DECEMBER 1991

FIELD STUDY OF MULTIDIMENSIONAL FLOW AND TRANSPORT IN THE VADOSE ZONE

WRRI Report No. 262

NEW MEXICO WATER RESOURCES RESEARCH INSTITUTE
New Mexico State University
Box 30001, Dept. 3167
Las Cruces, New Mexico 88003-0001
Telephone (505) 646-4337 FAX (505) 646-6418

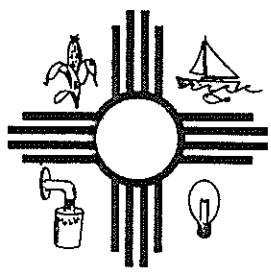

FIELD STUDY OF MULTIDIMENSIONAL FLOW AND TRANSPORT IN THE VADOSE ZONE

By

Robert S. Bowman
Daniel B. Stephens
Principal Investigators
Department of Geoscience and Geophysical Research Center
New Mexico Institute of Mining and Technology

and

Paula Arnet
David P. Grabka
Rolf I. Schmidt-Petersen
Ann M. Stark
Graduate Research Assistants
Department of Geoscience
New Mexico Institute of Mining and Technology

TECHNICAL COMPLETION REPORT

Grant Number 1423621-1345683
14-08-0001-G1645

December 1991

New Mexico Water Resources Research Institute

in cooperation with

Department of Geoscience
Geophysical Research Center
New Mexico Institute of Mining and Technology

The research on which this report is based was financed in part by the U.S. Department of the Interior, Geological Survey, through the New Mexico Water Resources Research Institute.

DISCLAIMER

The purpose of Water Resources Research Institute technical reports is to provide a timely outlet for research results obtained on projects supported in whole or in part by the institute. Through these reports, we are promoting the free exchange of information and ideas, and hope to stimulate thoughtful discussion and actions that may lead to resolution of water problems. The WRRI, through peer review of draft reports, attempts to substantiate the accuracy of information contained in its reports, but the views expressed are those of the author(s) and do not necessarily reflect those of the WRRI or its reviewers. Contents of this publication do not necessarily reflect the views and policies of the U.S. Department of the Interior, nor does mention of trade names or commercial products constitute their endorsement by the United States government.

ACKNOWLEDGEMENTS

The financial support of the U.S. Geological Survey, the New Mexico Water Resources Research Institute, and the Geophysical Research Center of the New Mexico Institute of Mining and Technology is gratefully acknowledged. Previous financial support from the University of Nevada Generic Center of the U.S. Bureau of Mines contributed to the success of the research reported herein.

Special thanks are due to Darlene Reeves and Catherine Ortega Klett of the Water Resources Research Institute, and to Anna McLain of New Mexico Institute of Mining and Technology, for administrative assistance.

Finally, the field site development work of former graduate students Earl Mattson, Alva Parsons, Kevin Flanigan, and Joseph Gibbens made this research possible. Their efforts, along with those of undergraduate students Grady Rhodes, Nikki West, Meiko Haushalter, and Mike Stephens are much appreciated.

ABSTRACT

A comprehensive field experiment was conducted to determine geologic controls on water flow and solute transport in a heterogeneous vadose zone. The experiment was conducted on a 10-m by 10-m plot underlain by heterogeneous beds of clays, sands, gravels, and cobbles of alluvial and fluvial origin. The plot and surrounding area were instrumented with 21 neutron probe access tubes, 168 tensiometers, and 62 solution samplers. Steady water application was provided by a drip irrigation system. Measurements of subsurface wetting and drainage, a multitracer transport experiment, in situ and laboratory determinations of hydraulic parameters, and destructive geologic characterization were conducted. The results of all determinations reflected the extreme short-scale geologic variability of the subsurface material. Attempts to model the flow and transport behavior were only partially successful.

The project provided a detailed characterization of a vadose zone typical of those found throughout the western U.S. The extensive data base developed under controlled conditions may be useful for future modeling activities.

Keywords: contaminant transport, groundwater recharge, hydrogeology, infiltration, model studies, soil physics, solute transport, stochastic hydrology, unsaturated flow.

TABLE OF CONTENTS

LIST OF FIGURES

List of Figures (cont'd)

LIST OF TABLES

INTRODUCTION

Groundwater contamination often results from transport through the vadose zone. Sources of chemical seepage near the land surface may include radioactive waste canisters, landfills, storage tanks, and fluid waste impoundments. In western states where the depth to the water table may be tens of meters, vadose zone processes become increasingly more important in assessing the potential for groundwater contamination. For example, characterizing the vadose zone is required by California statutes for hazardous waste disposal facilities.

The vadose zone often is comprised of relatively dry, stratified geologic materials. Recent theories and laboratory experiments suggest this stratification may cause seepage to spread laterally to a great extent under some conditions. That is, flow paths through the vadose zone are likely to be threedimensional. Numerical models of two- and three-dimensional, variably saturated flow are tools available to hydrologists to predict impacts of seepage on groundwater.

Great effort has been expended recently to develop theories and predictive models to describe moisture and solute movement in unsaturated porous media. Very little effort has been made thus far to validate the theories and models. The field experiments necessary to validate a numerical model are tedious, time-consuming, and often require extensive manpower. Site characterization comprises one of the most important elements of such field experiments. Data collected during site characterization must include unsaturated hydraulic properties which will be used in the predictive models. In most cases, the predictive tool is a numerical model. To evaluate the accuracy of a numerical code, it is imperative that the field data and laboratory measurements are accurate and representative of the hydrogeologic system. In natural settings the hydraulic properties are spatially variable. Therefore, numerical models must incorporate this variability where practical. This project was designed to obtain field data on site hydraulic properties and to apply a numerical code which incorporates spatial variability to simulate a field-scale flow and transport experiment.

OBJECTIVES

The objectives of this investigation were to:

1. Evaluate quantitative hydrogeologic information to describe the physical processes which affect multi-dimensional, field-scale transport of water and solutes in the vadose zone.

2. Test the capability of multi-dimensional numerical models to predict flow and transport in the vadose zone at field scale.

3. Develop a practical approach for characterizing the geologic and hydraulic properties of the vadose zone most relevant to predicting flow and transport.

The research focused on flow and transport in the vadose zone. In particular, we investigated processes associated with seepage from relatively localized sources such as canisters of radioactive waste, fluid waste disposal facilities, underground tanks, pipelines or ponds. The research differed from previous work primarily because it addressed:

1. Multi-dimensional unsaturated flow.
2. Spatial variability of hydrologic properties.
3. Field-scale observations and predictions.

This report summarizes two and one-half years of research by the principal investigators and four graduate students. Further details may be found in Arnet (1991), Grabka (1991), and Schmidt-Petersen (1991). A fourth independent study related to this project will be completed in early 1992 (A. Stark 1991, personal communication).

MATERIALS AND METHODS

FIELD SITE INSTALLATION

Site Location

A field site was established in a dry wash on the New Mexico Institute of Mining and Technology campus in Socorro. The site chosen lay in an arroyo bottom that was diked off to prevent runoff events. Figures 1 and 2 give the field site location relative to the rest of New Mexico and the campus. The soil is highly stratified and heterogeneous. Two distinct facies have been defined. The upper alluvial unit consists of interbedded silts, silty sands, sands, pebbles and distinct cobble layers. The lower facies consists of relatively uniform fluvial sands of ancestral Rio Grande origin. The water table is approximately 24 meters below ground surface at the beginning of water application to the site. The site had never been irrigated prior to the experiment. The site chosen overlay a 3O-m by 3O-m square section of soil oriented roughly north-south. Water was applied to the site over a 10-m by 10-m square section centered within this plot. The coordinate system had the southwest corner of the plot labelled (0,0) and the northeast corner labelled (30,30). The first number represents the distance in meters north from the southwest corner of the plot and the second number represents the distance east from this point.

Water Application System

A 30-m by 30-m area was cleared out and levelled. The water application system was constructed in the summer and fall of 1986. Details can be found in Mattson (1989). Alterations to the water application system were carried out in the spring of 1989.
The central 10-m by 10-m area was excavated to 60 cm below land surface. On this, 2 cm of sand were deposited as a base for the water application system. Twenty-one 10-m long polyethylene drip lines, with emitters spaced 50 cm apart, were laid down. The drip lines were placed 30 cm apart running east to west. This formed a 50 cm by 50 cm spaced grid of 441 drip emitters to evenly distribute water to the soil.

The drip lines were numbered 1 to 21 from south to north. The drip emitters were connected at their east and west ends to 3/4" PVC manifold headers, which ran north to

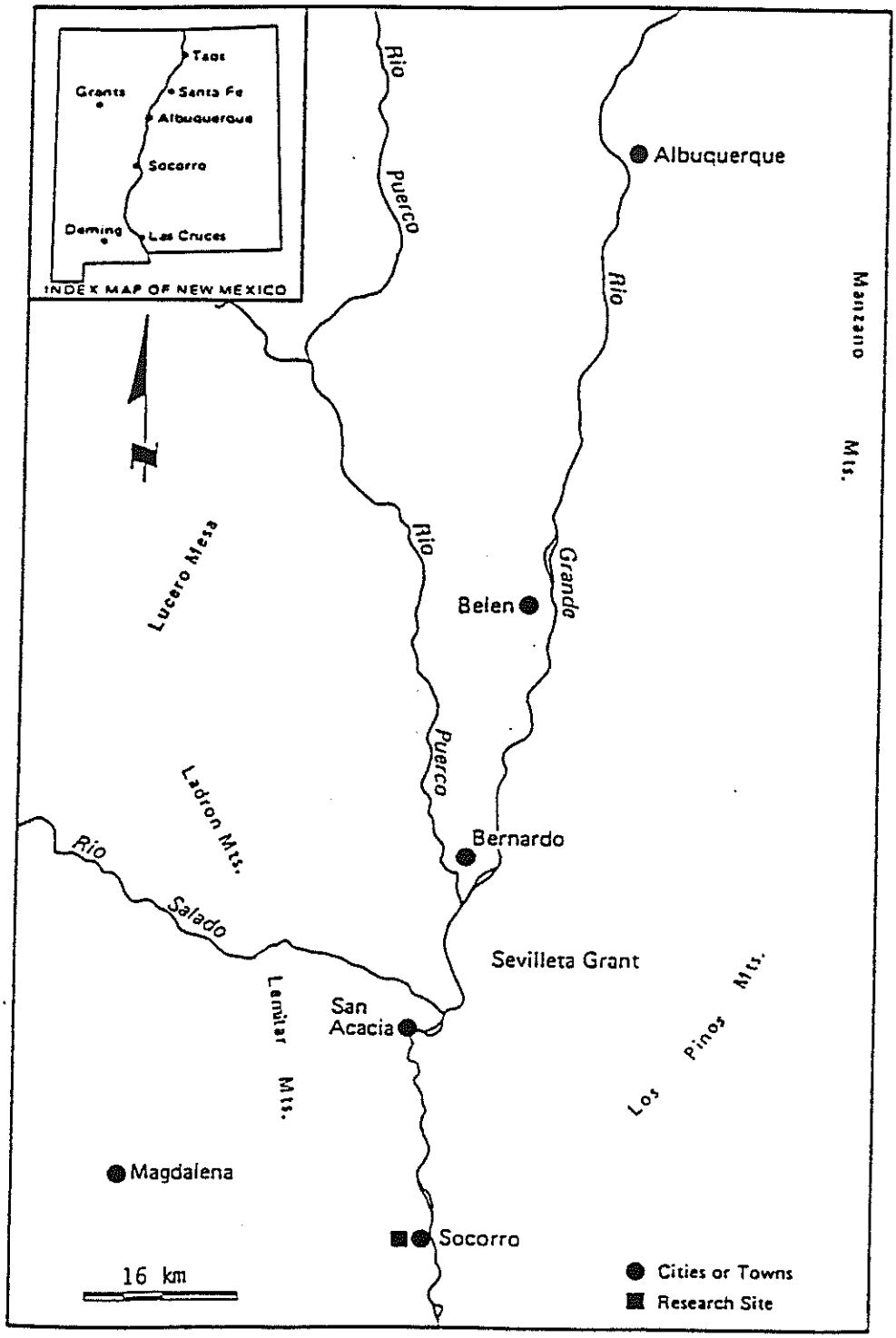

Figure 1. Index map (from Parsons 1988)

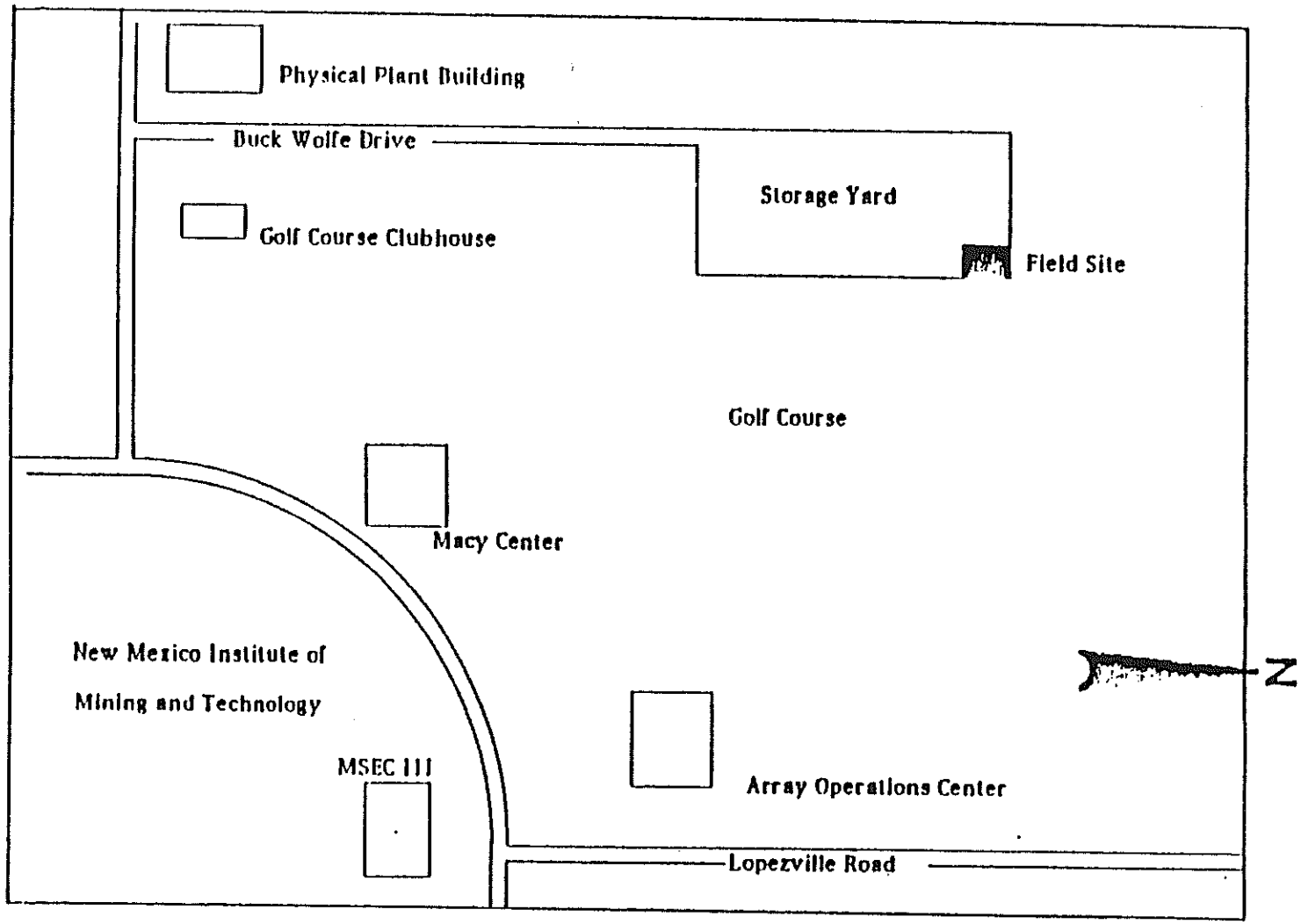

Figure 2. Site location map from Gibbens (1989). Not to scale.

south. The ends of the headers were capped. Originally, water was pumped into the eastern manifold header through two lines intersecting the header between drip lines 10 and 11. The northern line supplied the northern half of the emitter grid and the southern line supplied the southern half. The original water application configuration is shown in figure 3. The initial rate of water application was 10^{-5} cm/sec. Three studies were done using this configuration. Parsons (1988) applied a one-dimensional analytical model to observed moisture movement after water was initially applied. Mattson (1989) provided details on the water application design and construction, and applied a two-dimensional analytical model to the observed moisture movement. Flanigan (1989) described a bromide tracer experiment conducted at the site, applying different variations of the one-dimensional advection- dispersion equation to breakthrough of bromide seen in porous cup samplers. He also reported on unsaturated column studies using site material. During the spring of 1989, alterations to the water application system were completed. The lines were grouped into four sections. Lines 1 through 5 composed section A; 6-10, section B; 11 - 16, section C; and 17 - 21, section D. Ball valves were installed on the eastern and western headers between lines 5 and 6, 10 and 11, and 16 and 17. The valves were closed to prevent any water mixing between the sections.

Water entered the eastern manifold header sections via four 3/4" PVC pipe networks. The network divided a single water source into four roughly equal ones. Each network of pipe was instrumented with gate valves, totalizing flow meters, and a port whereby a tracer solution could be injected into the water stream. The gate valves allowed the adjustment of water flow to a particular section. Flow meters indicated the amount of water actually flowing into each section. The valves were adjusted to transmit 5/21 of the total water applied to the site to section A, 5/21 to section B, 6/21 to section C, and 5/21 to section D. Each emitter was then assumed to discharge an equal amount of water during any particular pump cycle. To periodically flush accumulated sediment from drip lines, a faucet was attached to each section of the western header. The western manifold headers ensured that pressure was evenly distributed among the drip emitters of a section. The headers on both sides and the pipe network supplying water to the site were encased in wood lined trenches which prevented damage to the pipes and allowed access for maintenance.

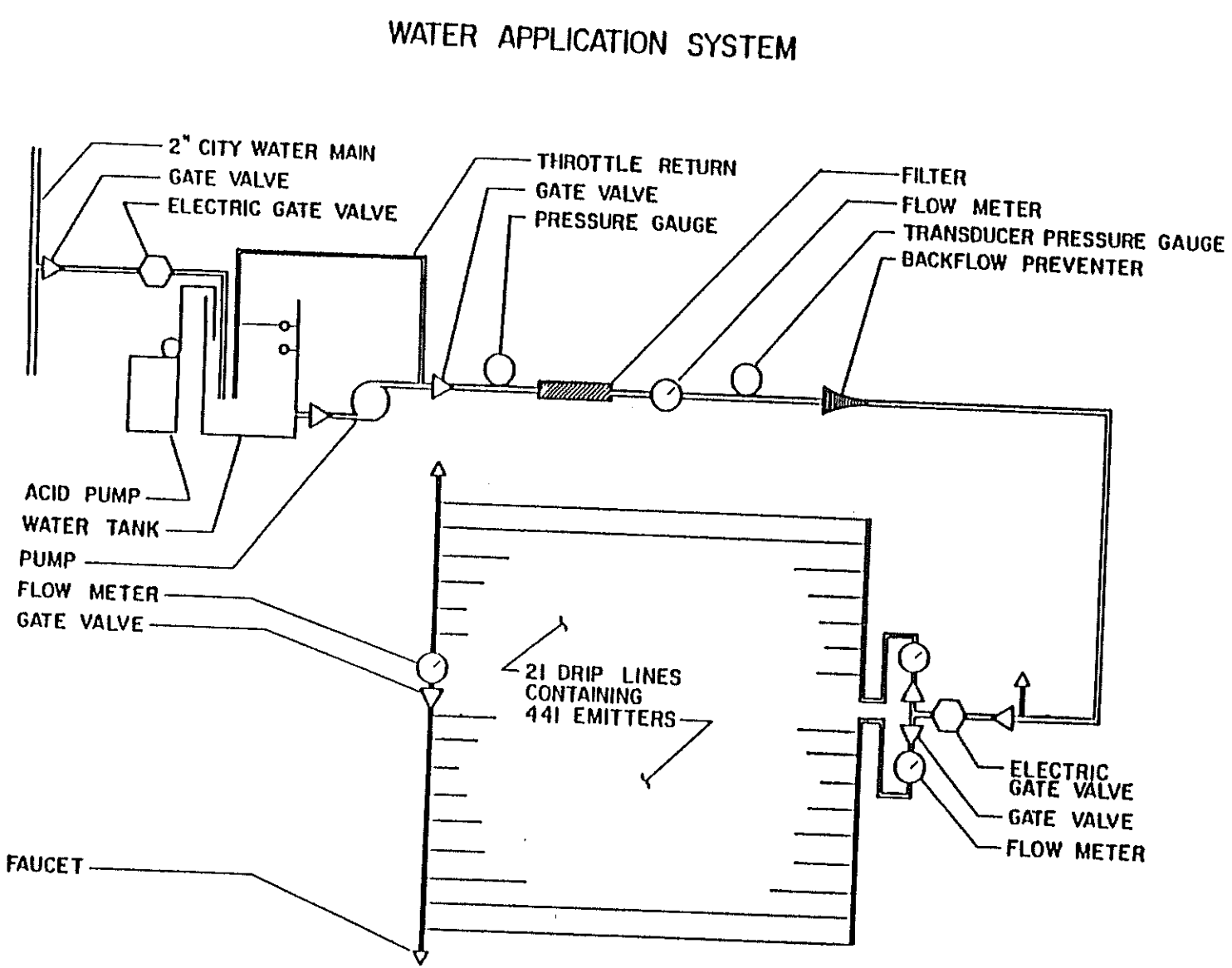

Figure 3. Schematic of initial water application system (from Parsons 1988)

Figure 4 is a schematic of the altered water application system.

Moisture/Pressure Head Instrumentation

Prior to constructing the water application system, tensiometers and neutron probe access tubes were installed at twenty-one stations in a symmetrical pattern across the site. Each station consisted of a 5-cm diameter, 10-m long aluminum tube that served as an access tube for the neutron moisture probe; and two tensiometer nests, each consisting of 8 tensiometers emplaced at depths from 1 to 5 meters. The location of these instruments is shown on figure 5. Moisture measurements from the neutron probe and measurements of matric potential in the soil were collected daily after the flux to the water application system was increased. Measurement data provided evidence that water flow through the instrumented area reached steady-state before the tracers were applied. The instruments were read twice weekly during the tracer experiment.

Monitoring Instrumentation

Tracer transport through the soil was measured with soil water samplers, also called suction lysimeters. Samplers beneath the drip lines ranged from 33 cm to 320 cm in depth; samplers outside the wetted region ranged in depth from approximately 100 cm to 700 cm.

Construction

Soil water samplers consisted of a length of 2" diameter PVC pvc pipe with a porous ceramic cup (No. 653X01-B2M2, Soil Moisture Equipment Corp., Santa Barbara, CA). epoxied to one end. A black rubber stopper, with two 1/4" black polyethylene hoses passing through it, sealed the other end of the PVC pipe. One hose reached the bottom of the ceramic cup to remove all solution pulled inside the sampler. The other hose reached two to four inches into the sampler. The rubber stopper was glued to the other end of the PVC pipe with liberal amounts of epoxy. Figure 6 illustrates the way the soil water samplers were designed.

Prior to installing the soil water samplers at the site, the porous ceramic cups and PVC pipes were cleaned to remove any chemicals that might interfere with tracer analysis. This was accomplished by drawing approximately one liter of 6N hydrochloric acid followed by two liters of distilled, de-aired water through the sampler's porous cup under vacuum.

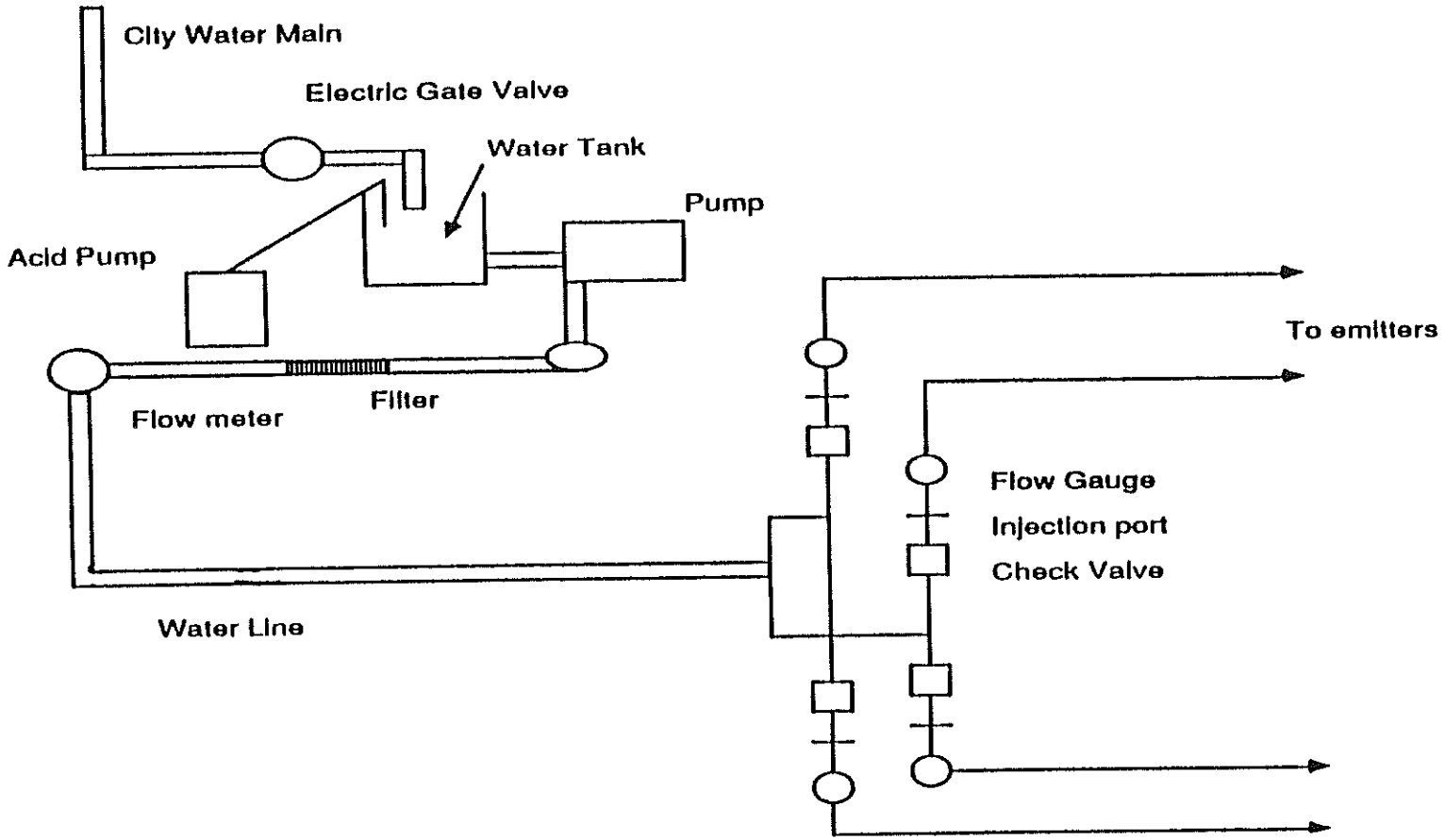

Figure 4. Schematic of water application system for use in tracer test (from Gibbens 1989)

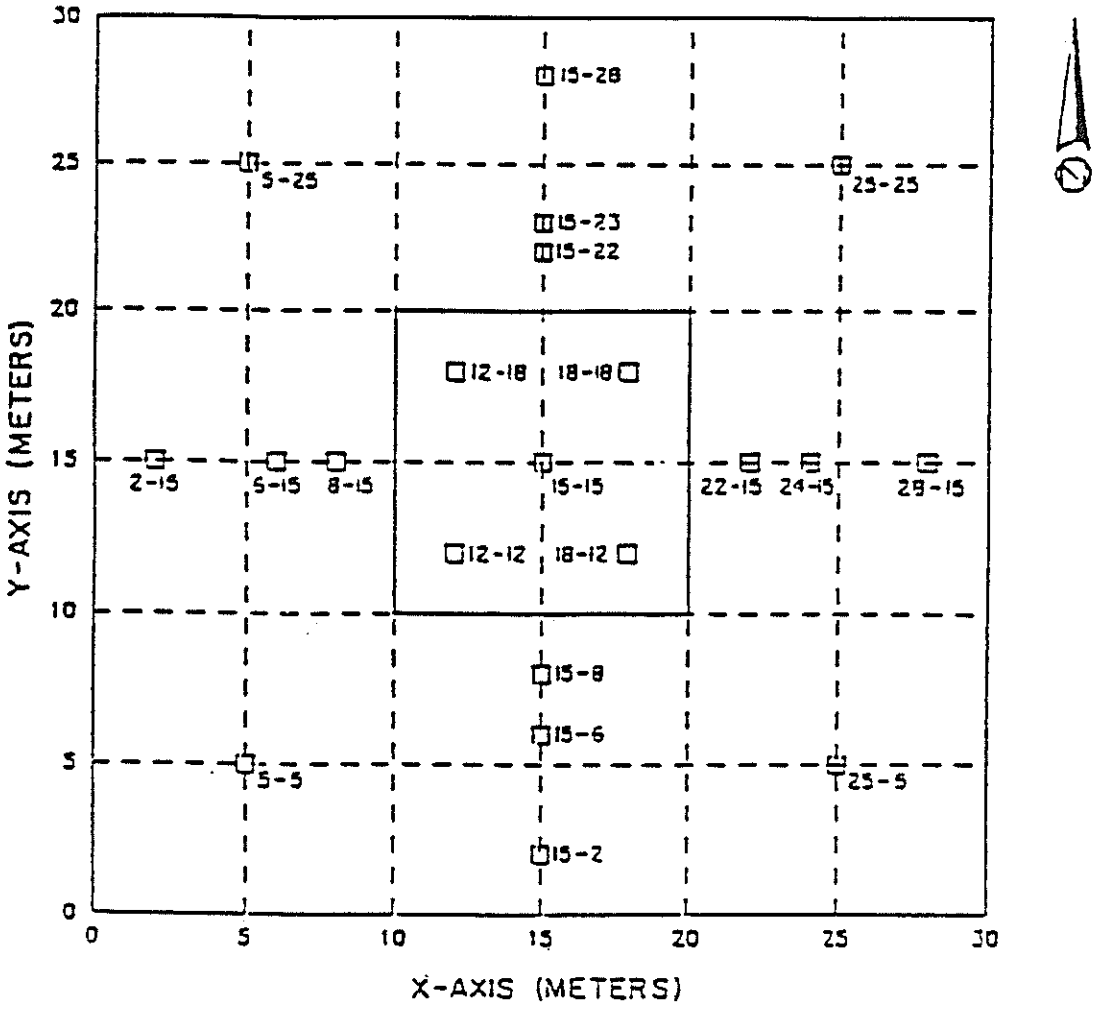

Figure 5. Diagram showing the location of instrument stations at the field site. Each square represents a neutron probe access tube and one or two tensiometer nests (from Parsons 1988).

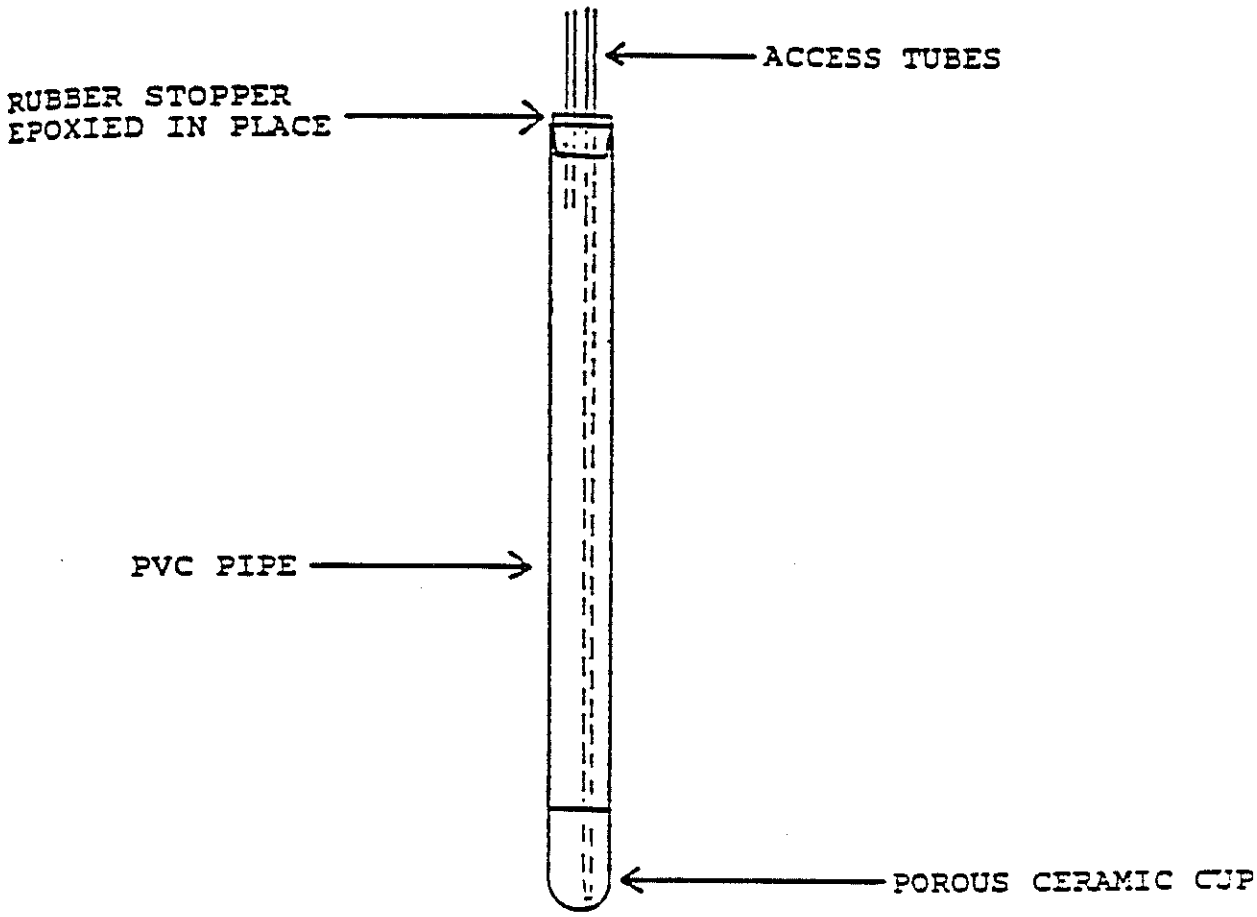

Figure 6. Soil water sampler (from Flanigan 1989)

Installation of Soil Water Samplers

Table 1 presents a list of soil water samplers, their coordinates and their depths below drip lines. The number part of each sampler's name corresponds to the hole in which it was emplaced. When a letter follows the number, like a, b, c, or d, it refers to several samplers placed at different depths in one hole. Figure 7 shows the location of the sampler stations installed before a previous bromide tracer experiment (Flanigan 1989). Figures 8 and 9 plot the location of samplers installed for this experiment within and without the wetted region, respectively. All samplers (except G24, H23, I22) within the wetted region were emplaced in holes dug with a 3" diameter hand auger. This digging method was employed because heavy machinery, such as a drill rig, could crush drip emitter lines and cause uneven water distribution across the site. Soil water samplers G24, H23, and I22 had been placed in holes made by a rotary drill rig with an 8" diameter auger before the drip lines were laid down.

The samplers were installed as follows. The black 1/4" plastic hoses were inserted into a 7/8" O.D. 5/8" I.D. PVC pipe, with 5" of hose sticking out, for protection. Silica flour (200 mesh) was funneled to the bottom of the augered hole, the sampler lowered to the bottom and enough silica flour added to cover the ceramic porous cup. Several inches of native sandy soil, sieved through a #4 (6.3 mm) sieve, were added and tamped; then two inches of a 15 percent mixture of bentonite and sieved soil were added. The bentonite was expected to swell around the PVC pipe of the sampler and inhibit flow down the sides. Sieved sandy soil was added and tamped till the elevation of the next sampler, or until the level of the drip lines. Just below and above drip line elevation, 5 cm of bentonite/soil mixture were placed to prevent evaporation out or precipitation into the augered hole. Native material was used to fill the hole to ground surface. Vinyl tubing was clamped onto the exposed ends of the black plastic hoses using hose clamps. Suction samplers placed outside of the wetted region were emplaced similarly, but holes were dug using a drill rig with a 20-cm auger. Names for these outside samplers correspond to points on a compass. For instance, SSW-C stands for a sampler placed at depth C in a hole drilled south-south west of the center of the drip emitter grid. Samplers 11 a,b,c,d were installed without silica flour or bentonite seals except just above and below the drip lines. This was done to

TABLE 1. x,y,z, locations of soil water samplers.

SAMPLER	x(m)	y(m)	z(cm)
1a	11.25	11.25	100
1b	11.25	11.25	191
1c	11.25	11.25	265
2a	16.25	11.25	100
2a	16.25	11.25	239
2c	13.75	11.75	100
3a	13.75	11.75	242
3c	18.75	11.75	100
4a	18.75	11.75	145
4c	11.25	12.75	100
5a	11.25	12.75	208
5c	16.25	12.75	100
6a	16.25	12.75	225
6c	13.75	13.75	100
7a	13.75	13.75	204
7c	18.75	13.75	112
8a	11.25	14.25	100
8c	11.25	14.25	219
9a	16.25	14.25	100
9c	13.75	15.25	33
10a	13.75	15.25	99
11a	13.75	15.25	148
11c	13.75	15.25	216
12a	13.75	15.25	100
12c	18.75	15.25	193
13a	18.75	16.25	100
13c	11.25	16.25	235
14a	11.25	16.25	100
14c	16.25	16.25	225
15a	13.75	17.25	100
15c	13.75	17.25	224
16a	18.75	17.25	100
16c	18.75	17.25	226
17a	11.25	18.25	100
17c	11.25	18.25	237
18a	16.25	18.25	100
18c	16.25	18.25	224
19a	13.75	19.25	100
19	13.75	19.25	248
20a	18.75	19.25	100
20c	18.75	19.25	199

Table 1. (Continued)

SAMPLER	x(m)	y(m)	z(cm)
20c	18.75	19.25	288
D29	14.50	12.25	138
G24	15.50	17.25	107
H23	15.50	17.25	244
I22	14.50	17.25	320
K25	14.00	15.25	158

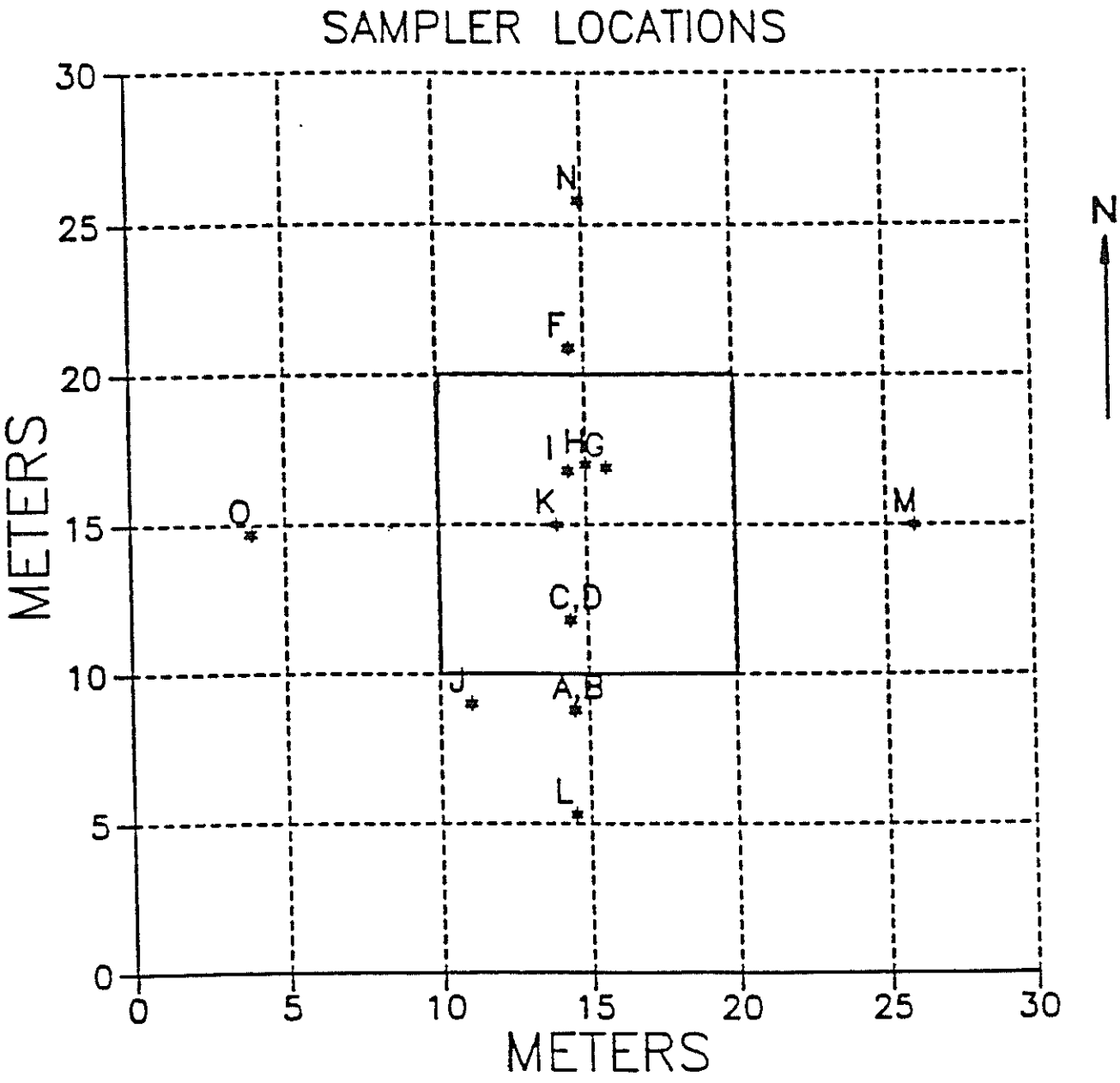

Figure 7. Locations of soil water samplers from the previous tracer experiment (from Flanigan 1989)

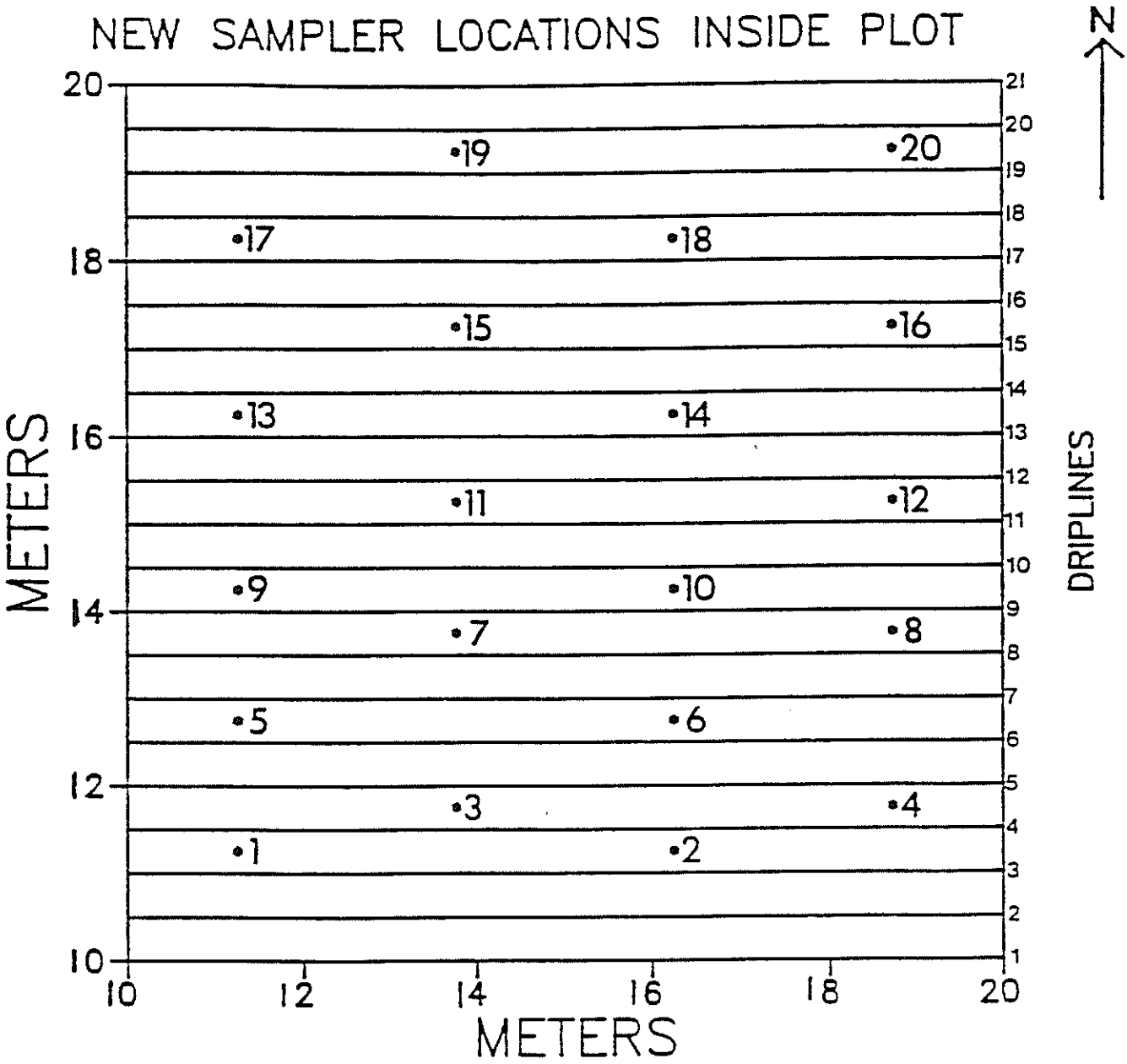

Figure 8. Location of sampler nests installed within drip lines for multiple tracer test.

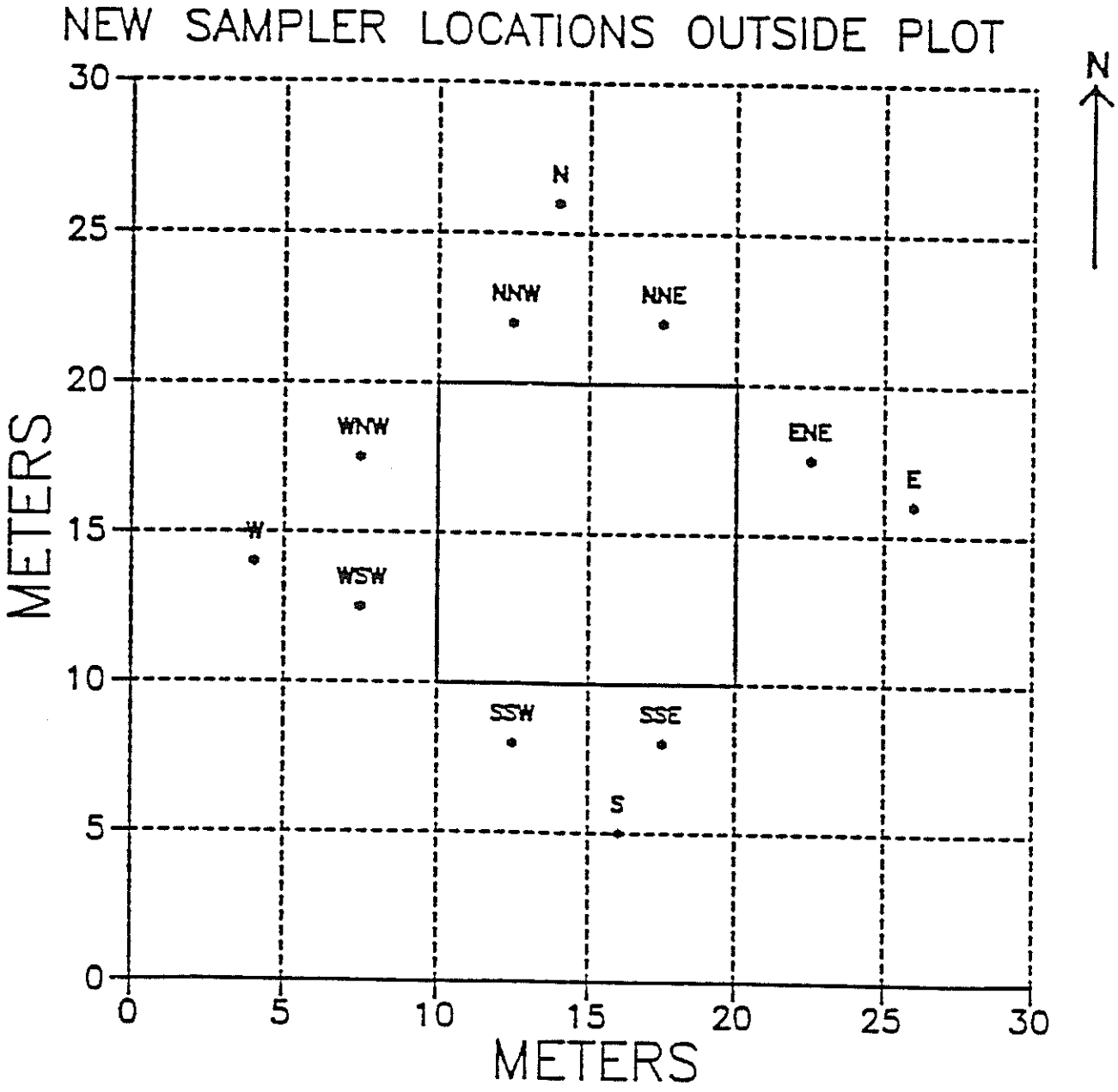

Figure 9. Location of sampler nests installed outside drip lines for multiple tracer test.

investigate how the installation of the porous cup samplers might influence tracer movement.

GEOLOGIC BACKGROUND

The study area's geologic characterization has been investigated on three major scales. The pertinent depositional history of the middle Rio Grande valley has been reviewed to establish the origin of the alluvial and fluvial environments encountered in the intermediate and small scale geologic investigations. The hydraulic vertical characterization study is focused on the heterogeneous alluvial piedmont slope facies, therefore the intermediate scale geologic investigation is centered on describing and classifying this alluvial fan environment. The small-scale investigation describes the geology beneath the site as applied toward textural control of fluid transport through the unsaturated zone.

Large Scale: Depositional History

The experimental field site is located in the easternmost part of the Basin and Range Province within the Rio Grande Depression (fig. 10). The field site is underlain by alluvial and fluvial sediments of the Sierra Ladrones Formation (Fm), the upper subdivision within the Santa Fe Group in central New Mexico. The following is an account of the regional depositional history, and a summary of the geologic classification history in the middle Rio Grande valley with a view of where the field site fits into these classifications.

Geologic History and Local Evidence

The Rio Grande Depression extends from central Colorado south to El Paso, Texas. In central New Mexico, the Rio Grande flows through a series of north-south trending structural basins underlain by Tertiary rocks and bordered in most places by highlands of older rocks. The valley is semiarid, with precipitation ranging from 10 inches on the piedmont to 20 inches in the highlands. The pediments rise steplike above the river and have been described as primarily stream-eroded surfaces graded to a successfully lowered base level, the Rio Grande. The lithologic composition of upper Santa Fe Group basin fills and post-Santa Fe valley fills reflect major structural and topographic elements of the Rio Grande rift that had formed by early Pliocene time (Chamberlain 1980). The erosional

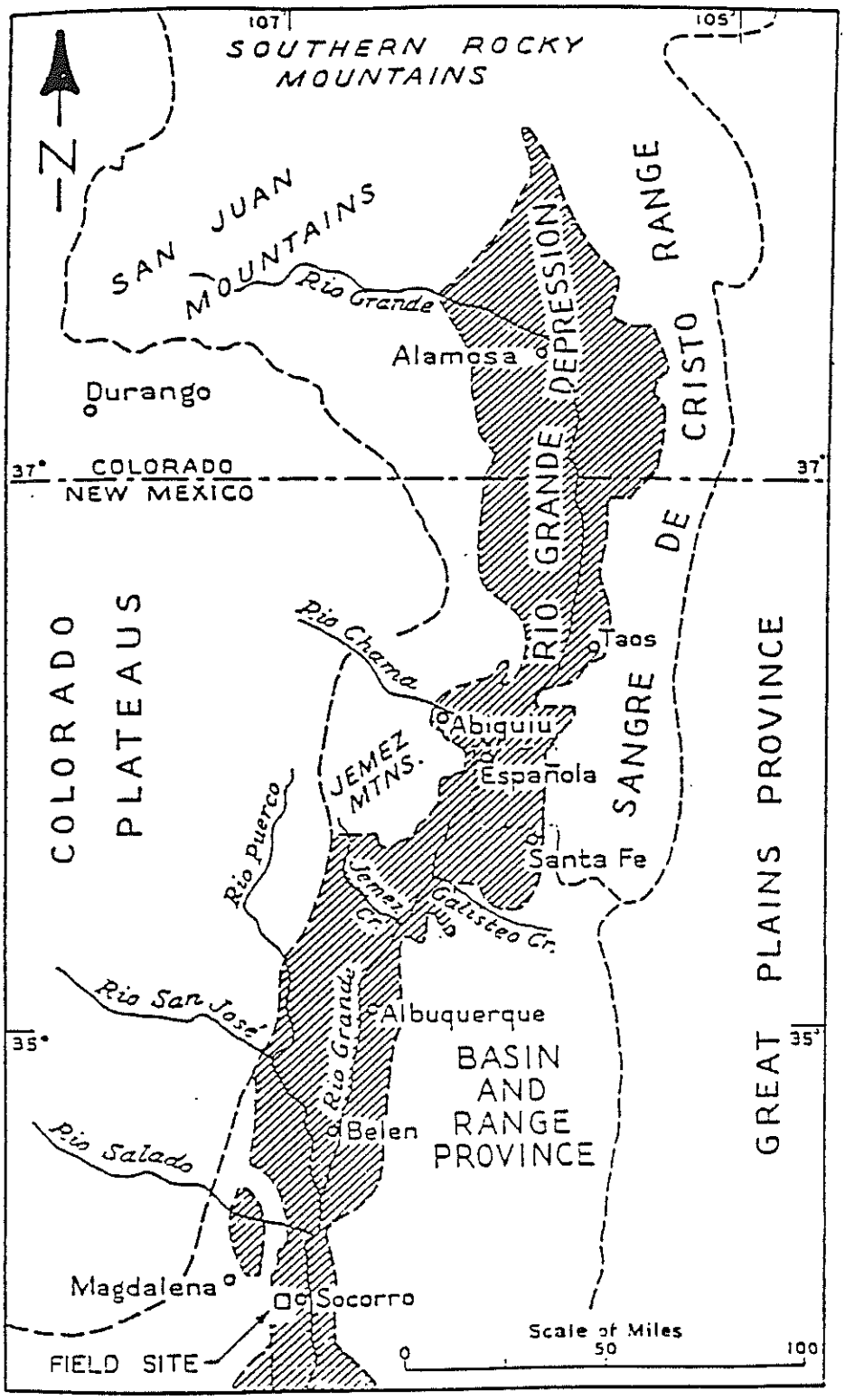

Figure 10. Rio Grande depression (after Denny, 1940).

valley of the Rio Grande, formed since mid-Pleistocene time, was the only major geomorphic feature not yet present. Previous deposits of volcanic basins, the bolson-fill facies and intrarift basins of the upper Oligocene-Miocene Popotosa Fm, are deeply buried in this area: they reflect Laramide-formed terrains largely obliterated by erosion, sedimentation, and structural deformation in the past 10 million years.

Sometime after 7 mybp and before 4 mybp, the Popotosa basin was disrupted by extensional forces breaking it into fault block uplifts and grabens (Chapin et al.1978). A combination of rifting and contemporaneous epirogenic uplifting of the southern Rocky Mountains and adjacent areas may explain the development of modern mountain ranges in the Socorro area at this time (Chamberlain 1980). Extensive pediment surfaces were carved across uplifted and tilted beds and older rocks. Alluvial fan material was deposited into the Socorro basin on the east, forming part of the lower Sierra Ladrones Fm. Concurrently, the regional drainage system integrated the Rio Grande into the Socorro basin. The river flowed along the eastern edge of the basin from San Acacia to San Antonio. Broad, gently sloping pediment plains graded into the tan well-sorted, arkosic sands and muddy overbank facies of the ancestral river. As regional uplifting occurred, an eastward prograding wedge of piedmont slope gravels (or alluvial fans) shed by the developing western mountain front caused the ancestral Rio Grande to retreat to the east, burying the older fluvial sands in the Socorro basin (Chamberlain 1980).

Early Sierra Ladrones facies do not indicate the presence of significant relief where the modern Lemitar, Socorro, and Chupadera mountains now exist; however, the coarsening sequence of mud, silt, sands, and gravels of this formation indicate an increase in topographical relief since late Miocene or early Pliocene time (approx. 4 to 7 mybp). Younger Sierra Ladrones piedmont slope gravels can be directly related to modern topography (Chamberlain 1980).

The diagrammatic cross-section in figure 11 (McLemore and Bowie 1987) from the Magdalena Mountains (southwest of Socorro) to the vicinity of Loma de las Canas, east of the Rio Grande illustrates the complex history of late stages of basin filling and the episodic nature of middle to late Pleistocene valley cutting. The earliest axial-river deposits (early Pliocene-3 to 5 mybp) were apparently emplaced along the western margin of the basin

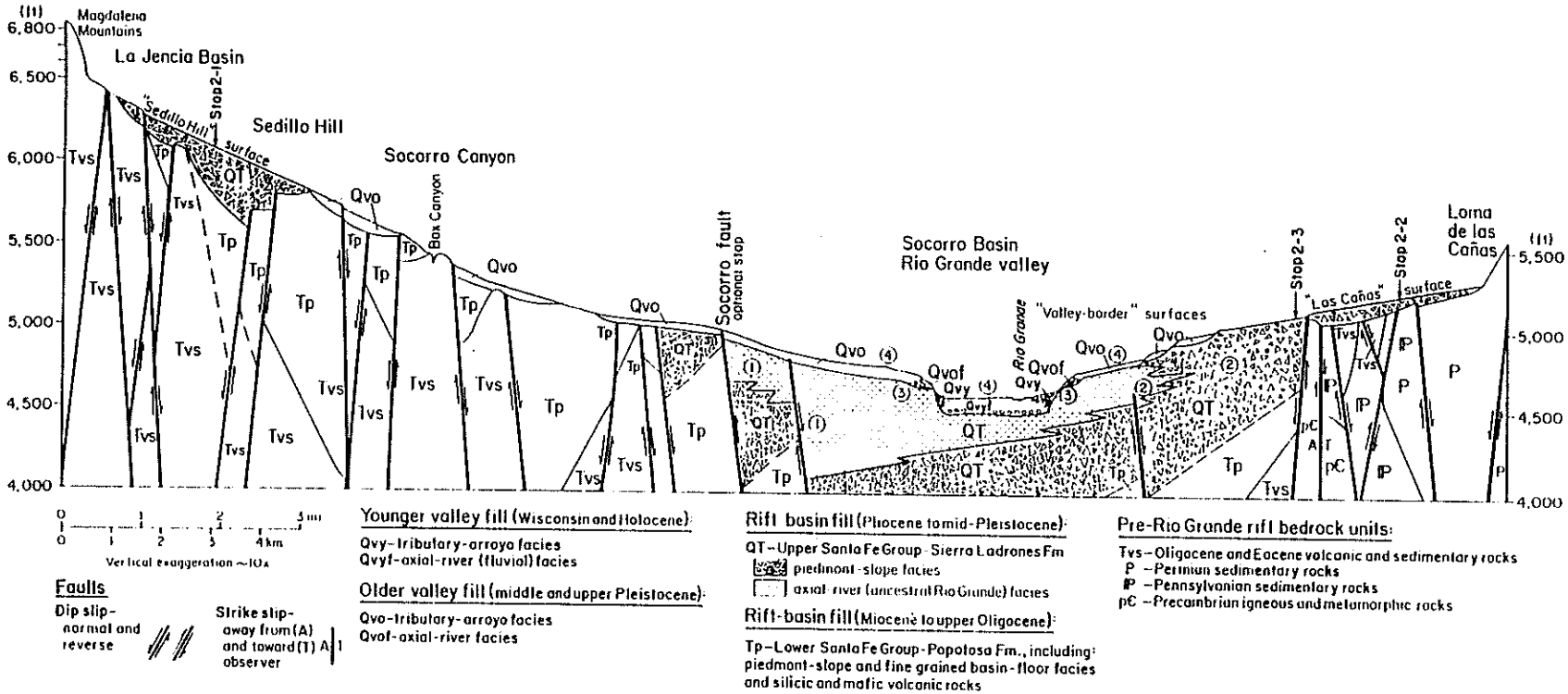

Figure 11. Diagrammatic cross-section near Socorro (after McLemore and Bowie, 1987)

and are now partly incorporated in the uplifted Socorro Mountain block (Chamberlain 1980). The site is located approximately 2 miles west of the Rio Grande lying above a unit of tributary arroyo facies with axial-river facies below.

Between 1.5 and 0.5 mybp ago, the ancestral Rio Grande again shifted westward to a position just west of the present valley in the Socorro-Escondida area. Volcanic ash from caldera-forming eruptions in the Jemez Mountains between 1.1 and 1.4 m.y. ago is present in axial-river deposits of the Sierra Ladrones Formation exposed in the Lopezville Road gravel pit about 1 mile north of the New Mexico Institute of Mining and Technology campus. Tephra from these eruptions is also present in Sierra Ladrones fluvial facies about 3 miles NE of San Antonio. Culmination of basin filling and the end of Santa Fe Group deposition occurred about 0.5 mybp ago throughout the Albuquerque to El Paso region (Hawley et al. 1976).

The Rio Grande system was internally drained until the capture of the ancestral Rio Grande at El Paso in middle Pleistocene time or 300,000 - 500,000 years ago (Kottlowski, 1958). This event lowered the river's baselevel throughout its course, creating deep entrenchment into earlier deposits. The highest outcrops of the ancestral Rio Grande surfaces in the Socorro area are about 180 meters above the present floodplain, due to entrenchment and localized effects of rifting (Chapin et al. 1978). Quaternary cycles of erosion and deposition correspond with the stage of recent glaciations (Chamberlain 1980). These events are evident in the stepped landscape of broad piedmont surfaces, terraces, (Qvy), and entrenched arroyos (Qvo) in the Socorro area. Much of Socorro Peak's eastern slopes are covered by a thin mantle of Quaternary surficial deposits consisting of alluvial fan and piedmont slope deposits resting unconformably on broad pediment surfaces, landslide deposits, colluvium, and young alluvium in arroyo flows, valley bottoms, and low drainages.

Valley landforms represent at least four major events of river entrenchments separated by periods of partial valley backfilling or relatively steady-state conditions in terms of local flood plain base levels. Along most of the river's course through the area, the boundary between the valley floor and sideslope is marked by a low bluff or scarp, here designated the inner-valley scarp. This erosional landform is the product of river trimming of the valley sides whenever the laterally shifting channel or flood flow impinges upon them. The site

exists on the outer limits, or rims, of the valley which vary considerably in terms of distinctiveness and regularity. The extensive remnants of graded surfaces flanking the inner Rio Grande valley in this region represent not only early valley degradational stages, but also long periods of valley-floor aggredation or relative gradational stability. The latter intervals probably reflect interglacial environments of the type exhibited in the Holocene (past 10,000 years) when tributary (or arroyo) drainage systems delivered more sediment to valley floors than master streams could remove from the middle Rio Grande basin.

In this discussion, the piedmont refers to the plain with locally complex topography that slopes from highland to playa or floodplain. The piedmont is an important part of the arid landscape of the Basin and Range province. Part of a piedmont may be more or less a bare rock surface, a pediment. Part is alluvium, and if its surface has the form of a section of a very low cone it is a fan. This fan-forming alluvium produces washes or arroyos.

The term arroyo is used throughout the project region (and many parts of the Southwest) to designate the channels of ephemeral streams, particularly those with broad, flat floors and vertical walls several feet or more in height. Valleys of these tributary streams comprise the dominant landforms of dissected terrains adjacent to the river floodplain, and they are termed arroyo valleys.

In the tributary-arroyo valleys of the project area, hillslope components include erosional slopes on older alluvial fill or bedrock, valley-floor depositional forms and valley-mouth alluvial fans graded to the Rio Grande. The most gentle longitudinal gradients of arroyo valley floors and valley-mouth fans are 1-2% and contrast markedly with the less than 0.1% slope of the river floodplain.

History of Classification - Today, most geologists agree that the Santa Fe deposits are a group and should include essentially all basin filling materials related to the Rio Grande rift ranging in age from Miocene to middle Pleistocene (Baldwin 1963; Hawley et al. 1969; Machette 1978; Chamberlain 1980). Its broad usage is an advantage in areas where the basin fill is not or cannot be subdivided (Baldwin 1963).

Machette (1978) mapped the San Acacia Quadrangle about 20 km north of the experimental field site, and subsequently redefined the Santa Fe deposits into an upper and lower unit; the Sierra Ladrones Fm and Popotosa Fm respectively. Machette reported the

upper Santa Fe unit as..."of early Pliocene to middle Pleistocene age is here named for the Sierra Ladrones (low foothills of the Ladron Mountains) and consists of alluvial fan, piedmont slope, alluvial flat, flood pain, and axial stream deposits, and locally derived basalt flows" (Machette 1978). These units had previously been called the Santa Fe Fm in San Acacia (Denny 1940). The Popotosa Fm had not been included in the Santa Fe Group before this time and represents the lower Santa Fe deposit in central New Mexico. The Popotosa Fm consists of several fanglomerates, qypsiferous playa beds, and piedmont slope deposits (Machette, 1978).

The axial stream deposits, also known as ancestral deposits of the Rio Grande, are the main characteristic to distinguishing the valley-fill sequence of the Sierra Ladrones Fm from the underlying Popotosa closed basin deposits. Debrine and others mapped ancestral sand deposits across the Rio Grande, east of Socorro. They found a grey, well-sorted sand and gravel unit composed of materials derived from sources to the north. The ancestral river deposits bed was dated as upper Pliocene by a fossil mastedon jaw found by Needham in 1936 (Debrine et al. 1963). Ancestral Rio Grande sands form a continuous stratum in the subsurface of the Rio Grande Valley between the type locality in San Acacia and Socorro (Chamberlain 1980). The sands crop out fairly continuously along the course of the present Rio Grande from as far north as Santa Fe to south of El Paso, Texas (Bachman and Mehnert 1978).

Chamberlain (1980) divides the Sierra Ladrones Fm into 3 sedimentary facies in the Socorro Peak area just west of Socorro. They are a mud and silt facies (Tslo), a fluvial facies (Tslf) of the ancestral Rio Grande River, and a piedmont slope facies (Tslp) derived from adjacent mountain ranges. In the Socorro Peak area, the Sierra Ladrones Formation lies in angular unconformity over the upper Popotosa Fm. The Sierra Ladrones Fm grades upward from alluvial flat mud and silts into lower axial stream sand deposits. The sands interfinger with the upper overlapping piedmont slope reddish brown sandstones and fanglomerates (Machette 1978). The top of the formation is placed at the base of thin veneers of gravelly alluvium which rest on piedmont surfaces cut across strata of Popotosa and Sierra Ladrones Fm. Thickness and extent of the Sierra Ladrones deposits are predominantly controlled by varying amounts of erosion across tilted faulted blocks. The thickest Sierra

Ladrones exposure crops out in Nogal Canyon where 350 meters of strata can be observed. The exact thickness in the Socorro Basin east of Socorro Peak is unknown but it may be significantly greater than 350 meters (Chamberlain 1980).

There is alluvial fan (or arroyo) material overlying ancestral Rio Grande deposits at the site. Chamberlain's divisions of the Sierra Ladrones Fm will be used to characterize the intermediate and small-scale geologic features of the study area. The fluvial facies (Tslt) exists below 5 meters at the site and the piedmont slope facies (Tslp) exists between the surface and 5 meters. These units and the contact between them are discussed further below.

Intermediate Scale: Alluvial Fan Characteristics

Alluvial fans are found in several arid and semi-arid parts of the world, including the southwestern United States, parts of India, South Africa and around the Mediterranean. Many potentially hazardous operations are located on these alluvial fans. The alluvial fan or tributary-arroyo facies is quite heterogeneous (as opposed to the fairly uniform sands of the ancestral Rio Grande), and therefore represents a complicated but common medium for contaminant or fluid transport. Therefore it is prudent to examine in detail the formation of alluvial fans and to identify the most useful and hydraulically applicable classification system for the various types of fan deposits. The classification system chosen is based on textural and therefore hydraulic differences between the units and is discussed below with respect to the units mapped at the site.

Formation of alluvial fans

Alluvial fans always occur in areas of decreased confinement (Bull 1977). Fans are usually wedge-shaped and up to tens of kilometers in area. From top (or source area) to valley bottom, they are divided into the apex, fanhead, midfan and distal fan. The fanhead usually consists of debris flows and channel-forming materials, while the midfan is dominated by sheetflood and braided stream deposits. The distal fan has similar deposits as the midfan though finer in grain size and tending to exhibit or interfinger with valley playa or eolian deposits. The tectonic setting for these fans is active, including fault blocks, mountain fronts, and volcanic highlands (McPherson et al. 1987). The characteristic facies associated with fans are conglomerates, sandstones, and mudstones with clasts up to boulder size. The gradients of fan surfaces are as steep as 25 degrees on small fans and less than 1

degree on large fans (Allen 1970). Sorting is usually poor with grading increasing downfan. Clast shape in fan deposits is angular to subrounded. Chemical characteristics for these deposits include a large degree of oxidation and a common association with pedogenic carbonates and evaporite containing playa-lake deposits (Bull 1972).

Other diagnostic features of fans include, vertical and lateral variability of lithofacies, a high bedload to total load ratio, a short distance from source to fan toe, and a low relative stability of distributaries found on the fan surface (McPherson et al. 1987). Each bed of a fan represents a single depositional event that has resulted from one of a spectrum of precipitation and erosion events within the source area. In radial sections of a fan, individual beds may be traced for long distances, while cross-fan sections reveal overlapping beds of limited extent that are interrupted by cut-and-fill structures (Bull 1972).

It should be noted that fan morphology and surface processes are controlled by allocyclic variables, such as climate and tectonism, and by autocyclic variables, such as channel diversion and bar migration that are inherent to fan depositional systems (Mack and Rasmussen 1984). Together these factors dictate the morphology of the fans with respect to their source areas.

To be able to understand the alluvial fan products at the site and their hydrologic roles, it is important to understand the allocyclic processes that contribute to their formation. The processes that most actively shaped these fans are climatic and tectonic in nature. These processes largely work independently of one another, but their effects can cause similar products, therefore creating a difficult task of recreating the climatic and/or tectonic past.

The climatic factors that produce deposits or affect the depositional slope of the semi-arid fans center around the abundance and regularity of precipitation events.

Semi-arid regions are known for precipitation events that are intermittent but strong and mostly short in duration. (Blissenbach 1954). In particular, these are the contributing factors behind debris flows. The more steady the rainfall, the larger the tendency for waterlaid deposits to form. The mountain ranges in these fan environments contribute to a larger amount of rainfall over the mountains than the surrounding area would receive, thereby adding to the transporting and depositing capabilities of flows.

In general, the more humid the climate (or the more precipitation), the more aggradation will take place further downfan, while fanhead entrenchment and stream incision will occur in response to more arid situations. For example, periods of accumulation of thin temporary alluvial fans may coincide with climatically controlled times of increased sediment yield of the source area, or decreased competence of transportational processes (Bull 1977). It is therefore seen that climatic changes may contribute to changes in the fan's depositional slope.

Tectonic factors are the second process responsible for fan deposits being discussed. Semi-arid fans are known to have existed in tectonically active areas, namely in rift valleys and along mountain front fault scarps as found in the Basin and Range province. Tectonic control on alluvial fan deposition can be summarized in the following manner: large scale coarsening-upward cycles in a fan sequence would represent uplift and fan progradation while large scale fining upward cycles would be a result of reduced relief between fan and source area or source area retreat (Mack and Rasmussen 1984).

In particular, the rate of uplift of the mountains relative to the adjacent basins, either by pulsatory or continuous uplift, largely determines the thickness or loci of fan deposition (Bull 1977). Uplift counteracts the tendency for the fanhead to entrench and it allows both channel downcutting in the mountains and fan deposition next to the mountains. The latter processes occur only when the rate of uplift equals or exceeds the sums of the two base-level trenching processes. On the other hand, recession of a mountain front results in the formation of a rock pediment normally covered by the fanhead portion of the fans. A rock pediment may be an important indicator of the extent of an alluvial fan at its maturity.

Classification System

Bedding of deposits is one of the best methods of identifying the alluvial-fan environment of deposition. Within a single outcrop a variety of strata generally can be observed, each bed representing a particular set of hydraulic conditions that determined the thickness, particle size and distribution, particle orientation, and type of contact with the underlying bed. For fans composed entirely of water-laid deposits, differences in flow result in marked differences in the sedimentological characteristics of the beds. Bedding differences are even more striking in the many fans composed of both water-laid and debris flow deposits. The

poorly sorted, massive beds of debris flow deposits stand out in marked contrast to the beds water-laid sediments.

A sheetflood-streamflood stream classification of alluvial fan deposits based upon lithofaciies classification will not be used because it is difficult to infer the shape of a deposit and the place of deposition from subsurface samples. This system of characterization focuses more on structural characteristics rather than textural characteristics that may be discerned in core samples. A useable classification (for the deposits found on alluvial fans) must include deposits of mudflows, and all the intermediate gradations. It should be applicable to both surface and subsurface deposits and should be adaptable to alluvial-fan deposits in any part of the world.

W. B. Bull's classification of alluvial fan deposits based on textural and sediment/water ratio during deposition is used in this study. This method of classification distinguishes between mudflow deposits and water-laid sediments which are distinct depositional types and are separated by deposits whose properties are intermediate between the two. The scheme can be used to classify subsurface samples because parameters from grain-size analyses can be used to help describe each type. The following are relevant characteristics of mudflow (or debris flow) deposits, water-laid deposits, and intermediate or between the two classes deposits. These products are directly related to the processes discussed above.

Debris flows are dense, viscous flows capable of transporting very large boulders in "suspension." As a result they are poorly sorted, with a very high sediment to water ratio. Debris flows are commonly formed near the apex of a fan but if the flow is persistent enough it will form lobate tongues extending from sheetlike deposits further downfan. Debris flows and mudflows have abrupt, well-defined margins along the sides and downslope edges of the deposit (Bull 1963). Farther downstream the mudflow overtops both banks and spreads out as a sheetlike deposit on the fan. Factors that promote debris flow formation (Bull 1963) are 1) abundant precipitation over short periods of time; 2) steep slopes with insufficient vegetative cover to prevent erosion; and 3) a source material that provides a matrix of silt and clay.

The relative viscosities of debris flows can be obtained by study of the position and orientation of the larger clasts. A low-viscosity debris flow will have grade bedding and a

horizontal or imbricated orientation of the tabular gravel fragments. The more viscous flows have the larger clasts distributed uniformly throughout the flow. The most viscous flows not only have uniform distribution of the larger clasts, but the tabular particles commonly have a vertical preferred orientation normal to the flow direction.

Mudflows are debris flows consisting mainly of sand-size and finer sediments with silt or clay matrix. Many debris flow deposits are so coarse grained that it is difficult to obtain a representative sample for determining the particle-size distribution of the material. As a result, few particle size analyses have been made of debris flows. Logarithmic plots of the coarsest one-percentile vs median particle size may make patterns distinctive of depositional environments on fans. For example sinuous patterns indicate shallow ephemeral-stream environments, while rectilinear patterns indicate debris flows (Bull 1962). W.B. Bull (1963) analyzed the grain size distribution of fan samples from Fresno County, CA and published an average clay content of 31% for debris flows.

Because the bulk of the fan deposits are deposited as sheets and lobes, uniform thickness for a given bed is common in most outcrops, particularly for debris-flow deposits. When individual beds can be identified at more than one outcrop, another diagnostic stratigraphic indicator becomes readily apparent-the extensive sheet-like aspect of the individual beds. The sheetlike character of the bedding commonly is not apparent in those fans consisting mainly of gravel. The braided-stream mode of deposition that is characteristic of these gravel deposits results in small-scale, cut-and-fill structures common in those exposures parallel to the fan contour.

Mudflows acquire air in two ways. Air may be incorporated into mudflows as they move down both tributary ravines and main stream channels. This entrained air actually may decrease the viscosity of the mudflow. The other air source is the deposits beneath the mudflow, as it spreads out on the alluvial fan. Part of the air in the soil moves upward and becomes trapped by the mudflow to form bubble cavities. Air may be trapped by water-laid sediments if they are deposited on soils that contain air which can move up into the saturated sediments.

Very few grain-size analyses and even fewer comparisons have been made of the sorting of debris flows and water-laid sediments. Bull (1964) made 50 particle size analyses of

mudflows. The cumulative curves (grain diameter vs cumulative percentage on semilog scale) have gentle slopes ranging range from clay to predominantly gravel. The grain size analyses supply quantitative information for some of the visual observations. For example, the clay content of the 50 mudflow samples analyzed ranged from 12 to 76% and averaged 31%.

The proportions of water-laid and debris-flow deposits vary greatly from fan to fan and may change during the accumulation of the deposits of a single fan. Most fans whose source areas produce debris flows also have flood events that result in water-laid deposits. Thus, the deposits of many fans consist of interbedded deposits of debris and water flows in varying proportions.

Water-laid flows consist of sheets of sand, silt, and gravel deposited by a network of braided distributary channels. More steady rainfall is needed for the formation of these flows. They are clast supported (with very little clay), well sorted, cross-bedded, and laminated. The laminations represent fluctuations or repeated periods of deposition (Bull 1963). These tend to fill in stream channels that were temporarily entrenched into the fan and they tend to occur on the lower parts of the fan. Sieve deposits are part of the water-laid category as they are formed when earlier surficial fan material is so coarse and permeable that even large discharges infiltrate into the fan completely before reaching the fan toe.

The nature of water-laid deposits shows progressive change downfan. There is an increase in the abundance of cross-bedding with transitions such as coarse gravel through clast-supported fine-grained gravel, and sand matrix-supported gravel to sand. These changes reflect a gradual decrease in the particle size to water depth ratio as stream competence decreases downfan.

Bull's study showed a 6% clay content for the water-laid samples from the Fresno County fans and they were marked by S-shaped grain size distributions indicating a coarse and fine portion as opposed to the flat (straight-line) plots of the mudflow deposits. Intermediate deposits are deposits between debris flows and water-laid deposits. They are better sorted than debris flow sediments with bedding defined partly due to horizontally oriented gravels in the lower parts of the beds and only partly defined margins. Intermediate flows have some clay grain coating but are not able to carry very large clasts. These deposits

include sheetflood sediments and streamchannel sediments, possibly the most abundant lithofacies of alluvial fan sequences (McPherson et al. 1987). Deposition of these sediments is caused by the widening of the flow into sheets as a result of more steady rainfall in the source area than for debris flows. These deposits are most likely found in the midfan area. Bull's (1963) fan study showed an average clay content of 17% for these beds with a grain size distribution slope intermediate between debris flows and water-laid sediments.

Small Scale: Geology of the Site

The detailed subsurface geology of the study area came from the initial study conducted by Parsons (1988), subsequent mapping of shallow and deep trenches (as discussed below), and 2-D and 3-D reconstructions of the plot down to 20 meters below datum using stratigraphic sections boreholes drilled at the site. As discussed above, the site consists of a piedmont slope facies underlain by the Rio Grande fluvial sand facies. The geologic heterogeneities of the piedmont slope facies must be defined to reconstruct and support the infiltration and drainage results discussed and interpreted in below. The nature of the piedmont slope facies/fluvial sand facies contact and the nature of the Rio Grande sand facies are also discussed.

Piedmont Slope Facies

As discussed by Parsons (1988) the profile beneath the 30 m x 30 m field site consists of "two distinct facies of the Sierra Ladrones Fm...The soil profile is stratified, consisting of an upper zone of red brown silty sands and pebbles interbedded with cobbles, and a lower zone of clean, tan fine sand and fine to coarse sands and pebbles. Clay lenses of undetermined extent are present throughout both zones. The underlying tan sands represent Chamberlain's (1980) ancient Rio Grande fluvial sand facies (Tslf), while the red brown silty sands and pebbles are piedmont slope facies (Tslp) derived from the Socorro Range to the west."

Following the tracer and infiltration experiments described below, study of the piedmont slope facies was undertaken. A 4 m wide by 15 m long by 4 m deep trench was dug by backhoe roughly oriented perpendicular (NW-SE) to the strike of the alluvial fan material coming off of the Socorro Peak area. The present relief between the top of Socorro Peak and

the trench units is about 2500 feet. The trench spanned the northeastern corner of the plot and the section studied was the western wall of this NW-SE trending trench.

MULTI-TRACER TRANSPORT EXPERIMENT

In May, 1989, flow to the emitter system was increased tenfold to 1 x 10-4 centimeters per second. The water was applied using a positive displacement pump, controlled by an electronic timer and a control box. At fifteen-minute intervals, water was pumped out of a tank for approximately four minutes. Water tank floats ensured the volume of water fed to the drip lines during each pump cycle remained constant. Water was pumped from the tank until a bottom float activated a switch and turned off the pump. Shortly afterwards, an electronic timer, controlling a solenoid valve, would open the valve and let the tank refill until an upper float in the tank activated a switch and closed the valve. The timer then reactivated the pump fifteen minutes after the last water application cycle and repeated the cycle. To prevent carbonate from precipitating out of the tap water and clogging the drip emitters, a chemical feed pump was occasionally turned on. This pump delivered a small amount of 1:13 solution of muriatic acid (31.45%) to tap water into the water tank (Flanigan 1989). This kept the water pH in the tank around 6.5.

On July 1, 1989, a multi-tracer field experiment was conducted at the site. The experiment consisted of injecting a different fluoro-organic acid tracer into each section of the water application system. Calcium bromide, potassium thiocyanate, and the herbicide bromacil were injected into all sections simultaneously with the fluoro-organic acids. The transport of the tracers was monitored using the soil moisture samplers.

Tracer Application

Four 50 L reservoirs of concentrated tracer solution were prepared, each consisting of one of four different fluoro-benzoic acids, bromide, thiocyanate, and the herbicide bromacil. The fluoro-benzoate tracers used were m-(trifluoromethyl)benzoic acid and acid (m-TFMBA), o- (trifluoromethyl)benzoic acid (o-TFMBA), 2,6-difluorobenzoic acid (2,6-DFBA) and pentafluorobenzoic acid (PFBA). The amount of tracer dissolved in each 50 liter reservoir is listed in table 2. Reservoir III had 20 percent more tracer since it supplied six, rather than five, driplines.

A multi-channel syringe pump (Soil Measurement Systems, Tucson, AZ) was used to inject concentrated tracer solution into the water stream flowing through the water application system, via four plastic syringes. The tracer application system was designed as follows. A 20-mL plastic luer lock syringe was connected to one end of a 5-cm long polyethylene tube, the other end of the tube connected to a "T" connection. Tubing ran from one end of the "T" to the tracer reservoir. The other end of the "T" had tubing running to an injection port, located between the gate valve and flow meter on the water application network previously described (see figure 4). High-flow uni-directional check valves were inserted into the lines running between the "T" and the reservoir and the "T" and the injection port. These check valves ensured that there was no backflow in the system. Hose clamps were placed on the tubing running from the solute reservoir to the "T." These clamps were pinched shut when the syringe pump was off. Otherwise, the head difference between the reservoir and the injection port would allow tracer to freely flow into the water application system.

An injection cycle consisted of two parts, a pull cycle and throw cycle. During the pull cycle, the stem of the syringe was pulled back, creating a suction that drew reservoir solution into the syringe bore, while a check valve prevented water from being sucked from the water application system. During the throw cycle, the stem was pushed into the syringe bore, creating a positive pressure that forced reservoir solution into the injection port. Presumably, the tracer solution mixed thoroughly with the water flowing through the drip emitter system, moderating the pulsing effect of the tracer injection cycle. The tracer application system was attached to the water application system in late June of 1989. Each reservoir was hooked to a separate syringe, which in turn was connected to one of the four sections (fig. 12). Reservoir I applied tracer to section A, reservoir II to section B, reservoir III to section C, and reservoir IV to section D. Tracer injection began at 7:00 am, July 1. The faucets on the western header were opened and mixed tracer solution and water allowed to fill the drip lines. The faucets were then closed and the experiment begun. The syringe pump was powered only when the water pump was activated. Tracer was applied for

Table 2. Masses of solutes added to 50 -L reservoirs (masses in grams)

	Fluorobenzoate				
Reservoir	**Acronym**	**Mass Added**	**$CaBr_2$**	**KSCN**	**Bromacil**
I.	PFBA	105	260	175	105
II.	2,6-DFBA	105	260	175	105
III.	o-TFMBA	125	310	210	125
IV.	m-TFMBA	105	260	175	105

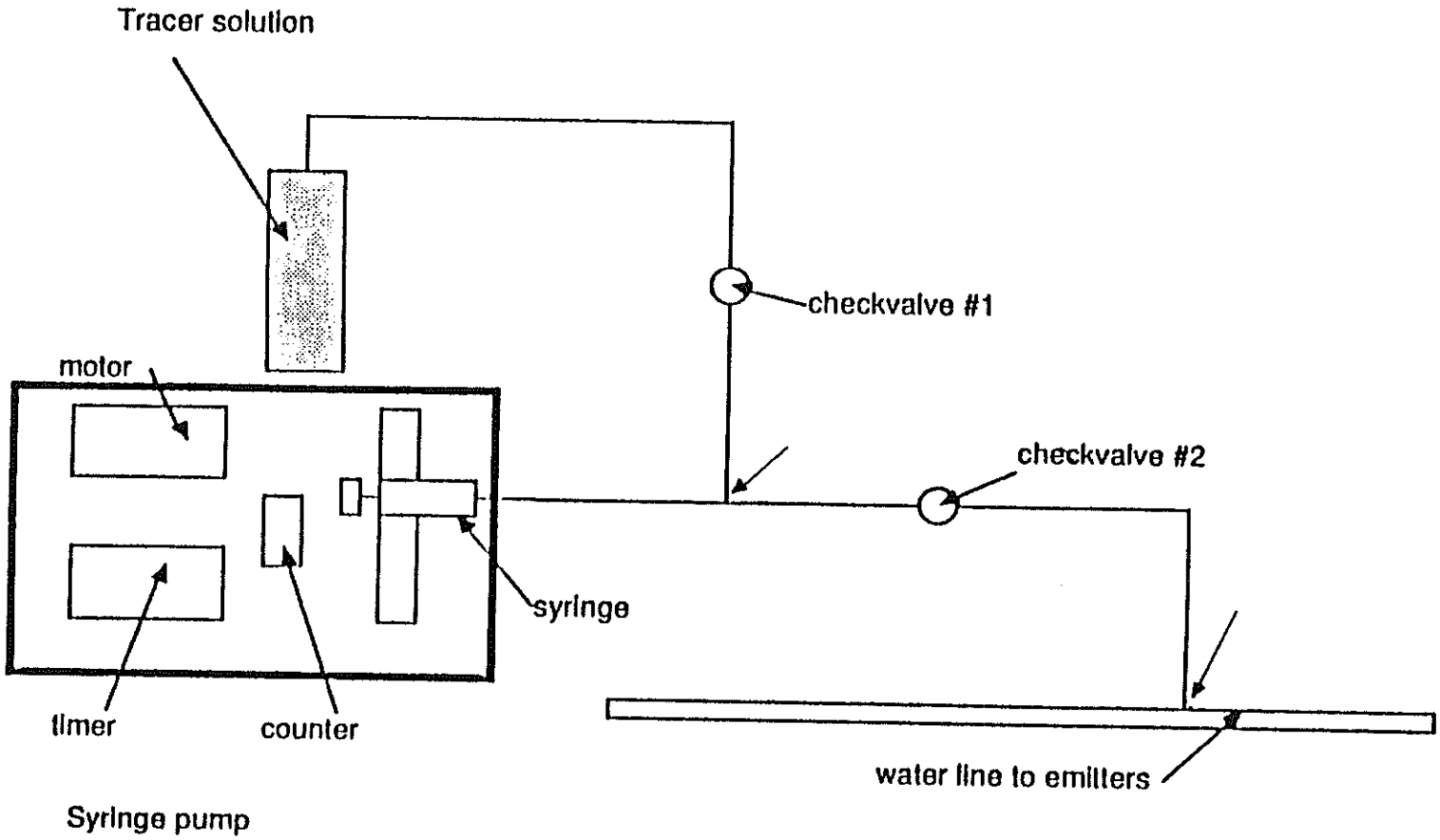

Figure 12. System for injecting tracer into water application system (from Gibbens 1989).

24 hours, consuming approximately 28 liters of each reservoir. While the tracer was being injected, drip line solution was sampled on three separate occasions. Samples were taken from the western header faucets one hour and 45 minutes, 14 hours and 45 minutes and 23 hours and 45 minutes after the start of tracer injection. These samples defined the initial tracer concentration entering each section of the site. After tracer application was discontinued, the faucets were opened and the lines flushed with tap water. To check for tracer still in the drip lines, water was sampled from the faucets during the next 3 pump cycles.

Sample Collection

Soil water samples from interior samplers were taken with a portable vacuum/pressure pump three times a day at approximately 0600, 1400, and 2200 hours for the first nine days after tracer injection was begun; then at steadily decreasing frequency through the remaining test period. Extraction of soil water samples took place in two phases. The first phase consisted of putting a vacuum in the sampler and allowing soil water to be pulled into the instrument through the porous cup. This was accomplished by closing one of the lines to the sampler and pulling a vacuum on the other line of 15 to 25 centibars on interior samplers and 30 to 40 centibars on exterior samplers. The vacuum line was clamped shut and soil water allowed to enter the porous cup. The second phase consisted of unclamping both lines and applying pressure to the line running to the top of the soil water sampler, thus forcing water out the other line. Almost all the water in the sampler was pumped out so that there would be no mixing between sampling runs. Samples were placed in 2-mL polyethylene sample bottles and the approximate volume of extracted water recorded. The volume of water varied from no water to 500 ml.

Dye Injection and Trenching

Immediately after the last soil water samples were taken, FD&C blue dye #1 was injected into the water flowing into the southern section of the site. This continued for five days. Afterwards, dye was applied over the entire site for one day. This was done to trace actual fluid flow paths from the drip emitters through the soil and to test drip emitter uniformity.

Trenches were dug across the site to observe the dye and to better understand the degree of soil heterogeneity. This paper will discuss only one particular trench. This trench was excavated to determine whether there was any piping of flow down instrument nests in the area. The hole was approximately 3-m deep, 2.75-m long running east to west, and 1.3-m wide. Figure 13 gives the approximate location of the trench within the plot. The nests studied were samplers 1a, 1b, 5a, 5c; neutron access tube 12-12 and tensiometer nest 12-12a.7

Analysis for Tracers in Water Samples

Water samples were analyzed for fluoro-benzoate, bromide, and thiocyanate using a model 501 HPLC pump, model 481 UV detector and model U6K injector (Millipore Corporation, Waters Chromatography Division, Milford, MA). The column used was a 25-cm x 4.5-mm I.D. Regis Rexchrom strong anion exchange column packed with 5pm solid phase (#728220, Regis Corporation, Morton Grove, IL). The mobile phase was 0.03M KH2PO4, pH 2.6, 20% CH3CN v/v. Periodic adjustment of the mobile phase was necessary to enhance separation of the tracers. Adjusting the concentration of KH_2PO_4 buffer sped up or slowed down the elution times for all the chemicals, while adjusting the pH permitted changing the elution times of the fluoro-benzoates relative to bromide and to each other. The mobile phase was pumped at 1 ml/min. The detection wavelength was 195 nm. High nitrate contamination at the site caused difficulties quantifying bromide in some samples. More information concerning the method for analyzing these tracers can be found in Bowman (1984). Figure 14 is a sample chromatogram showing an analysis of sampler 20b for bromide and m-TFMBA.

DETERMINATION OF HYDRAULIC PROPERTIES

Disc Permeameter

The disc permeameter (also known as a tension infiltrometer) is a compact field instrument for determining in situ hydraulic properties of soils. It was used to determine 119 in situ sorptivities and hydraulic conductivities at preselected supply pressures in this study. The device evolved from the sorptivity tube design of Clothier and White (1981). In addition to sorptivity and hydraulic conductivity, the characteristic mean pore size in which flow is occurring can be determined. The idea for measuring in situ unsaturated hydraulic

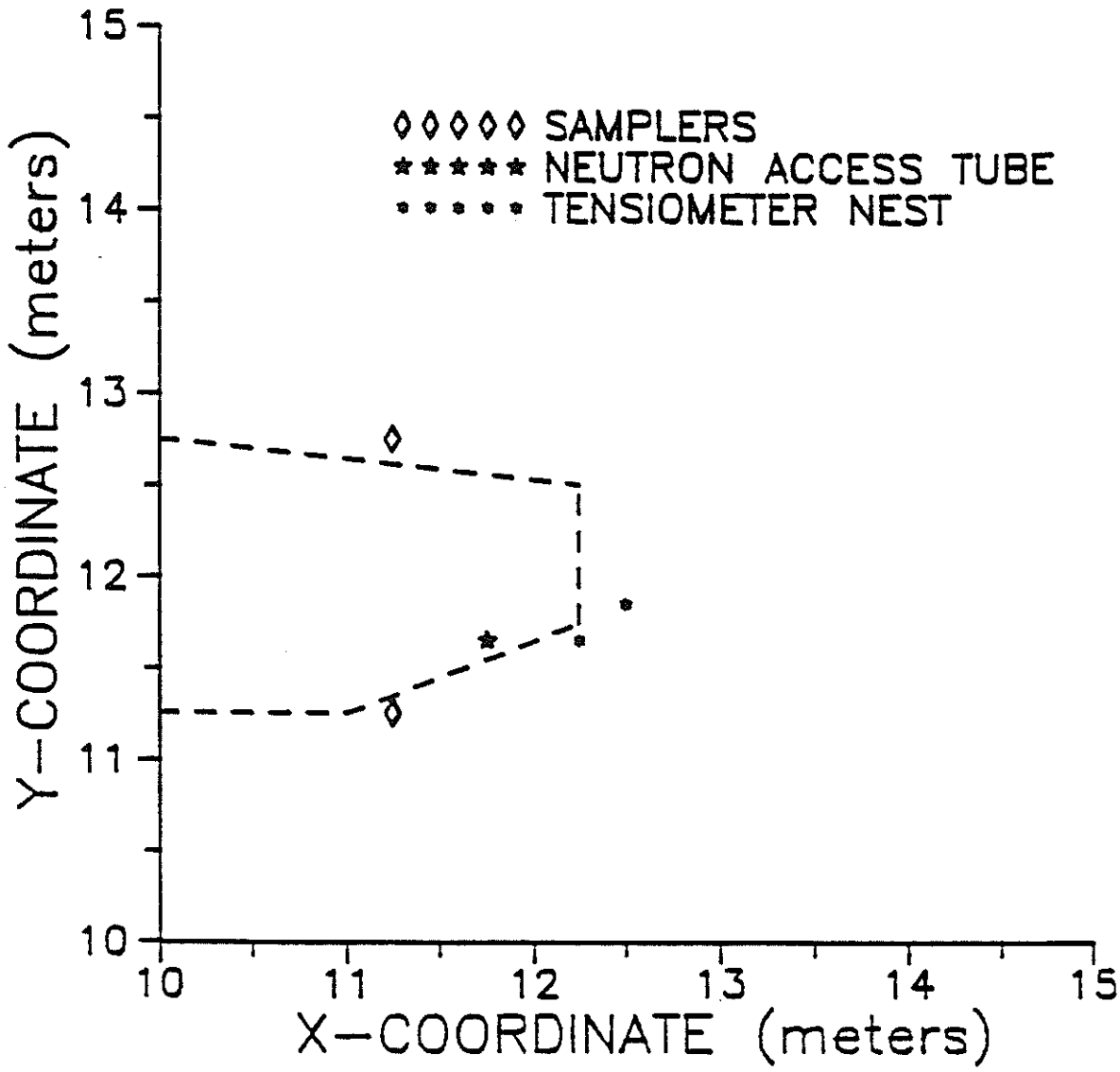

Figure 13. Trench location. Area inside dotted lines is location of trench (approximately 3 meters deep below ground surface).

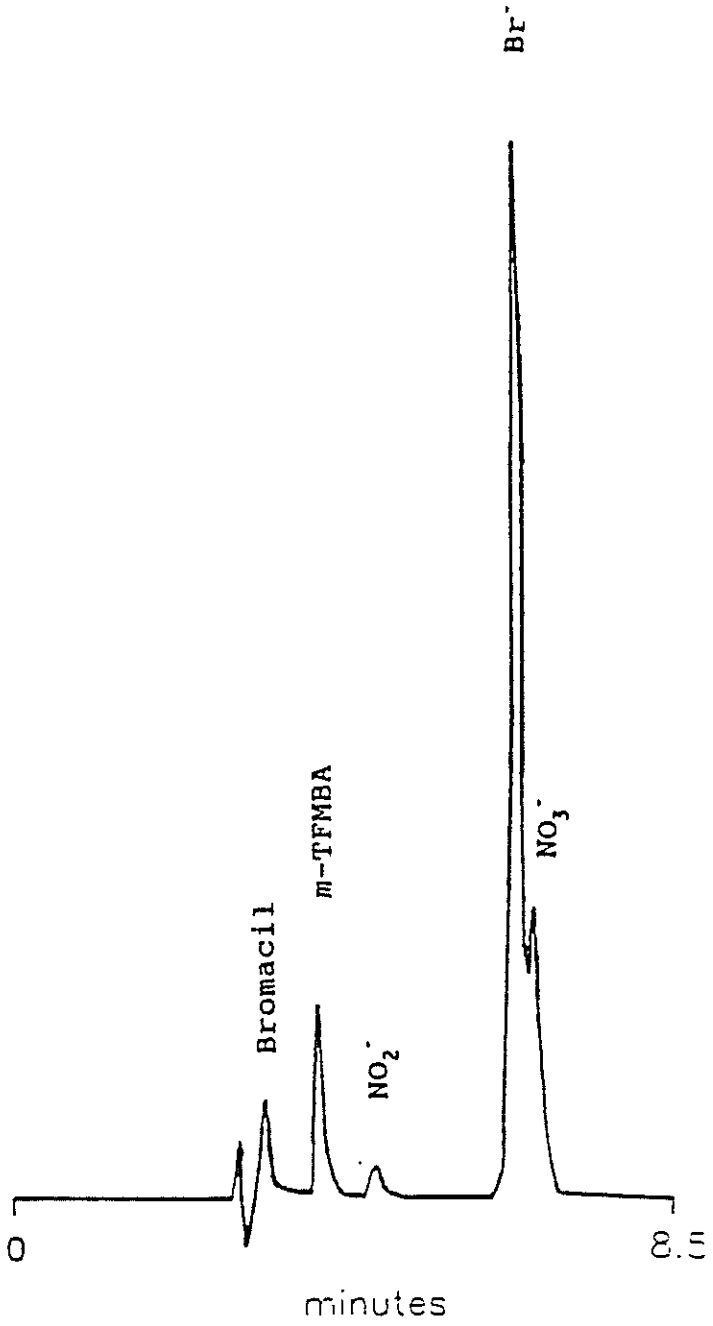

Figure 14. Sample chromatogram from sampler 20B. Sample was taken 7/6/90 at 14:00

properties is not new. Talsma (1969) measured in situ sorptivities but with a device restricting supply pressures to greater than zero. A closed top infiltrometer was designed by Dixon (1975) to study soil macroporosity and roughness at supply pressures between -3 cm and +1 cm of water. However, the device is complicated and may be hard to use in the field (Perroux and White 1988). Following the work of Smiles and Harvey (1973), Dirksen (1975) proposed a method to measure sorptivity with a mariotte type device. The method determined the dependence of conductivity on water content or pressure head in the tensiometer range.

According to Perroux and White (1988), the simplicity of Dirksen's device makes it attractive for field use. Using some of Dirksen's permeameter features, Clothier and White (1981) produced a simple field device known as the sorptivity tube. Water flow occurs through a sintered glass plate. Tension is determined by the bubbling pressure of a hypoder mic needle which allows air to enter a reservoir. The effective range of supply pressures for the sorptivity tube is from -10 cm to 0 cm of water. Chong and Green (1983) modified the supply plate design of the sorptivity tube. The modification, however, restricts supply pressures to a narrower range (Perroux and White 1988). Perroux and White (1988) identified several limitations in the sorptivity tube design: 1) the limited size of the sintered glass plates available restricted disc sizes to less than 0.1 meter; 2) air entry through the capillary was insufficient to maintain constant pressure during the initial stages of infiltration on high sorptivity materials; 3) the hypodermic needle used to regulate supply pressures clog easily under field conditions. Therefore, they designed the disc permeameter to retain the sorptivity tube simplicity, while increasing its versatility. Other permeameters have been used in field studies. Jarvis et al. (1987), for example, designed and operated a tension infiltrometer at supply pressures of -0.5, -2, and -9 cm of water. They compared the calculated hydraulic conductivities to the number of conducting macropores counted from a dye experiment. Perroux and White ' s permeameter has been used by numerous researchers (Sully and White 1987; Watson and Luxmoore 1986; Perroux and White 1988 ; Greene and Tongway 1989). Several researchers have used the disc permeameter to determine transport parameters such as infiltration, macroporosity and mesoporosity on forest watersheds. Watson and Luxmoore (1986) determined that, in general, the larger the total water flux, the

larger the macropore contribution to total water flux. They analyzed the spatial variability of infiltration under ponded conditions as well as 2, 5, and 14 cm of water tension. Perroux and White (1988) used the dependence of sorptivity on water supply potential to find the dependence of soil water diffusivity, hydraulic conductivity, and soil water characteristic on water content. Chisholm et al. (1987) compared the disc permeameter, drip infiltrometer, and disc rainfall simulator for sorptivity measurements. Only the rainfall simulator approxim ated the situation for natural rain, but the sorptivity measurements for all three devices could be logically explained.

The design, operation, and theory of the disc permeameter used in this study is described by Perroux and White (1988). The paper discusses the effects of the water supply membrane and soil cap materials as well as limitations imposed by restricted air entry. Ankeny et. al. (1988) proposed the design of an automated tension infiltrometer that can be used for tensions ranging from 2 cm to 50 cm and infiltration rates of 1.0 x 10-6 cm/sec to 5.0 x 10-2 cm/sec. This modification allows quick and accurate pressure control at low tension and improved measurement precision as well as automating data collection. More recently, White and Sully (1989) compared disc permeameter measurements of saturated hydraulic conductivity and sorptivity, developed analytical expressions for hydraulic conductivity and sorptivity, and compared them to results calculated from field measurements of time to ponding with a rainfall simulator on gravelly silty clay loam. They found good agreement between the three methods.

Smettem and Clothier (1989) describe a new method for obtaining unsaturated hydraulic conductivity and sorptivity from tension disc permeameter measurements. As sorptivity is often difficult to measure, they extended the ponded twin ring method to unsaturated discs of varying diameters. Long-time quasi-steady discharge, at the same water supply potential for all measurements, is needed to determine the hydraulic properties. Time domain reflectometry is used to estimate moisture content prior to the first measurement, but apparently not for subsequent measurements. Final moisture content is estimated from a soil-water/pressure head relationship. Comparisons with laboratory methods of determining unsaturated and saturated hydraulic conductivity on two contrasting soils corresponded well with near saturated field results. One soil, however, with large connected pores showed a

conductivity change of 3 orders of magnitude as pressure head decreased from -1 to 0 cm of water.

White and Perroux (1988) used field sorptivity measurements with the disc permeameter to estimate unsaturated hydraulic conductivities. They derived approximations that relate K(psi) to sorptivity measured over a range of supply pressures. Comparisons with conventio nally determined K(psi) for repacked and intact soil samples showed good agreement.

Ankeny et al. (1990a) measured field infiltration rates at selected tensions with a tension infiltrometer to develop new methods of characterizing the effects of wheel traffic and tillage on pore structure as measured by water flow through macropores. In a subsequent paper (Ankeny et al 1990b), a new field method for determining in situ unsaturated hydraulic conductivity is presented. Unsaturated hydraulic conductivity is determined from consecutive tension infiltration measurements on the same surface. Steady state infiltration rate is the only parameter needed for determining unsaturated hydraulic conductivity. Initial moisture content is not required. They state the method is valuable because it is simple, faster than lab methods, and less disruptive of soil pore structure than other field techniques such as the Guelph Infiltrometer.

Disc Permeameter Measurement Method

The disc permeameter was used interchangeably in this study for saturated and unsaturated hydraulic conductivity measurements. The methods of operation are similar and are described, briefly, by Perroux and White (1988). Detailed operation procedures are described below and in the CSIRO Disc Permeameter Instruction Manual (1988).

Positive Supply Pressures

Thirty-four measurements were conducted at positive pressures in this study (fig. 15). A thin-walled stainless steel cylinder, having an interior diameter just larger than the disc, is driven several millimeters in the soil. The interior soil is levelled, and the exterior disturbed soil is tamped down. A bentonite or mud seal is placed around the cylinder to limit leakage during infiltration. The permeameter is then placed within the cylinder and adjusted to

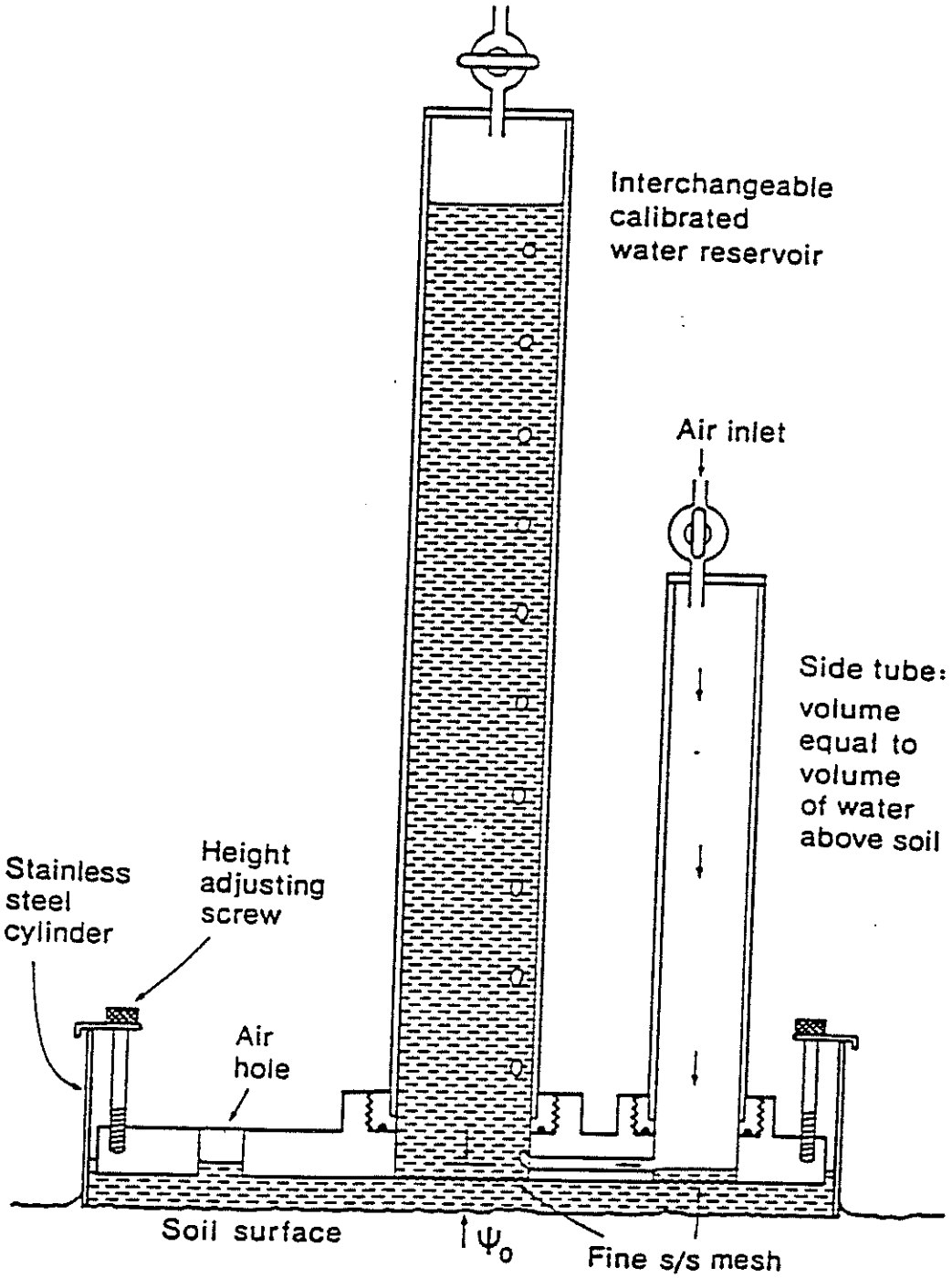

Figure 15. Positive pressure disc permeameter (CSIRO Instruction Manual 1988)

contain a selected head of water (0.5 cm for this study). The permeameter is taken from the cylinder and the reservoir filled with water. This is accomplished by closing the air-inlet stopcock, placing the base of the permeameter in a tub of water, and evacuating air from the reservoir. A hand vacuum works well to fill the reservoir. Similarly, the side tube is filled to the volume needed for ponded infiltration to occur.

Infiltration is initiated by placing the permeameter within the cylinder and opening the side tube stopcock to deposit water on the soil. Infiltration versus time is recorded. Timing when the first air bubble appears in the permeameter reservoir. High conductivity materials will require several reservoir volumes before steady state flow is achieved.

Negative Supply Pressures

Eighty-five measurements were conducted at very low tensions. The -1.3 cm tension was employed to exclude flow from cracks formed by evaporation after trench construction (fig. 16). The method is quite similar to that for positive pressures. First, the disc must be soaked in water for several hours prior to measurement to ensure it will remain airtight. The desired tension is fixed by raising or lowering water in the bubbling tower (fig. 16). The supply pressure at the membrane is calculated by $Z = z_2 - z_1 \cdot Z_2$, is fixed for each disc and was O.7mm for our disc. Therefore, z_1, the height of water in the bubbling tower above the air inlet, is used to set the desired supply pressure.

The measurement site is prepared by removing vegetation and large rocks, and levelling the soil. A level surface is imperative for good measurements. In many cases, a cap of contact material (normally a fine sand) is needed to ensure a flat measurement surface. The impact of the cap is discussed in Perroux and White (1988) and in the disc calculation section of this study. In any case, the thinnest cap needed for good soil contact with the membrane was used.

The permeameter reservoir is filled as in the positive supply case. The instruction manual (CSIRO 1988) suggests the following steps be conducted before measurements are started:

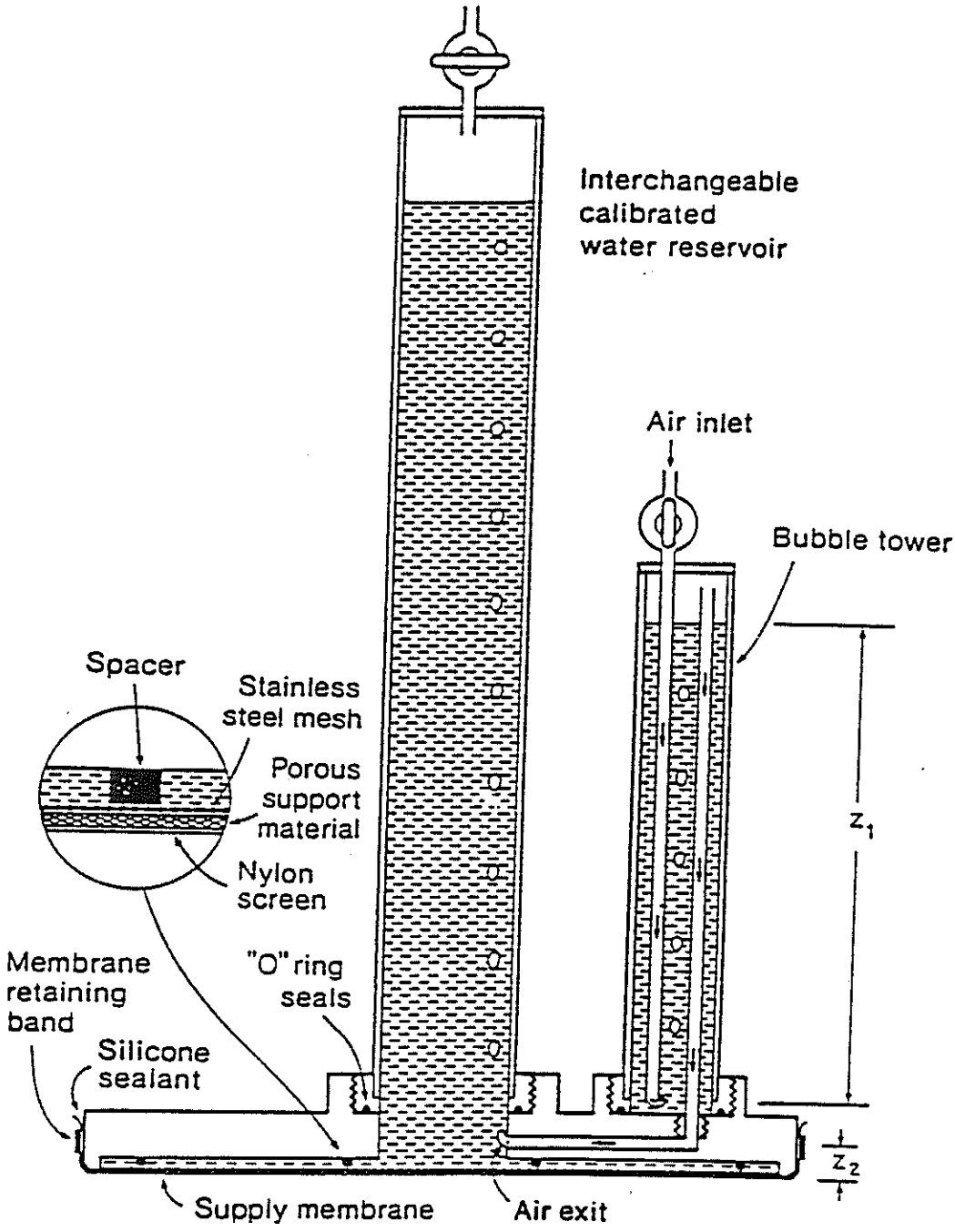

Figure 16. Negative pressure disc permeameter

(CSIRO Instruction Manual 1988)

1) Wet the stopcock to ensure it does not leak.
2) Check the water level in the bubbling tower for the desired supply pressures.
3) Examine the disc for air bubbles. If present, rewet the disc and evacuate the bubbles. Reexamine and if the bubbles continue, the membrane should be changed.

Measurements commence as soon as bubbling begins in the tower after placing the disc firmly on the contact material. Good contact is imperative for meaningful measurements. Infiltration is recorded with time as quickly as possible during early infiltration times. Measurements of consecutive 0.5 cm changes in water level were effective in this study for sorptivity determinations, although not always possible for highly conductive materials. An automated design such as that of Ankeny et al. (1988) would increase accuracy and decrease the labor. Recordings should continue at a lessening pace until steady state flow is achieved. Constant measurements over a 5-10 minute period are necessary for good results.

Calibration

Each permeameter reservoir is different. Therefore, they must be calibrated. Calculated calibrations for the two reservoirs used are:

Reservoir 1: $dV = 17.48 \times (dX) + 2.24$

Reservoir 2: $dV = 17.31 \times (dX) - 0.352$

dV is the volume of water infiltrated for a specified water level drop in the reservoir (mL), dX is the specified drop in water level (cm), and 17.48 and 17.31 are areas for each reservoir (cm^2). Assuming essentially pure water at 20 C, cubic centimeters (cm^3) are equivalent to milliliters (mL).

Moisture Contents

Prior to the infiltration measurement, a soil sample (approximately 100-150 g) is collected from the top centimeter of soil near the measurement location for initial moisture content determination. Samples should be collected within 10 to 15 cm of the permeameter. At the end of infiltration a final moisture content sample is taken from the top few millimeters of soil and placed in an airtight container for weighing. For positive supply measurements, sampling for moisture content is conducted as soon as the free water infiltrates the soil surface after removing the permeameter from the ring. Under tension

conditions, the cap is quickly scraped from the soil surface, and a sample of soil beneath the cap is taken.

In both cases, samples taken too late or too deep will give incorrect, low values of the change in moisture content from the infiltration event. This is quite frustrating inasmuch as the calculated conductivity is highly dependent on the change in moisture content. Final moisture content samples were also analyzed in the laboratory to determine particle size distributions.

CHARACTERIZATION OF SOLUTE FLOW PATHS

Spatial characterization of vadose zone parameters such as unsaturated hydraulic conductivity was discussed above. The qualitative estimation of fluid pathways is also vital in flow field analysis. Several studies were conducted involving application of dyes to an irrigated or ponded field site and subsequent excavation of their trace in the soil in order to provide a visual determination of fluid behavior in the substrata. Ghodrati and Jury (1990) applied Acid-Red 1 (water-soluble, anionic) dye and Dispersed-Orange 3 dye in solution to eight 1.5 X 1.5 m plots (all loamy sand to gravely sand), some of which had disturbed top layers. Four plots were irrigated by sprinkler while the others were ponded. Albrecht, et al. (1989) applied water containing two fluorescent dyes to a small 3 X 9 X 0.9 m compacted earthen liner to examine preferential patterns of water movement through the material. Omoti and Wild (1979) also used fluorescent dyes as solute markers. They wished to determine reasons behind asymmetric leaching of nitrate and chloride in the soil profile.

To characterize the flow field in terms of actual pathways taken by the infiltrating water, a similar qualitative analysis was undertaken at the site. Prior to the drainage phase of the field experiment, blue dye solution was injected over a 4-day period via the irrigation system. A blue food coloring (FD&C no. 1) was used as it dissolved readily in water forming a solution which significantly stained the soil in uniformly packed soil columns. A syringe pump fed the solution into the southern portion of the "main" line every 15 minutes (water pump activation period). A steady quantity of dyed water was applied to the soil through driplines 1-5. During the fifth day, the last day of plot irrigation, the remaining solution was dumped into the water tank and injected into all driplines. Drainage commenced on the sixth day (early September, 1989).

Following intensive drainage monitoring, a series of trenches were completed with a backhoe throughout the 30 X 30 m plot. A shallow (1.5 m deep below site datum) SE-NW trench was excavated in three phases. Initially, the channel was dug from the corners of the 30 X 30 m plot to the corners of the irrigated plot during the latter stages of drainage. The second phase brought the trench to the edges of the wooden trench containing the main water line. Finally, the trench became continuous along a SE-NW transect upon removal of the wooden trench. A second trench near Station 12-12 was constructed mid-summer 1990 and provided a study of instrument performance as suggested by dyed pathways in the vicinity.

The first dye study area was located in the southeast corner of the irrigated plot (fig. 17). This 2.5 X 4.0 m region encompassed portions of six driplines. This area is expanded in fig. 18. Eight cross-sections or "cuts" are displayed. Each cut contains one or more "sections" which were cleaned of backhoe marks, brushed, drafted (noting dye paths and geology) and in some cases photographed. Once again, the emitter locations are included as the extent of dye movement (the stippled pattern in the cross-sections) can be explained by emitter uniformity and proximity.

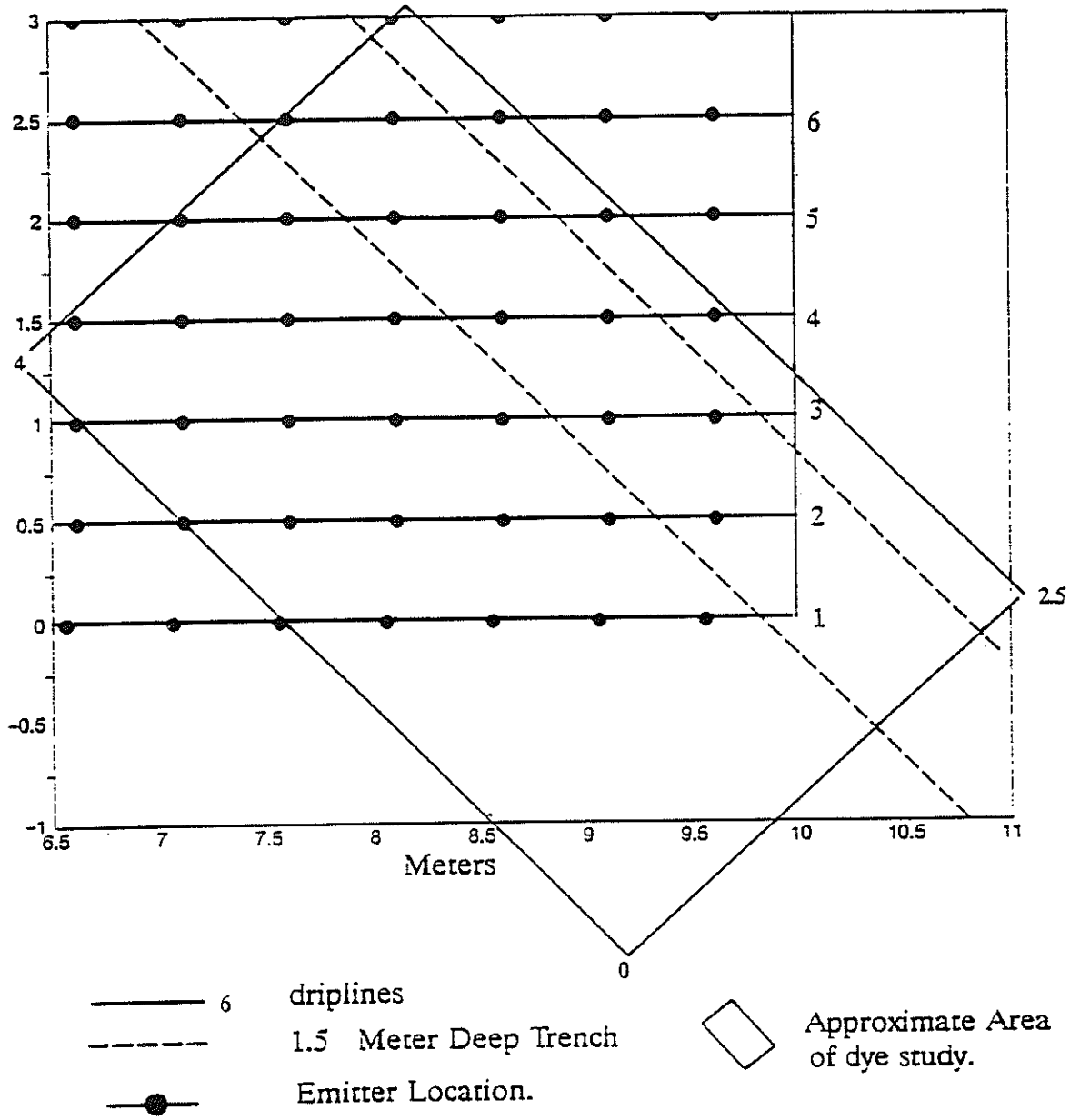

SOUTHEAST CORNER OF IRRIGATED PLOT

(SEE FIGURE FOR DIAGRAM OF 2.5 X 4.0 M STUDY AREA)

Figure 17. Southeast corner of irrigated plot

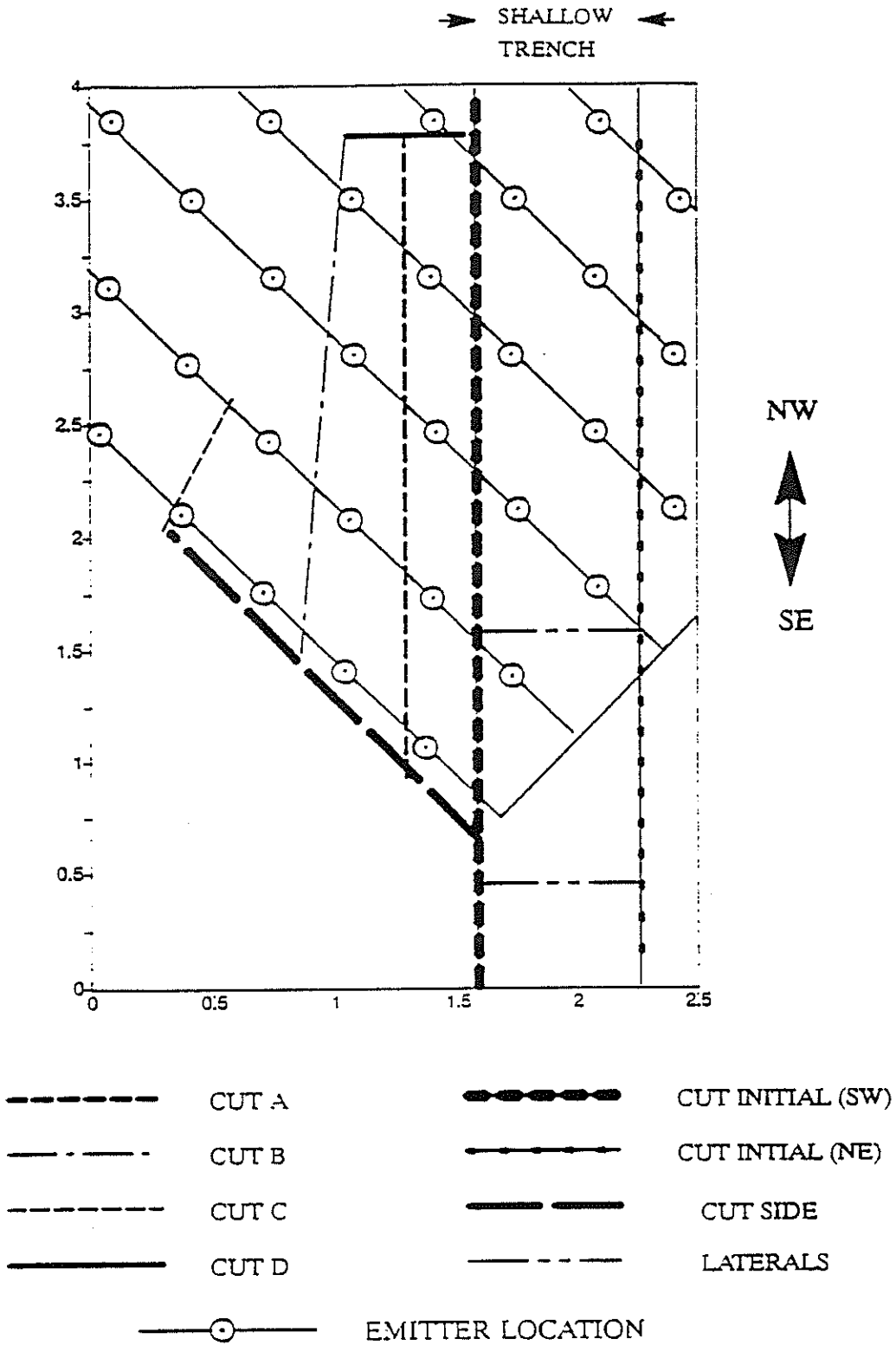

Figure 18. Locations of excavations in dye study area
Both axes in meters

RESULTS AND DISCUSSION

MULTI-TRACER TRANSPORT

Concentration data from the water samples were used to construct breakthrough curves (BTCs) at each sampling location for each tracer. Tracer breakthrough curves were generated by plotting the tracer concentration seen in a soil water sample versus the time at which that sample was drawn. This time was considered to be two hours after vacuum was applied to the sampler. The solution samples were assumed to yield flux concentrations.

Problem Solution Samplers

Piping of dye down the instrumentation was seen only at sampler la. It was also noticed that the bentonite seal around the tube had pulled away from the PVC and that there were large voids in the silica flour around the porous cup. The silica flour around samplers 5a and 5c was intact and the bentonite seemed to make a good seal.

Breakthrough curves were plotted for sampler la and the two samplers directly beneath it. The BTCs of sampler la and lb were distinctly different from most of the other BTCs that were plotted. The tracer flowed very quickly to sampler la, far less quickly to sampler lb. The mass recovered from sampler lb was also much less than that recovered from either sampler la or lc. It is hypothesized that the quick movement of tracer to sampler la was due to piping down the side of the tube and that the diminished mass seen in sampler lb was due to the direct extraction of the tracer directly above it. Figure 19 shows the breakthrough curves of bromide for samplers la, lb, and lc. For the reasons cited above, samplers la and lb will not be used in modelling the tracer movement at the site.

The tracer breakthrough curve of sampler D29 also showed extraordinarily fast tracer movement, faster even than sampler la. This sampler, used in a previous tracer experiment, had been removed once, because of clogging of the porous cup, and then replaced. The sampler tube extended above ground surface, so it was possible to observe the seal between the soil and the sampler. It appeared that the sampler was not in sound contact with the soil as the sampler could be wiggled in its hole. For these reasons, this sampler was not used in modelling the tracer movement either. Figure 20 shows the breakthrough curve for sampler D29. Samplers 3a, llb, and 2Oc would not hold a suction so no soil water samples could be

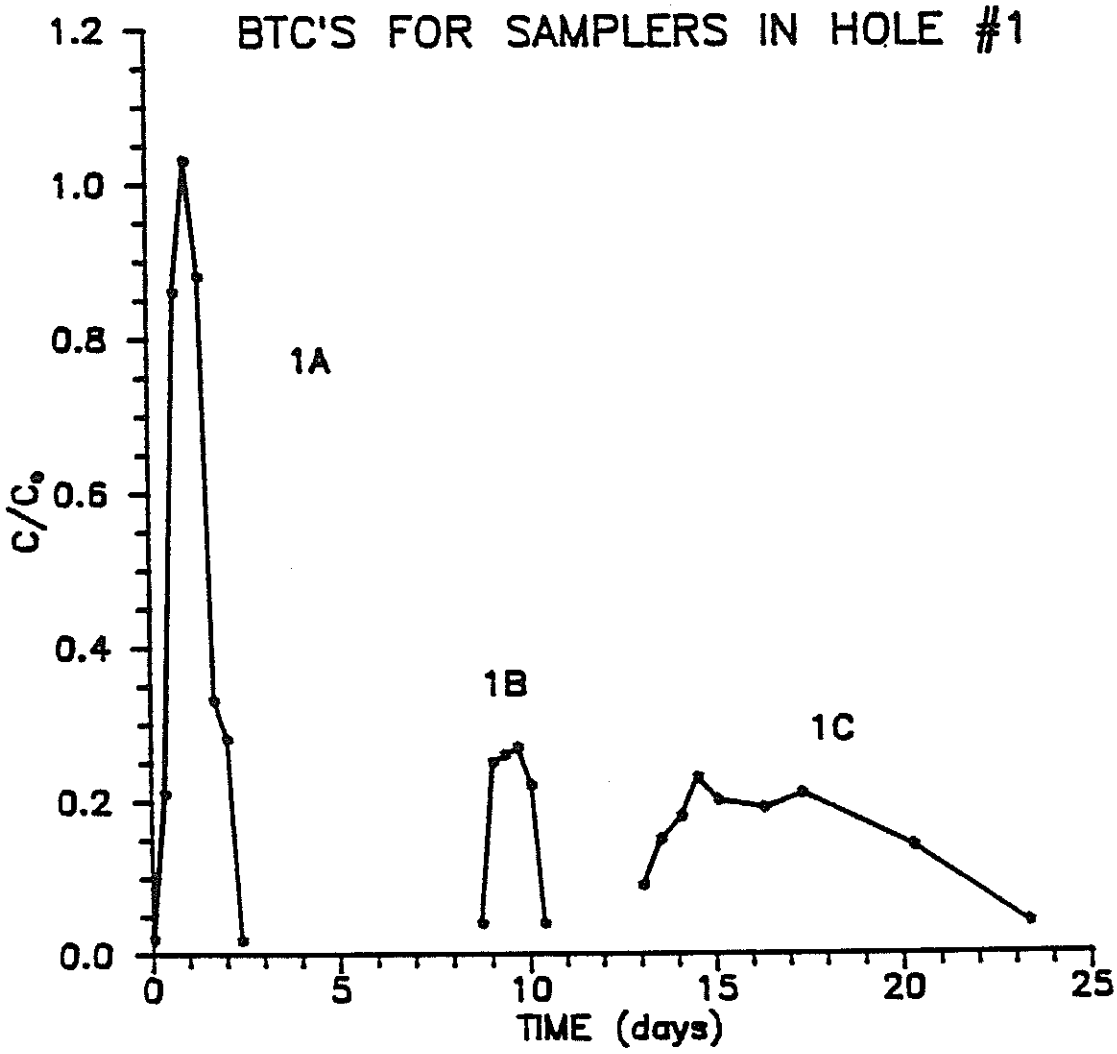

Figure 19. Bromide breakthrough curves for samplers 1a, 1b, and 1c.

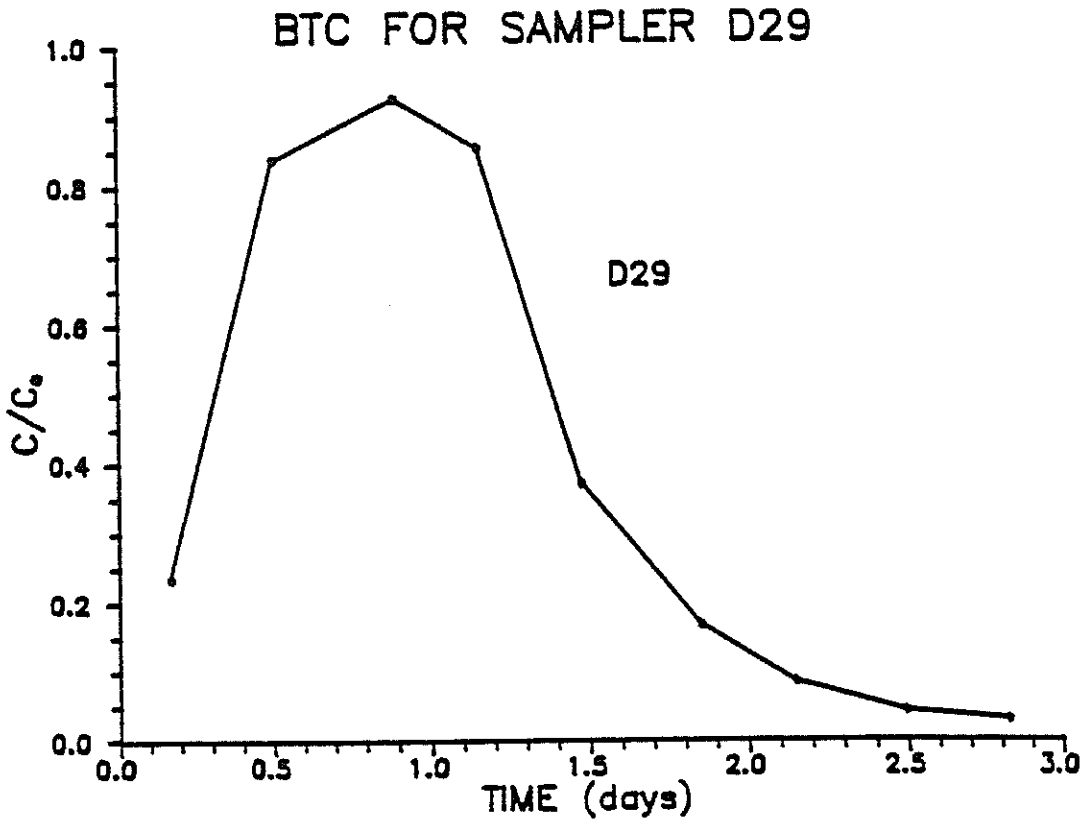

Figure 20. Bromide breakthrough curve for sampler D29.

taken from them. Soil water samples were taken from samplers 2a and 6c, but no tracer was detected in either of them. This could be explained by tracer movement around the sampler drawn, but not close enough to be pulled into it. It was also possible that much of the water pulled into the sampler was not removed during the extraction process. This could have happened if there were a hole in the extraction line well above the porous cup. The water that remained in the sampler would dilute the water that was pulled in the subsequent soil water extraction, possibly to the point of diluting it below detection limits. These samplers, like the ones mentioned above, have been disregarded for modelling purposes.

Determination of Transport Parameters From Breakthrough Curves

Soil water samples were used to determine the movement of tracer through the unsaturated zone beneath the site. Relative concentrations were calculated by dividing the concentration of tracer in a particular sampler by the average concentration seen in three "standards," samples taken from the faucets during tracer application. The deviation of individual "standard" samples from the average concentration was no greater than 20 %. Plots of the standards compared with the average concentration, set equal to 1.0, are shown in fig. 21 along with the residual concentration seen in the drip lines after the tracer application was stopped.

Two methods were used to determine hydrodynamic parameters from the breakthrough curves. The first used was the program CXTFIT of Parker and van Genuchten (1984). This program uses a non-linear least squares method to fit the parameters velocity (v), dispersion coefficient (D), and mass recovered (t_0) to the one-dimensional advection dispersion equation (1-D ADE). Mode 2 of the program, which assumes flux concentrations, was used. Flanigan (1989) suggested that flux concentrations more nearly represent the concentrations seen in porous cup sampling. The retardation factor was set equal to 1.0 as bromide and the fluoro-organic tracers are relatively non-reactive. The retardation factor is quite possibly not one, as anion exclusion of bromide was observed by Flanigan (1989) in repacked columnstudies of material from the site. Relative concentrations were input into the code. These concentrations were calculated by dividing sample concentrations by the average concentration seen in the lines during tracer injection. Table 3 lists the parameters and goodness of fit calculated for the solution samplers.

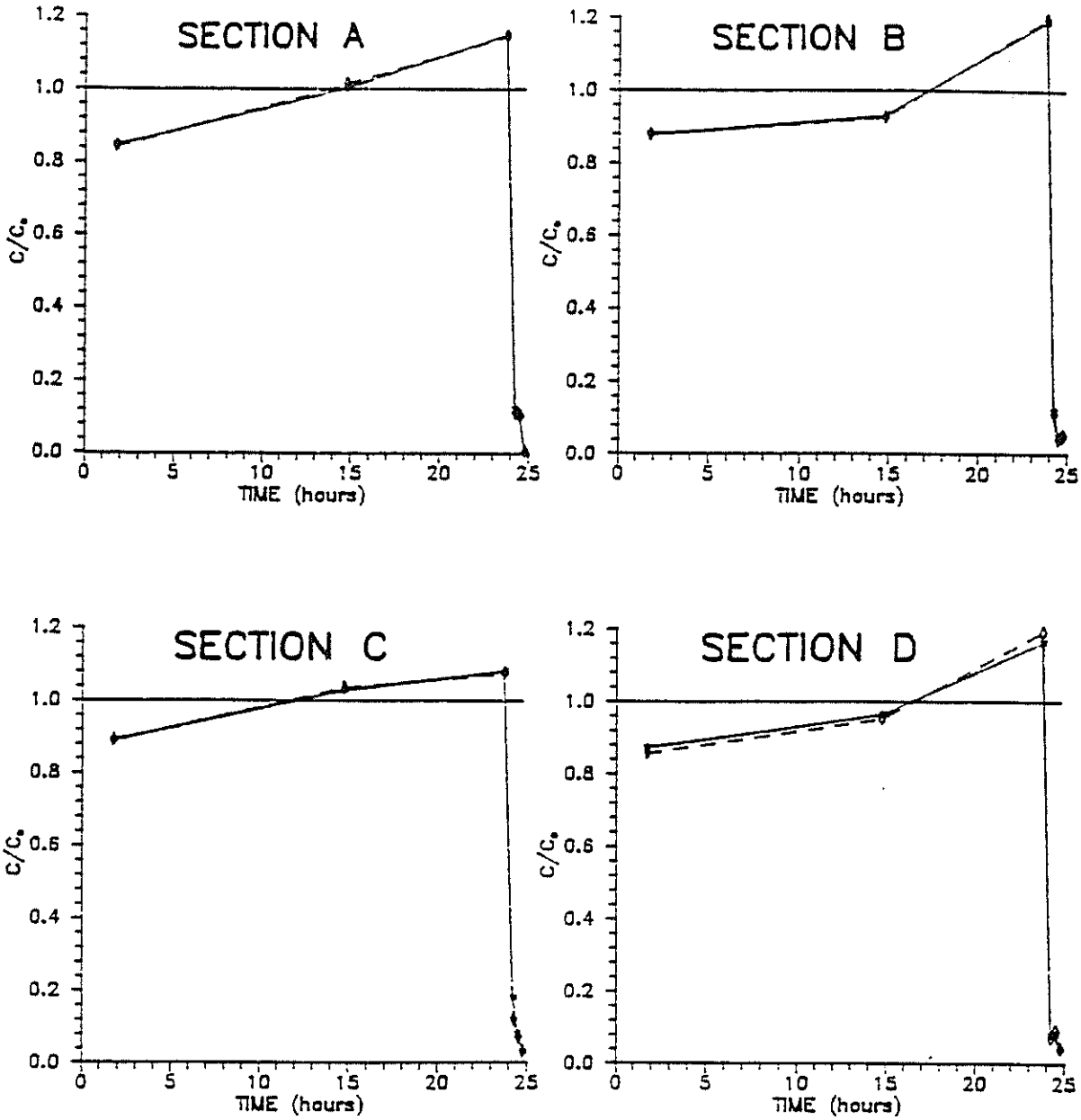

Figure 21. Tracer input concentrations in drip lines (during tracer application) for each section.

The second method applied a moment analysis to the curves. There are two ways in which the concentration vs. time data was considered. The first was as a normal distribution, where the zeroth moment is the mass recovered in a particular sampler; the first moment, divided by the zeroth moment, is the time at which fifty percent of the tracer seen has passed the sampler; and the second moment, also divided by the zeroth moment, defines the spread of the tracer about the center of mass or first moment. The second way to look at the data is as a log-normal distribution of travel times. This is most likely a better description of the curve as it not only confines the data, in that there can be no tracer appearing before it has been injected, but better represents the tailing seen in the BTCs.

It is not clear whether, when applying a moment analysis to the raw data, it is more appropriate to use travel times from the time the tracer was first applied or to use travel times from the time at which half the tracer has been applied. For breakthrough curves showing very fast tracer movement, subtracting half a day from the time at which the tracer was seen leads to some negative times. This makes it impossible to determine the log-normal moments, as one cannot take the logarithm of a negative number. Table 4 lists the normal distribution moments.

Statistics of Transport Parameters

Fractile diagrams of fitted transport parameters v, D, t_0' dispersivity (α) and the observed parameter volume pulled (Vp) are shown in figures 22 through 26. It is seen that a log-normal distribution of velocity, dispersion coefficient one dimensional advection dispersion equation and dispersivity more clearly represents the fitted parameters while normal distributions characterize the mass recovered and volume pulled. Log-normal distributions of velocity, dispersion coefficient and dispersivity were seen in similar studies by Biggar and Nielsen (1976) and Nielsen et. al. (1973). Little correlation can be seen between the parameters. Fractile diagrams of the zeroeth, first and second moments (normal distribution) are illustrated in figures 27 through 29. The zeroeth moment corresponds to the mass recoved T. A plot of the zeroeth moment against the t calculated from CXTFIT is shown in figure 30. It can be seen that the zeroeth moment is larger than that determined from the l-D ADE. This was believed to be because the one-dimensional advection-dispersion equation usually underpredicts the concentration of tracer on the tail of the breakthrough.

Table 3 1-D ADE FITTED PARAMETERS FOR INDIVIDUAL SAMPLER BREAKTHROUGH CURVES.

SAMPLER	v(cm/d)	D(cm^2/d)	α(cm)	t_o(d)	R^2
1c	16.1	98.7	6.1	1.88	.87
2c	7.6	237.1	31.2	2.25	.93
3c	7.8	400.2	51.3	2.37	.86
4a	9.3	28.2	3.0	1.05	.68
4c	21.5	87.2	4.1	0.73	.86
5a	16.7	228.5	13.7	1.16	.96
5c	18.7	227.4	12.2	0.79	.92
6a	7.4	118.8	16.1	1.99	.93
7a	10.3	175.4	17.0	1.52	.90
7c	8.3	153.1	18.4	1.98	.97
8a	23.7	113.0	4.8	0.40	.94
9a	24.6	144.2	5.9	1.04	.99
9c	17.3	309.5	17.9	0.78	.90
10a	18.8	214.9	11.4	0.96	.98
11a	36.1	252.9	7.0	0.36	.88
11c	38.7	192.0	5.0	0.93	1.00
11d	22.5	192.9	8.6	0.72	.97
12a	4.9	148.3	30.3	2.56	.94
12c	12.9	652.4	50.6	1.52	.88

13a	15.0	197.7	13.2	1.23	.88
13c	27.2	189.1	7.0	.89	.88
14a	49.1	383.6	7.8	1.12	.94
14c	36.1	412.7	11.4	0.85	.95
15a	15.1	145.7	9.6	1.04	.87
15c	26.6	669.0	25.2	1.15	.74
16a	46.3	338.3	7.3	0.96	.98
16c	15.0	372.9	24.9	1.26	.83
17a	11.9	82.8	7.0	0.96	.79
17c	21.9	244.3	11.2	1.20	.95
18a	8.2	28.8	3.5	0.76	.94
18c	11.1	169.2	15.4	1.48	.97
19a	8.5	30.1	3.5	0.45	.89
19c	12.8	182.4	14.3	1.51	.86
20a	30.7	247.1	8.0	1.35	.98
20b	45.0	880.6	19.6	1.40	.99
G24	93.3	627.8	6.7	1.07	1.00
H23	48.7	518.1	10.6	1.08	.90
I22	42.6	306.5	7.2	1.04	.98
K25	43.5	673.7	15.5	1.25	.93
AVERAGE	23.9	273.7	13.9	1.21	
STD. DEV.	17.3	198.5	11.1	0.51	

Table 4 PARAMETERS DETERMINED BY MOMENT ANALYSIS

SAMPLER	0^{th} MOM []	1^{st} MOM [DAYS]	2^{nd} MOM [$DAYS^2$]
1c	2.20	14.70	245.6
2c	1.17	21.56	490.9
3c	2.14	29.40	1029.1
4a	0.09	10.92	122.8
4c	0.68	7.11	52.5
5a	1.21	7.01	58.9
5c	1.02	14.21	234.5
6a	1.93	13.43	214.1
7a	1.52	10.37	133.3
7c	2.01	25.79	767.2
8a	0.46	5.74	38.2
9a	1.07	4.79	25.9
9c	0.80	13.67	214.7
10a	1.06	6.37	50.3
11a	0.37	1.04	1.6
11c	0.96	4.31	20.0
11d	0.81	10.83	132.6
12a	1.26	11.18	137.3
12c	1.39	16.53	331.6

13a	1.72	10.96	164.2
13c	1.24	10.33	128.8
14a	1.56	4.50	31.6
14c	0.99	8.01	73.9
15a	1.18	8.55	90.0
15c	1.39	11.15	160.5
16a	1.00	2.81	9.1
16c	1.39	17.64	372.9
17a	2.05	22.27	670.2
17c	1.82	19.67	574.5
18a	0.69	12.33	160.0
18c	1.51	20.32	472.4
19a	0.37	11.30	132.5
19c	1.62	21.86	534.2
20a	1.36	4.00	18.3
20b	1.40	5.09	29.6
G24	1.10	1.76	3.5
H23	1.08	5.34	30.4
I22	1.01	7.78	62.8
K25	1.29	4.56	24.4

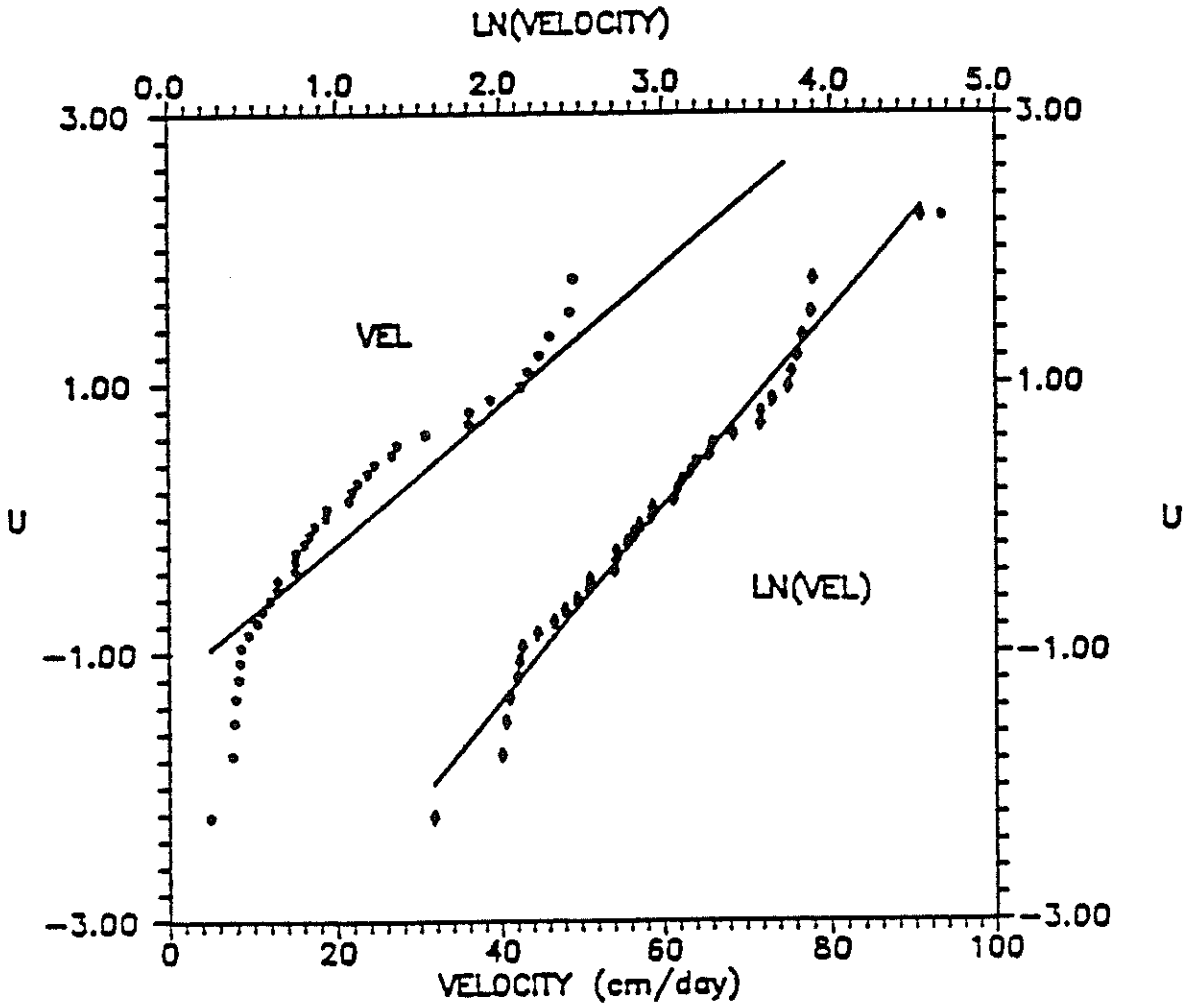

Figure 22. Fractile diagram of velocities determined from one dimensional advection dispersion equation.

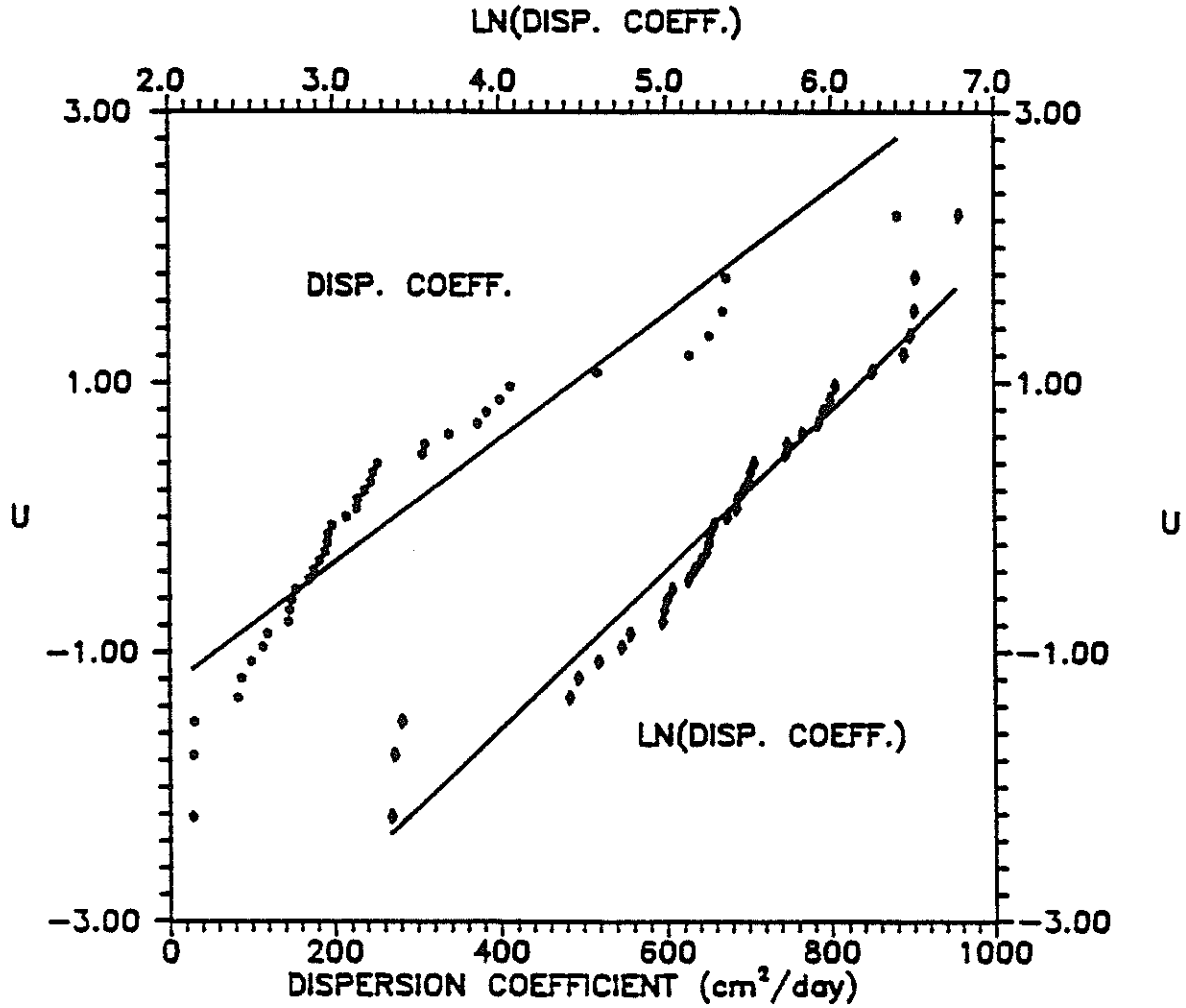

Figure 23. Fractile diagram of dispersion coefficient determined from 1-D ADE.

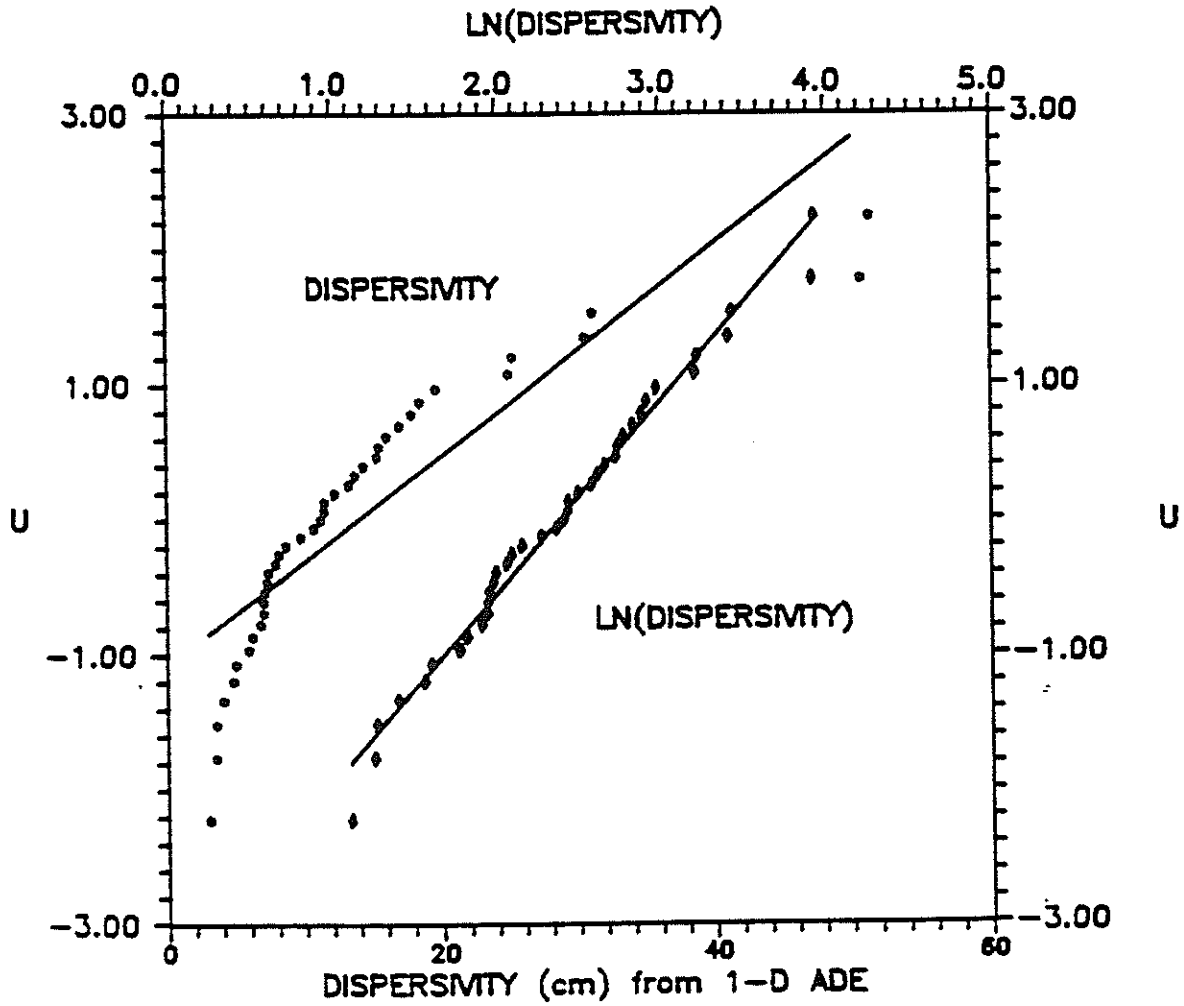

Figure 24. Fractile diagram of dispersivity determined from 1-D ADE.

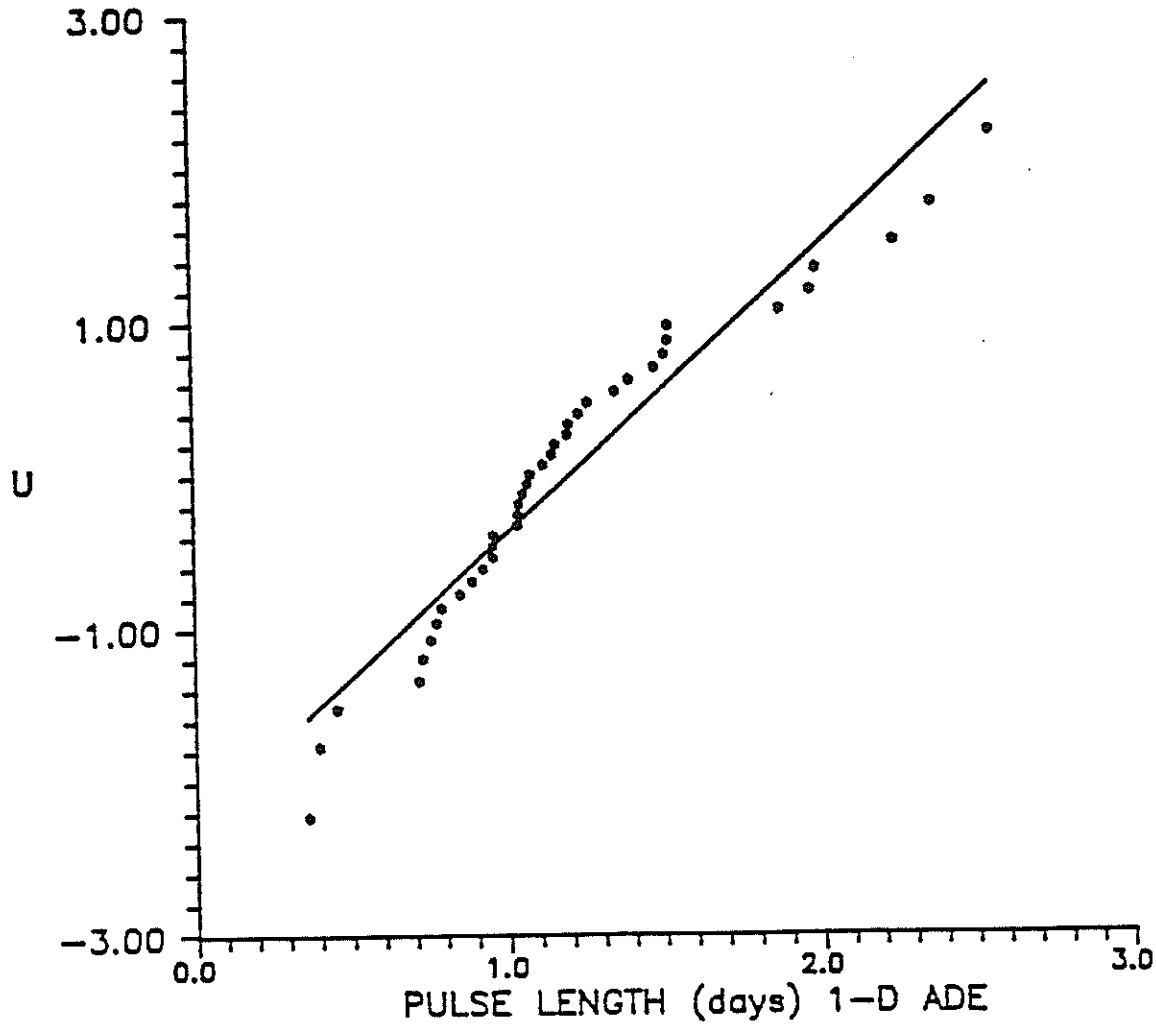

Figure 25. Fractile diagram of pulse duration determined from 1-D ADE.

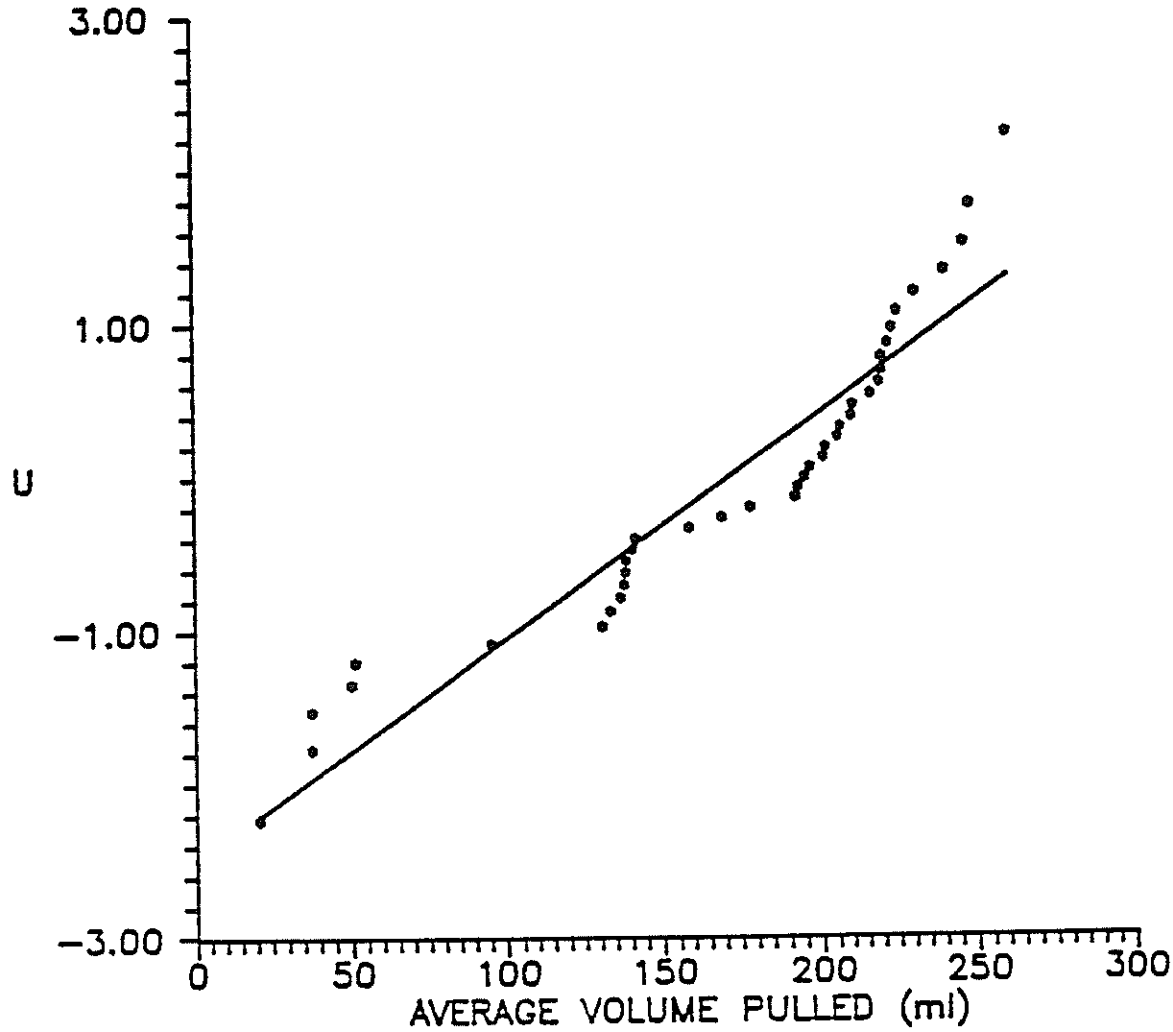

Figure 26. Fractile diagram of average volume pulled per sampler.

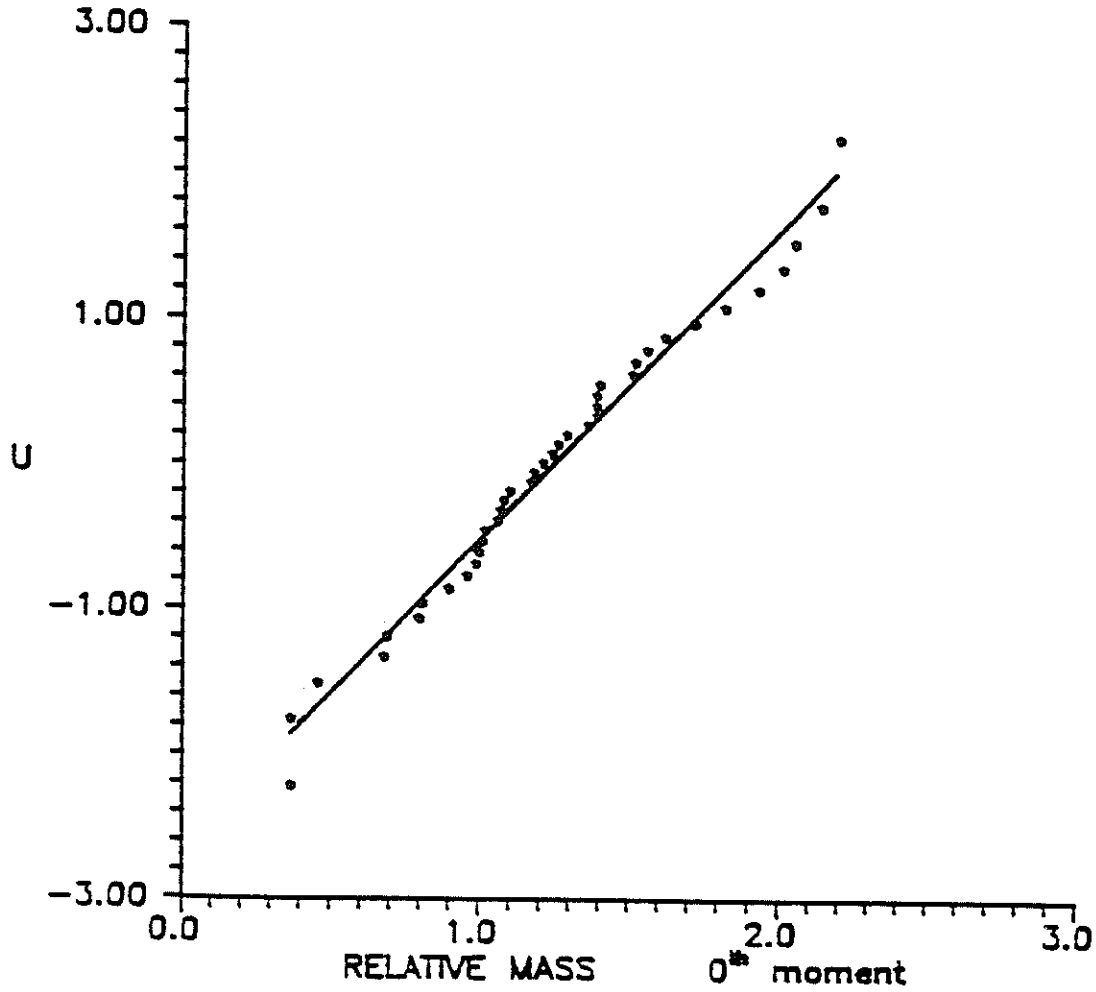

Figure 27. Fractile diagram of relative mass recovered from moment analysis.

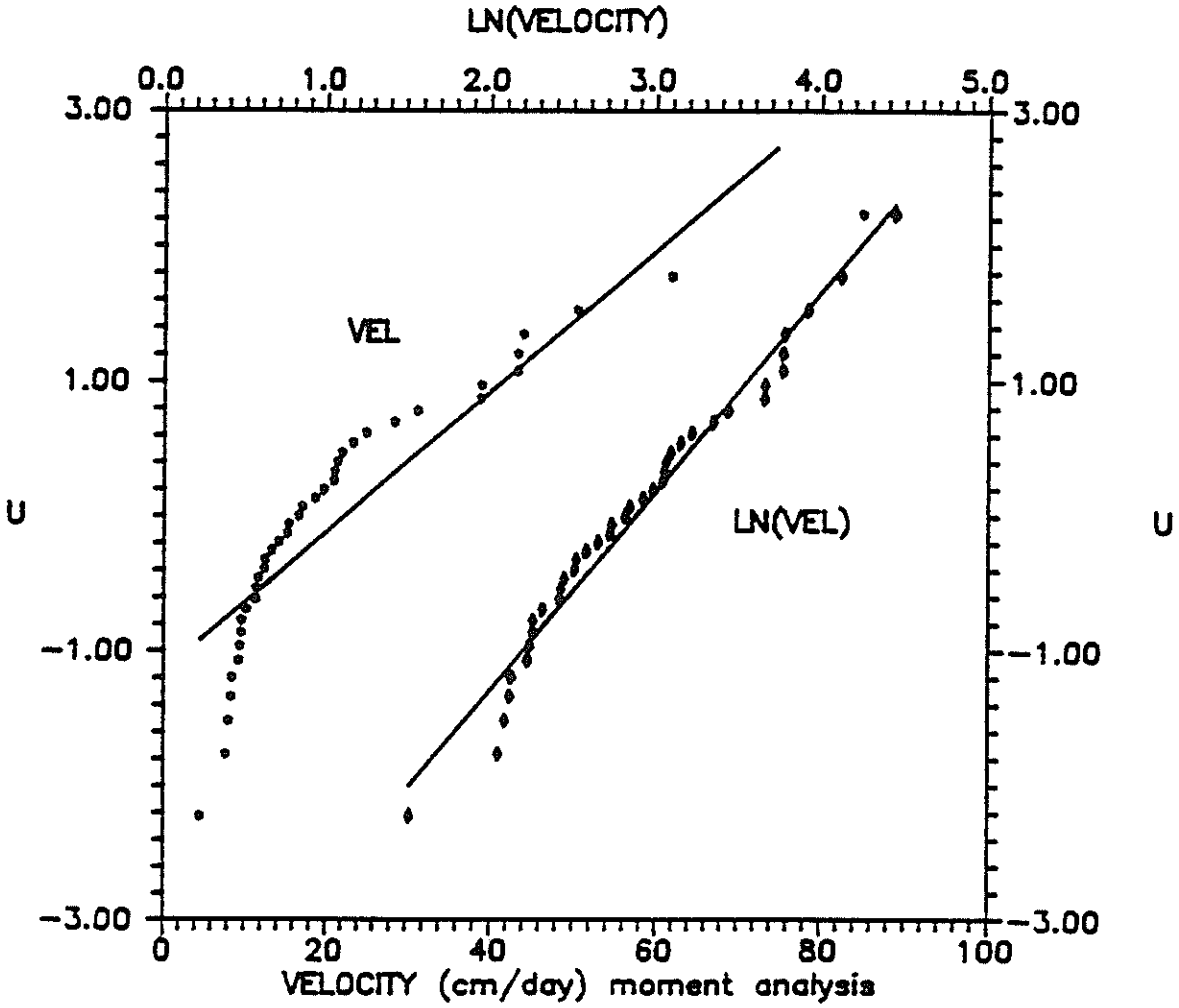

Figure 28. Fractile diagram of velocities calculated from first moments.

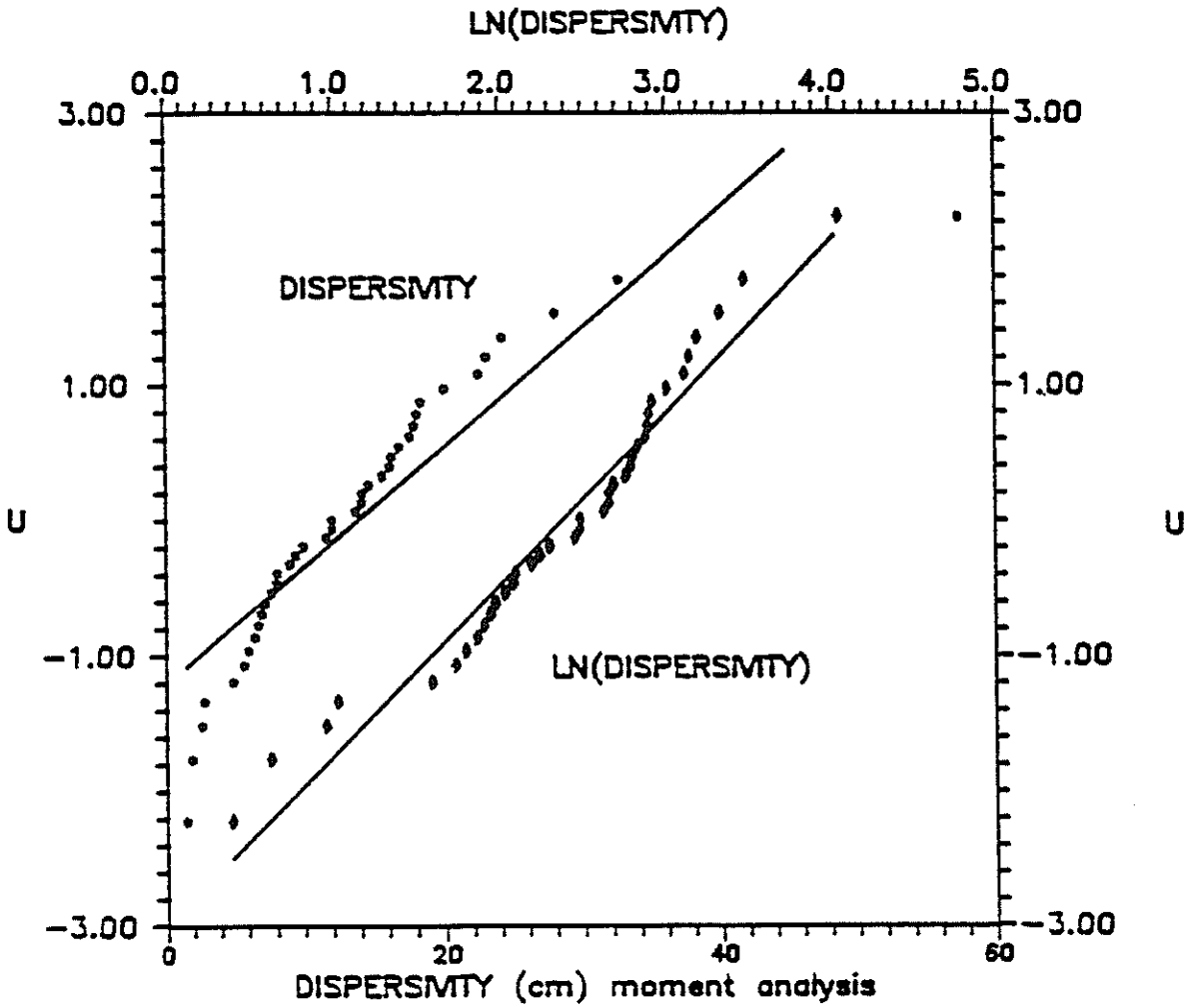

Figure 29. Fractile diagram of dispersivities calculated from first and second moments.

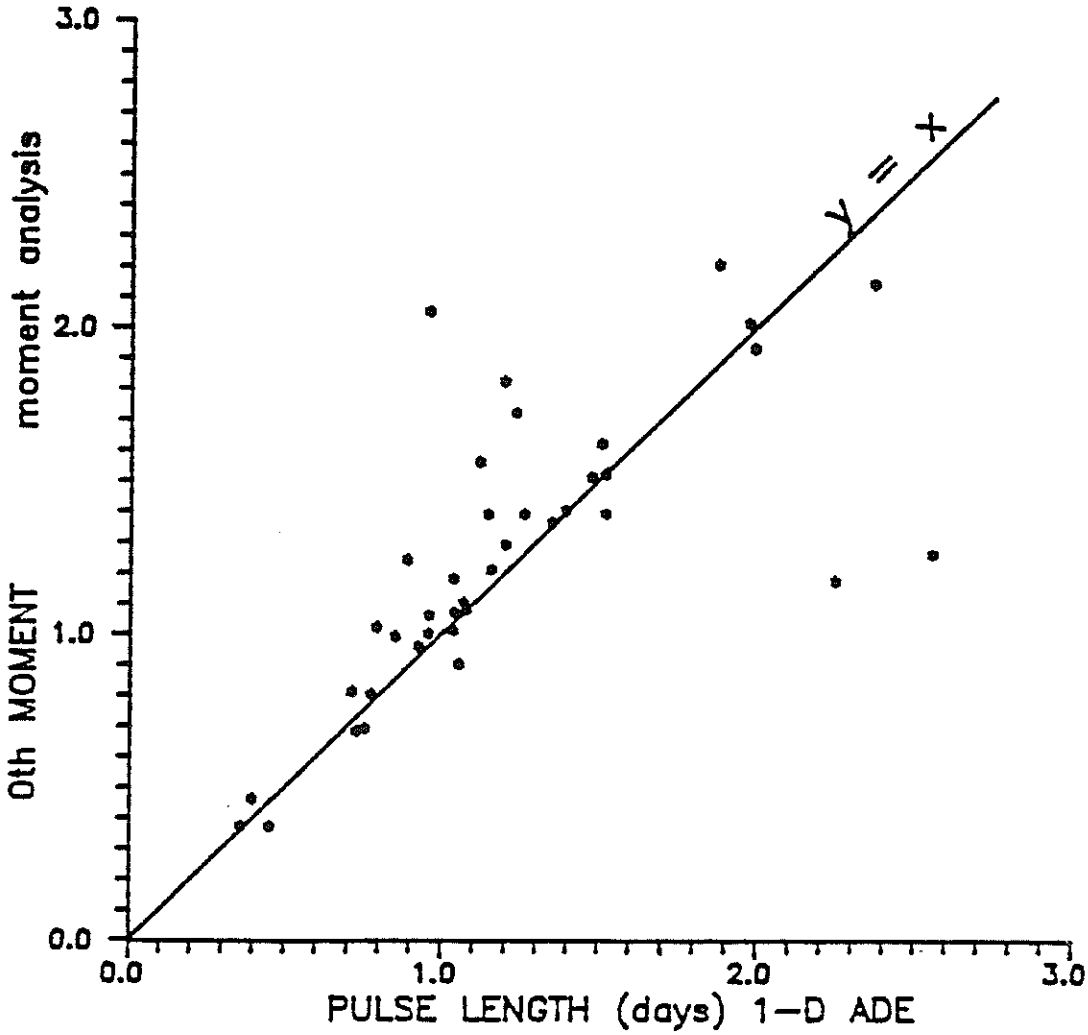

Figure 30. Comparison of pulse duration and mass recovered.

The first moment can be converted into a velocity. Figure 31 plots the velocity calculated from the first moment against the velocity fitted by the one-dimensional advection- dispersion equation. It is seen that neither model consistently predicts larger velocities than the other. It is known that the pulse duration for this experiment was relatively long, but dispersivities were still calculated for each sampler. Figure 32 plots the dispersivities calculated from moments versus those determined from the 1-D ADE. Neither seems to consistently predict higher dispersivities than the other.

Variogram Analysis

In order to look at the correlation between BTCs of samplers at different locations but at approximately the same depth, variograms were taken looking at the parameters' velocity and dispersivity. The parameters were taken from the least-squares analysis of the one-dimensional advection-dispersion equation. Variograms of the parameters at the 1-m depth and the 2.25-m depth (+/-0.15 m) show little correlation between the samplers. This is believed to be because the samplers were emplaced in a grid which placed them at a distance apart greater than the correlation scale of the geology, either vertically or horizontally. Non-ergodic variograms provided a better visual representation of the lack of correlation as it removes trends in the parameter that is being analyzed.

Horizontal Movement of Tracer

Some horizontal movement of the fluoro-organic tracers beneath the drip emitters was observed as evidenced by two different fluorobenzoate tracers appearing in samplers along with bromide. The addition of the relative concentrations of the organic tracers yielded a very close approximation to the relative bromide concentration, suggesting that the fluorobenzoate tracers were conserved. Samplers 6a, 17c, and 18c showed evidence of lateral spreading of solute. Figures 33 through 35 illustrate the breakthrough curves of the fluorobenzoate tracers, bromide and the addition of the two fluorobenzoate tracers. From the figures it is seen that the curve made from the addition of the two organic tracers approximately follows the bromide curve.

In all three cases, tracer moved northward, from a section to the south of the soil water sampler, to the sampler located in an adjacent northern section. Movement of tracer in the other direction was never observed, leading the author to believe that in general, there is a

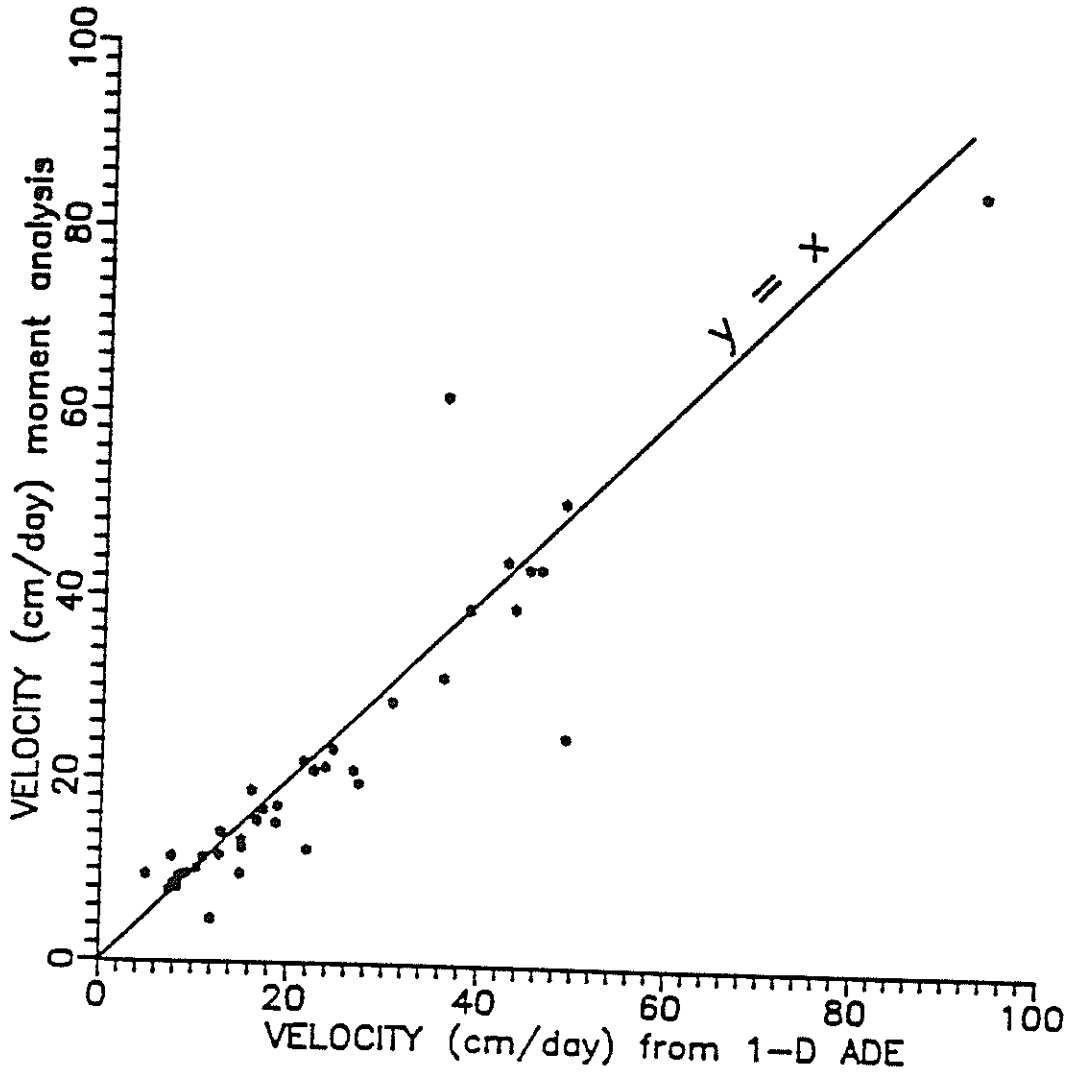

Figure 31. Comparison of velocities determined from 1-D ADE and from moment analysis.

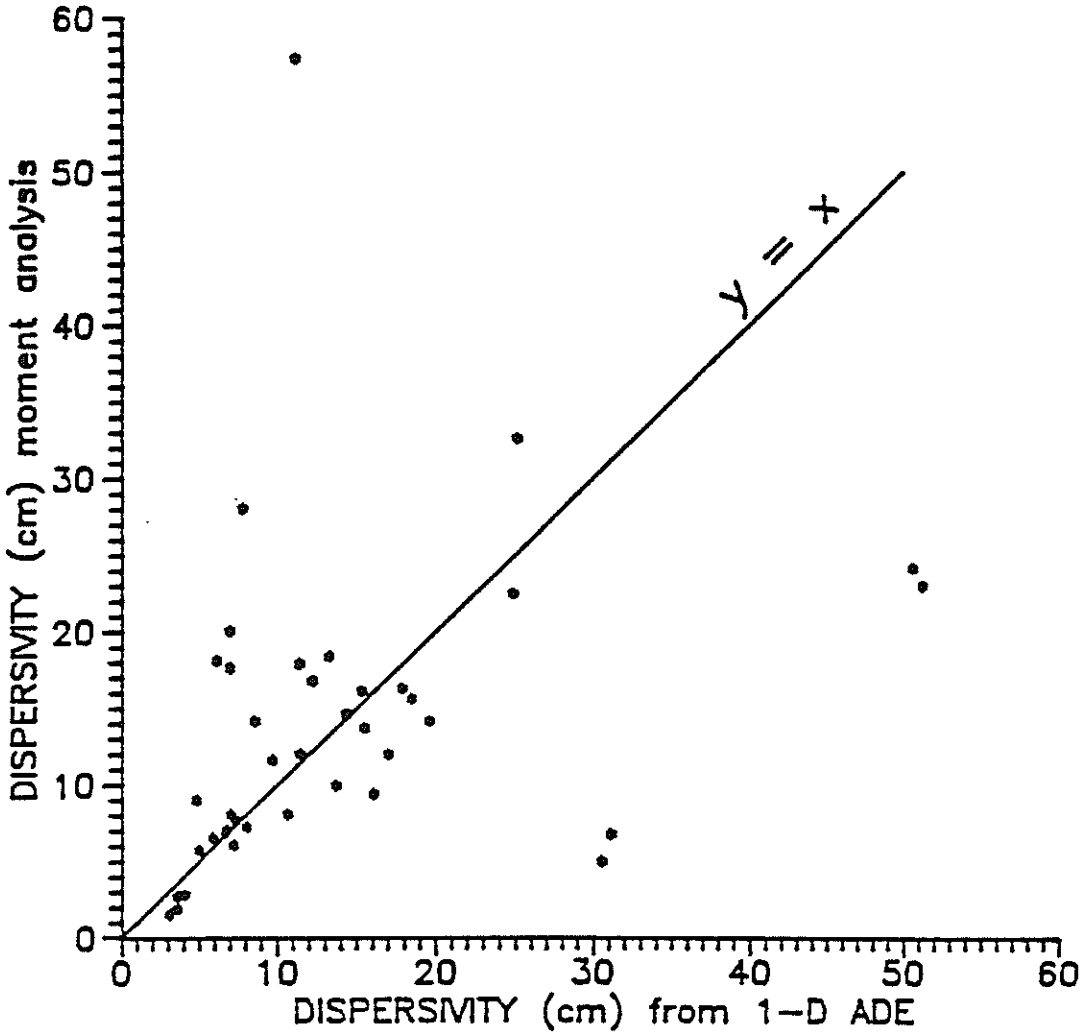

Figure 32. Comparison of dispersivities determined from 1-D ADE and from moment analysis.

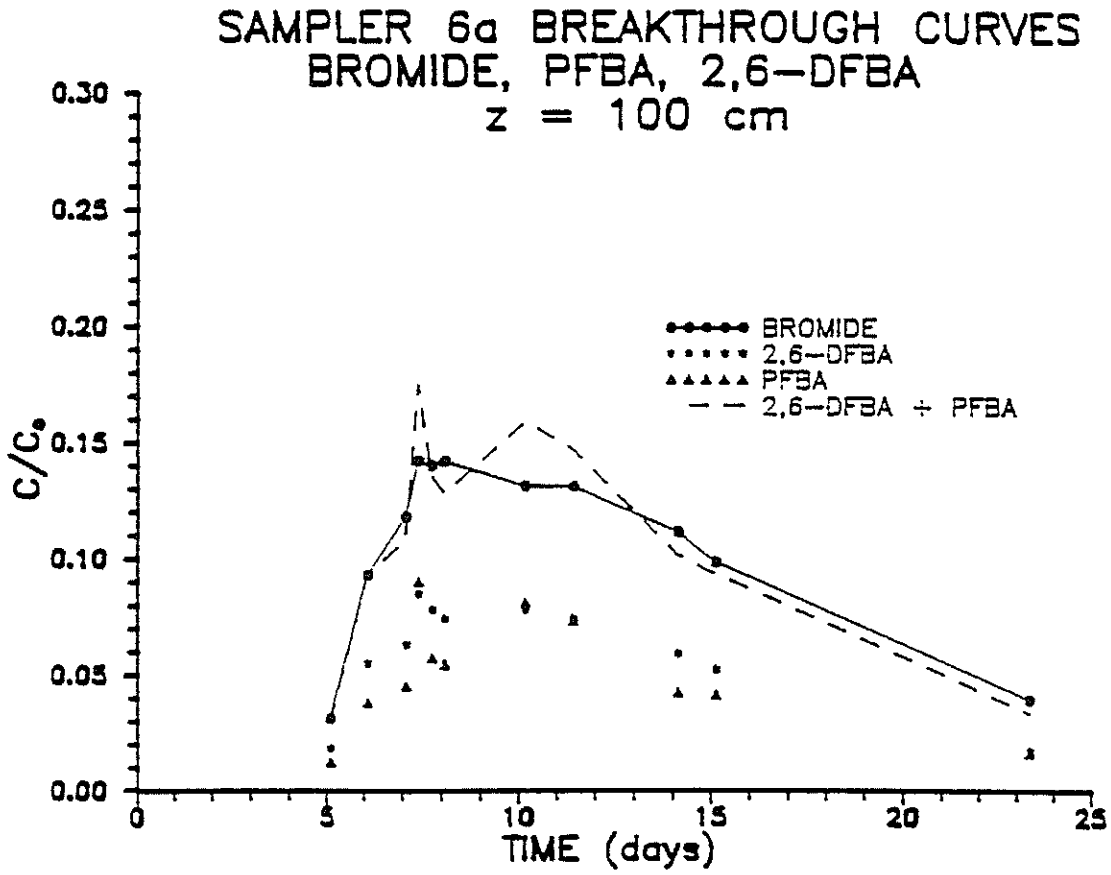

Figure 33. Sampler 6a breakthrough curve.

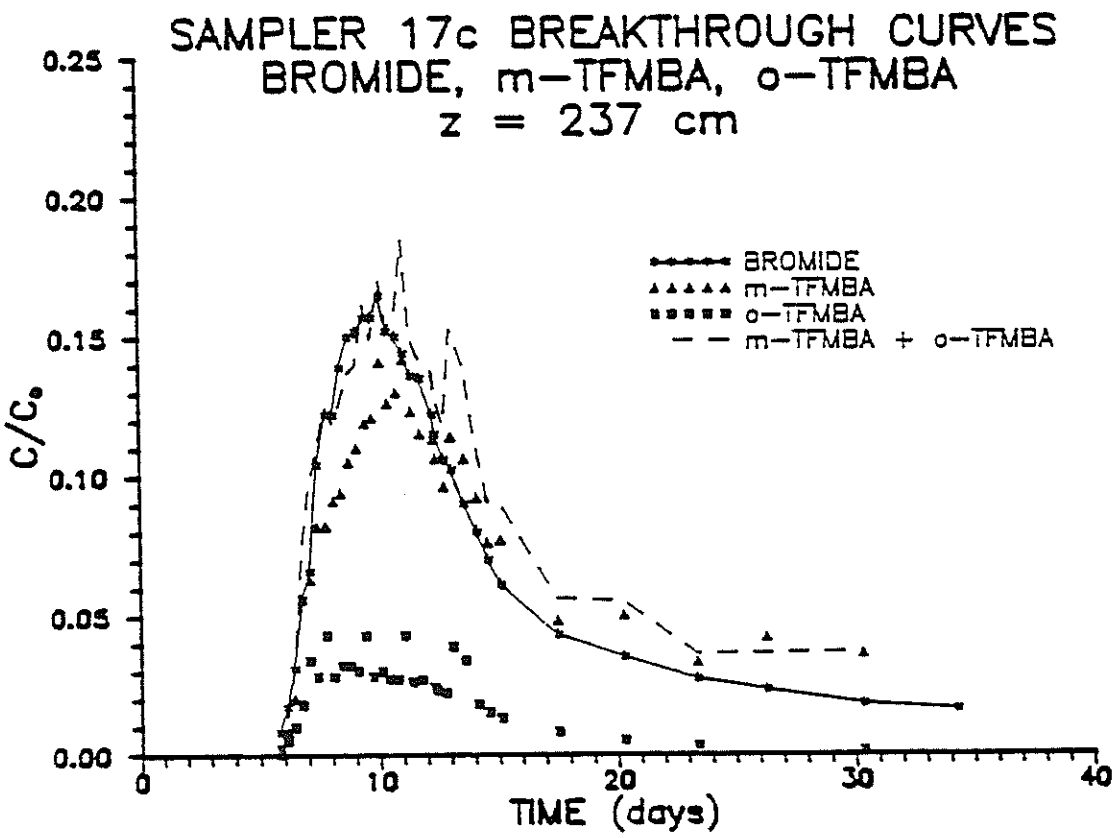

Figure 34. Sampler 17c breakthrough curve.

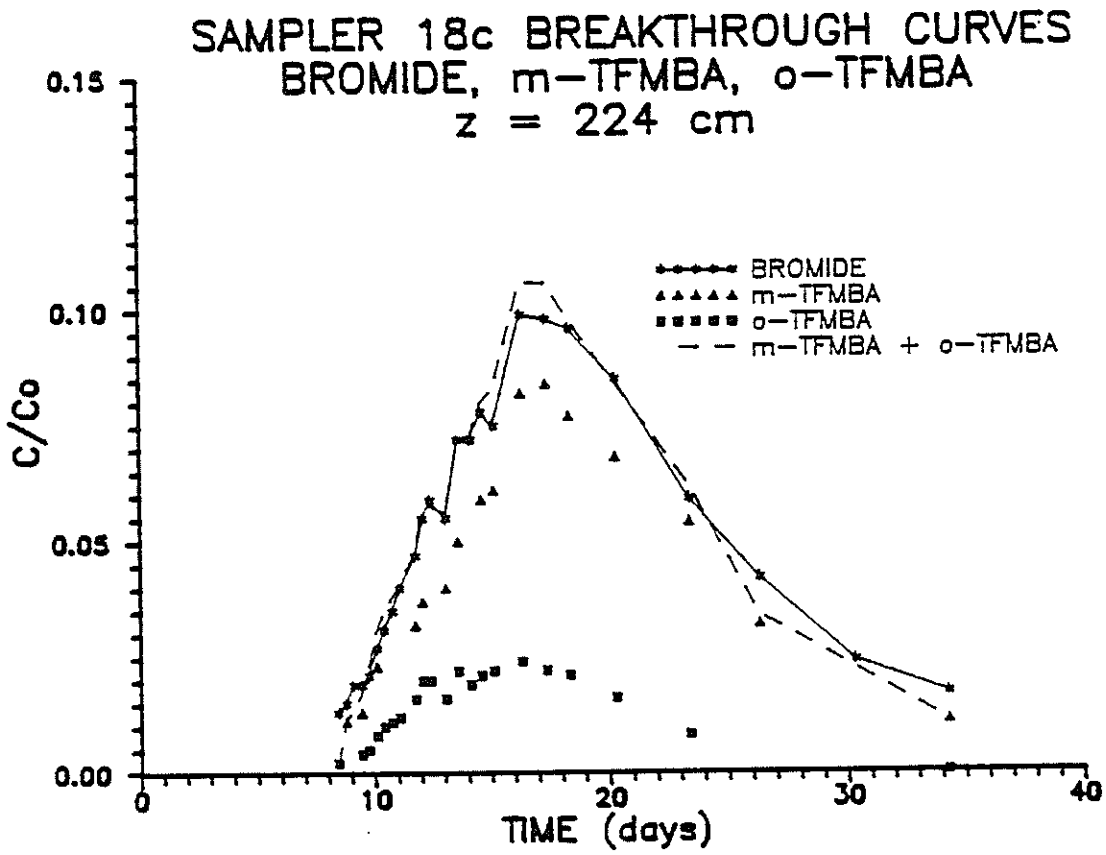

Figure 35. Sampler 18c breakthrough curve.

northward component to flow beneath the wetted region. Horizontal movement of tracer away from the wetted region was also observed. Breakthrough curves were made for outside samplers ENE-a, ENE-b, ENE-c and MEC. These BTCs suggest a significant eastward component to the flow away from the emitters and possibly suggest a slightly northward component to the flow. Figures 36 and 37 show the analyzed relative sampler concentrations vs. time methods of aerially averaging concentration.

Three methods of aerially averaging concentration at a given depth were studied: 1) average resident concentration (ARC); 2) average flux weighted concentration AFWC); and 3) concentration determined from averaging transport parameters from fitted breakthrough curves (ATPC). To the author's knowledge, it has not been convincingly proven which of the three methods apply in a heterogeneous system with three-dimensional fluid flow occurring. Two particular depths were chosen because they were considered sufficient samplers at approximately those depths to get a meaningful average. Seventeen samplers were chosen from approximately the one-meter depth and sixteen samplers from a depth of 2.25 meters, plus or minus .15 meters.

Because water samples were taken at different times from the porous cup samplers and concentration data were not determined at all times, a method was needed to determine the concentration at each sampler at given times. The method used was to input the parameters determined from CXTFIT back into the one-dimensional advection-dispersion equation and thus calculate an idealized concentration for each sampler at various fixed times. These concentrations were then averaged using the three methods discussed earlier.

The ARC breakthrough curve for a particular depth was created by adding the concentrations of all the samplers at that depth at particular times and then dividing this number by the number of samplers observed. This gives the average concentration breakthrough curve at a particular depth, but does not necessarily denote the mass passing through the plane at that depth, because it does not take into account that the water flux is not constant at every point in the plane. If the flux is a constant over the plane, then only variations in the moisture content should determine velocity variations.

The AFWC breakthrough curve for a particular depth was created in a similar manner, but variations in the water flux through the plane were used to weight the concentrations of

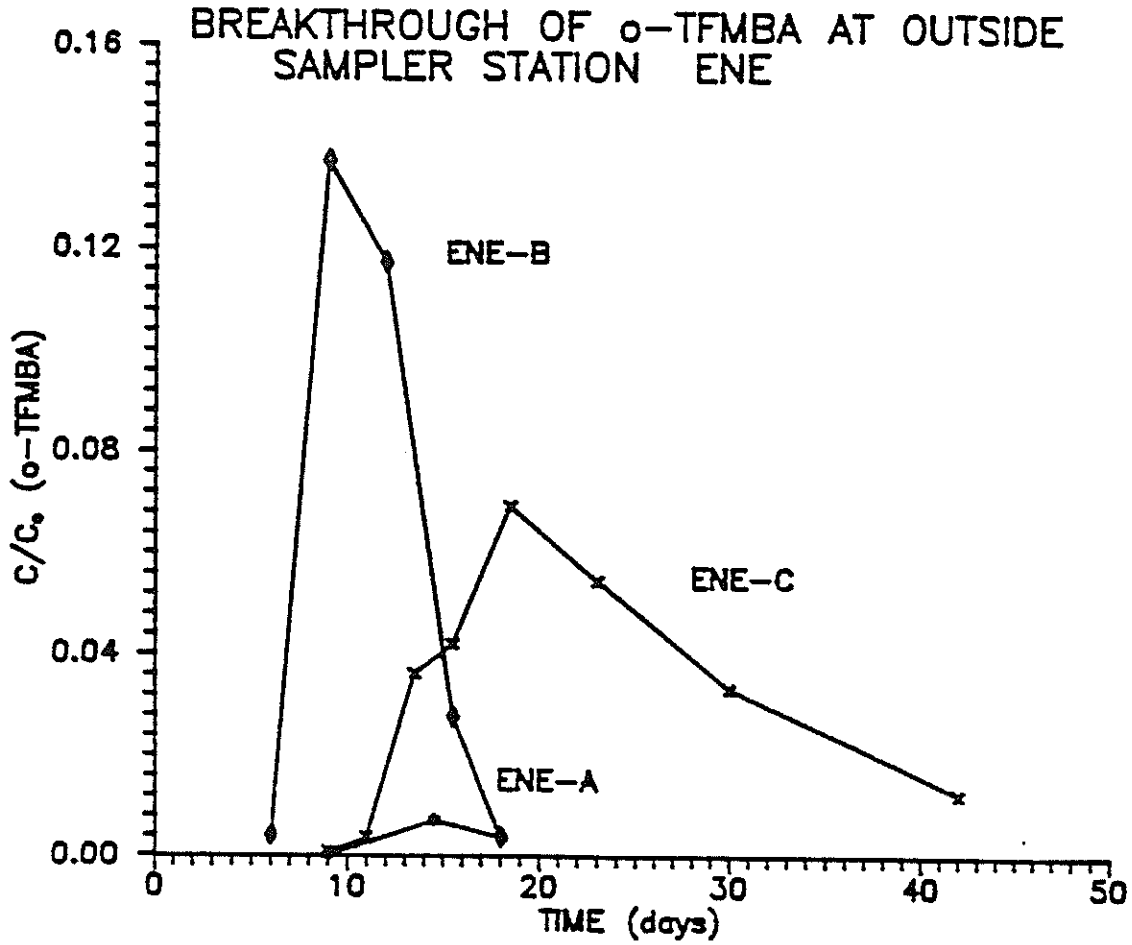

Figure 36. Concentration of tracers seen in samplers ENE-a, ENE-b, and ENE-c.

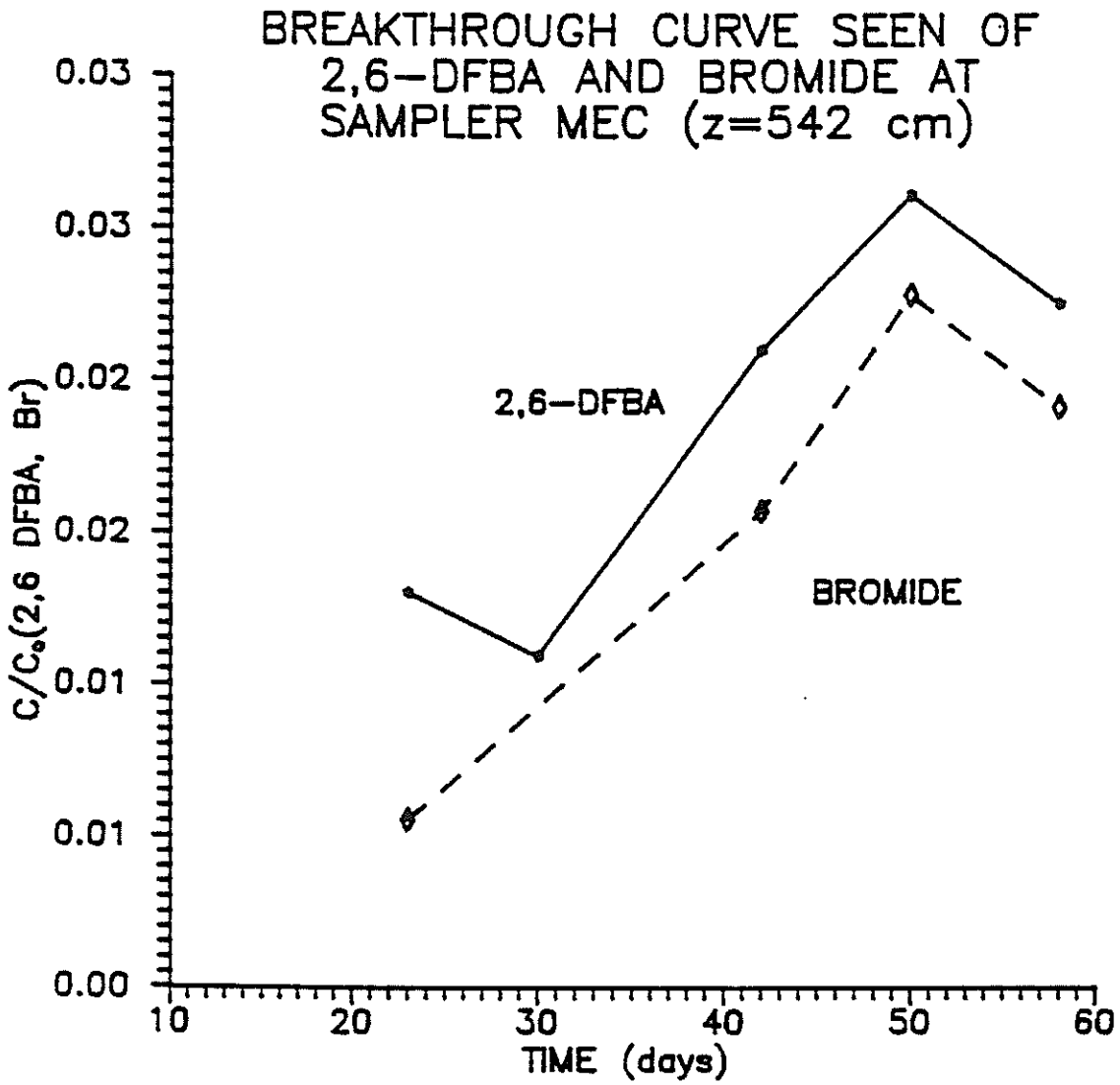

Figure 37. Concentration of tracer seen in sampler MEC.

particular samplers. The flux values were calculated by multiplying the fitted velocity calculated from the 1-D ADE by the average moisture content to that depth determined from neutron moisture measurements. Little variation was seen in the moisture content at a particular depth, so the average used was taken from all the neutron moisture measurements at the given depth. The flux values were multiplied by the concentrations seen in that sampler. This provided qC values at various times for all the soil solution samplers. The qC values for a given time were added together and were then divided by the sum of the flux values. This provided flux weighted concentrations at various times which were used to construct a AFWC BTC. The effect of weighting the concentration by the flux is to make the breakthrough curve peak earlier, because samplers showing fast movement of tracer will necessarily have higher fluxes and will gain greater weight. This method is thought by the authors to better represent the mass of tracer passing through a horizontal plane than that of the average resident concentration.

The concentrations from averaging transport parameters (ATPC) were calculated by first finding the average of the parameters v, D, and t. for a given depth. These average values were then plugged into the 1-D ADE to provide breakthrough curves for the two depths. The ATPC BTCs gave a later breakthrough of tracer than the AFWC but earlier than the ATC. It also removed much of the tailing seen in the BTCs calculated by the other methods. Figure 38 shows the breakthrough curves calculated by all three methods for the 1-m depth and fig. 39 illustrates the curves for the 2.25-m depth. The hydrodynamic parameters v, D, Q, and t_0 were calculated from the curves generated by these averaging techniques using CXTFIT, with Q calculated by dividing D by v. Table 5 lists these values. Using average resident concentrations predicts lower solute velocities, while the other two methods predict similar, higher velocities. From ARC data, there is a large increase in velocity with depth. The other averaging methods have velocity decreasing slightly with depth. Also, averaging transport parameters (ATPC) gives much lower dispersion coefficients than the other methods. This leads to ATPC curves predicting the lowest dispersivity and ARC curves predicting the highest dispersivity. Several authors have suggested that dispersivity increases with depth. The dispersivities calculated from ARC and AFWC curves decreased with depth, while the ATPC curve has it increasing with depth.

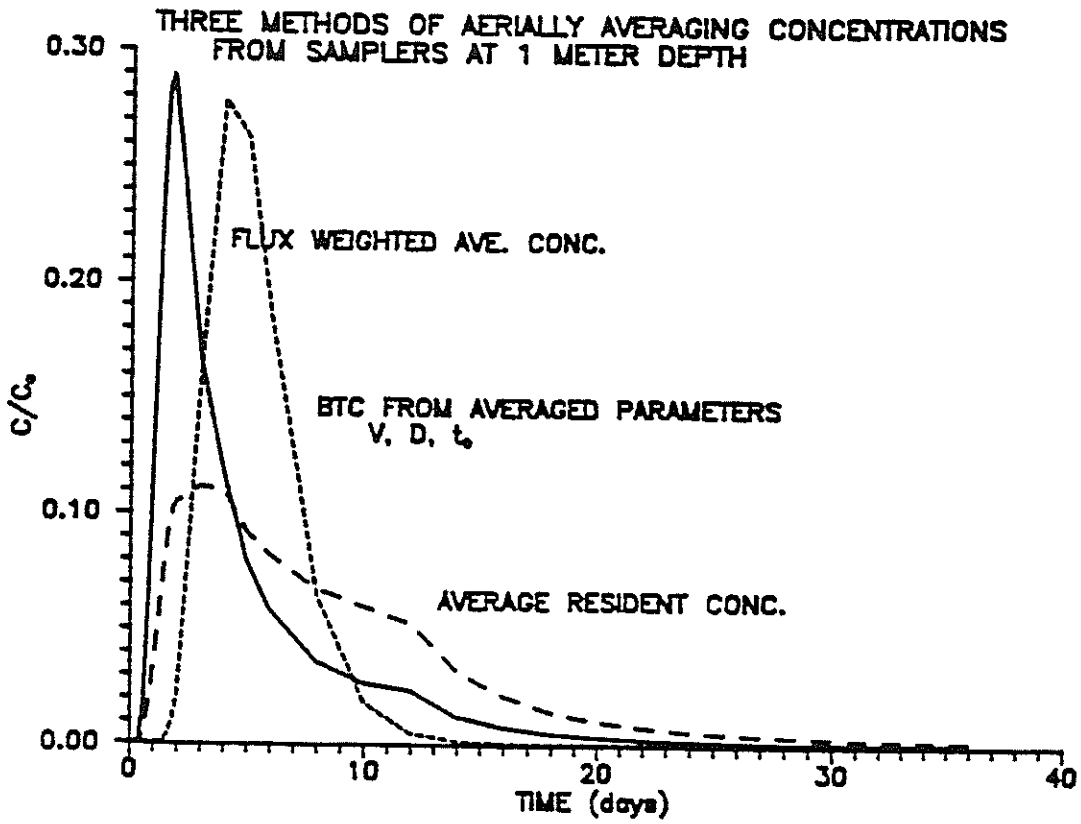

Figure 38. Breakthrough curves from three methods of aerially averaging concentration (ARC, AFWC, and ATPC) for samplers at one meter depth.

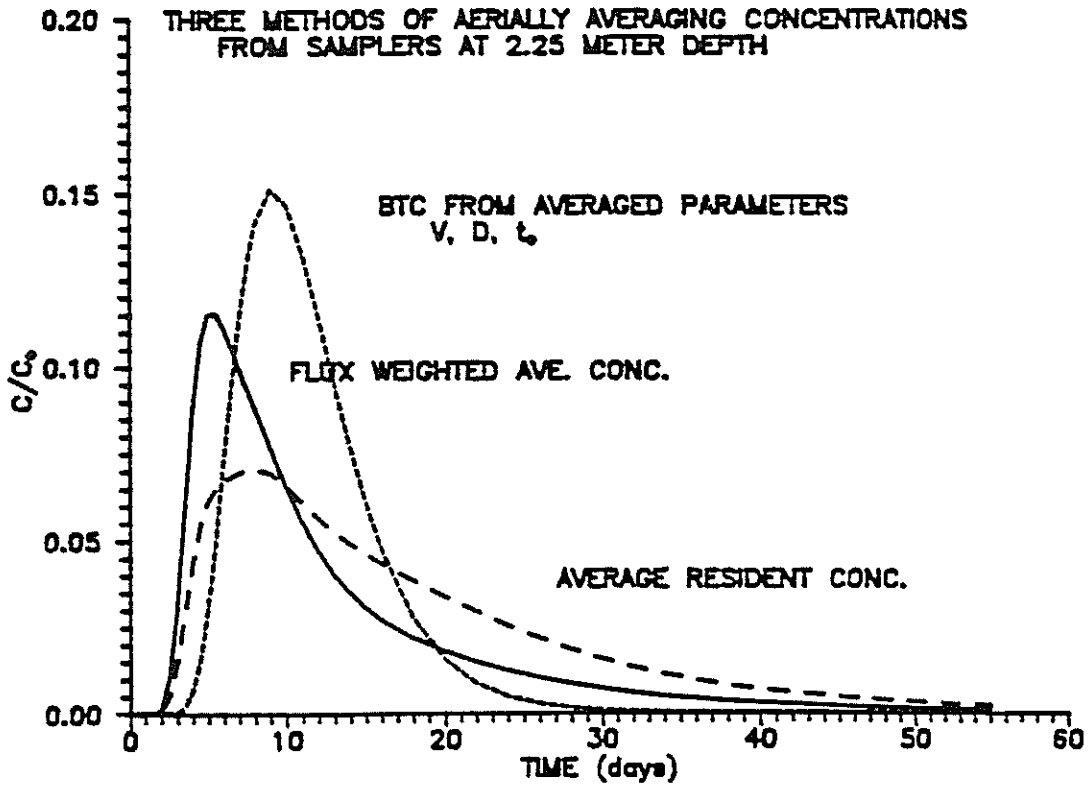

Figure 39. Breakthrough curves from three methods of aerially averaging concentration (ARC, AFWC, and ATPC) for samplers at 2.25 meter depth.

Moment analysis was used on the three BTCs and velocity, dispersivity, and zeroth moment calculated. The parameters are listed in table 6. The ARC method predicts lower solute velocities than the other two methods, but does not have velocity increasing with depth as drastically as from CXTFIT calculated velocities. Using moment analysis, the average flux weighted concentration curve is more dispersed than the other two. In contrast to ADE calculated dispersivities, moment analysis predicts increased dispersivity with depth using any of the averaging techniques.

It is interesting to note that the velocities calculated are all substantially less than the predicted solute velocity calculated from the water flux added to the site, 10^{-4} cm/sec, and moisture contents from the neutron probe data: $\theta_1 = 0.258$ and $\theta_{2.25} = 0.226$. q/θ or v thus becomes 33.5 cm/day at 1 meter and 38.2 cm/day at 2.25 meters. The lower velocities calculated from the three averaging methods are most likely due to lateral flow components.

Transfer Function Model

A transfer function model was applied to the data. Trial and error was used to determine the parameters from average resident concentration curves at the calibration depth. Using a single calibration depth, such as one-meter concentration data, one can in principle predict the BTC for any other depth. The parameters $C_0. = 1.14$, $\mu = 1.85$, and $\sigma = 0.95$ optimized the transfer function curve to the ARC 1-m data. Figure 40 is a comparison of the curves determined from the transfer function model (calibrated against samplers at 1-m depth) and the curves of the average resident concentration. The parameters $C_0. = 1.30$, $\mu = 2.55$, and $\sigma = 0.75$ fit the 2.25-m ARC data. Figure 41 is a similar graph depicting the transfer function curves calibrated at the 2.25-m depth. It was observed that the parameters from either calibration did not produce a good fit with the ARC curve of the uncalibrated depth. Due to the large degree of layering and heterogeneity, there was probably little correlation between flow paths to the two depths.

To predict the loading of tracer on the water table (approximately 20 m below drip lines), the parameters from two models were used. A tracer breakthrough curve was generated from transfer function theory with 2.25-m being the calibration depth. A second curve was generated using the one-dimensional advection dispersion equation, inputting

TABLE 5 Transport parameters, v, D, α, and t_o of the curves generated by the three averaging methods mentioned (generated from CXTFIT.)

TYPE OF AVERAGE	Z(CM)	v(cm/day)	D(cm^2/day)	α(cm)	t_o
ARC	100	6.53	874	134	1.2
	225	11.30	1140	101	1.4
AFWC	100	28.18	1293	46	1.0
	225	24.35	1082	45	1.0
ATPC	100	23.17	191	8.3	1.2
	225	21.27	363	17	1.3

TABLE 6 Transport parameters v_m, α_m, and T of the averaged breakthrough curves (m subscript denotes from moment analysis).

TYPE OF AVERAGE	Z(CM)	v_m(cm/day)	α_m(cm)	t_o
ARC	100	12.34	26.8	1.1
	225	13.84	46.7	1.3
AFWC	100	21.75	42.1	1.1
	225	19.28	61.2	1.2
ATPC	100	20.56	7.0	1.2
	225	20.85	15.5	1.3

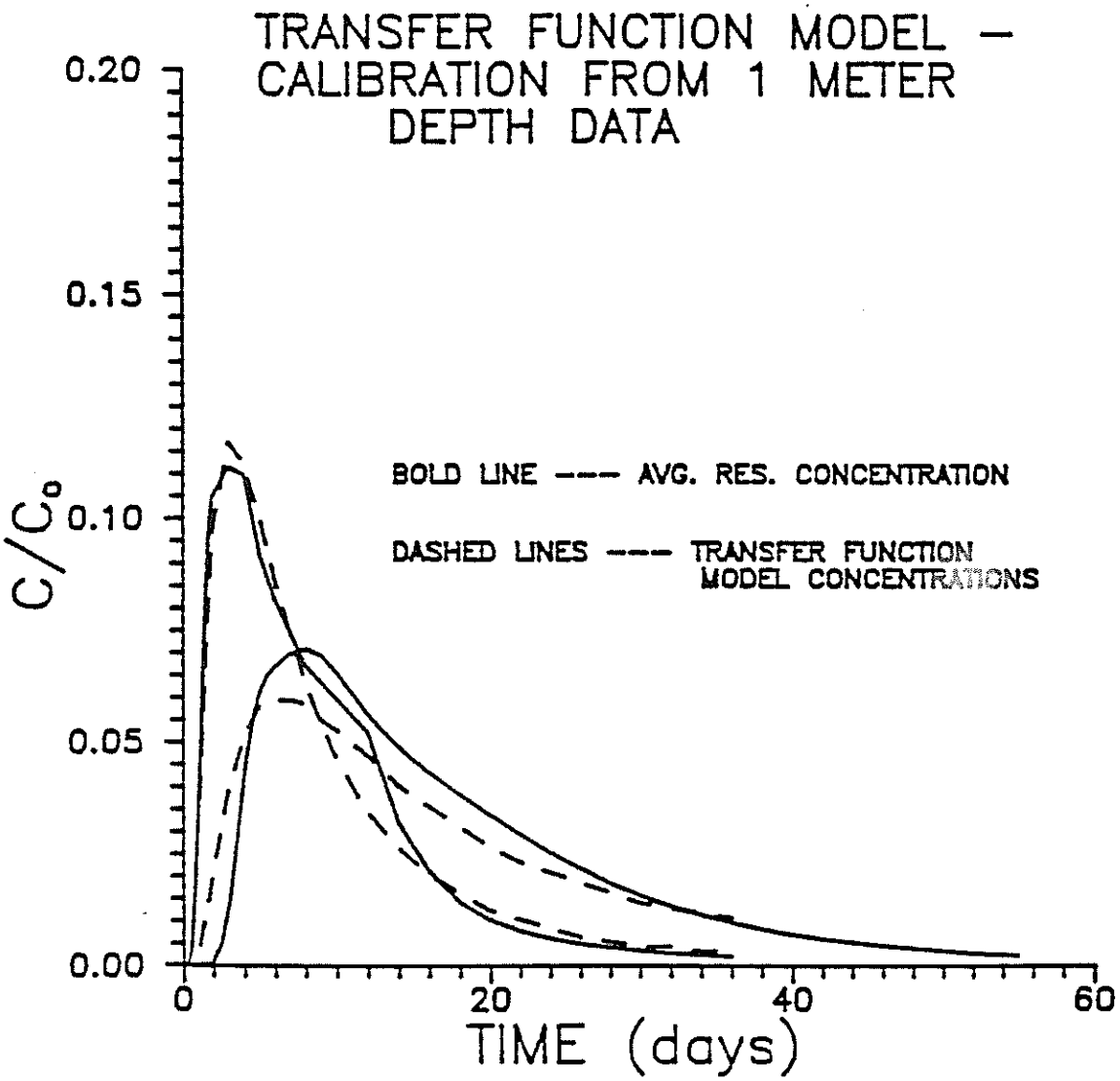

Figure 40. Comparison of ARC curves to curves generated from the transfer function calibrated at one meter.

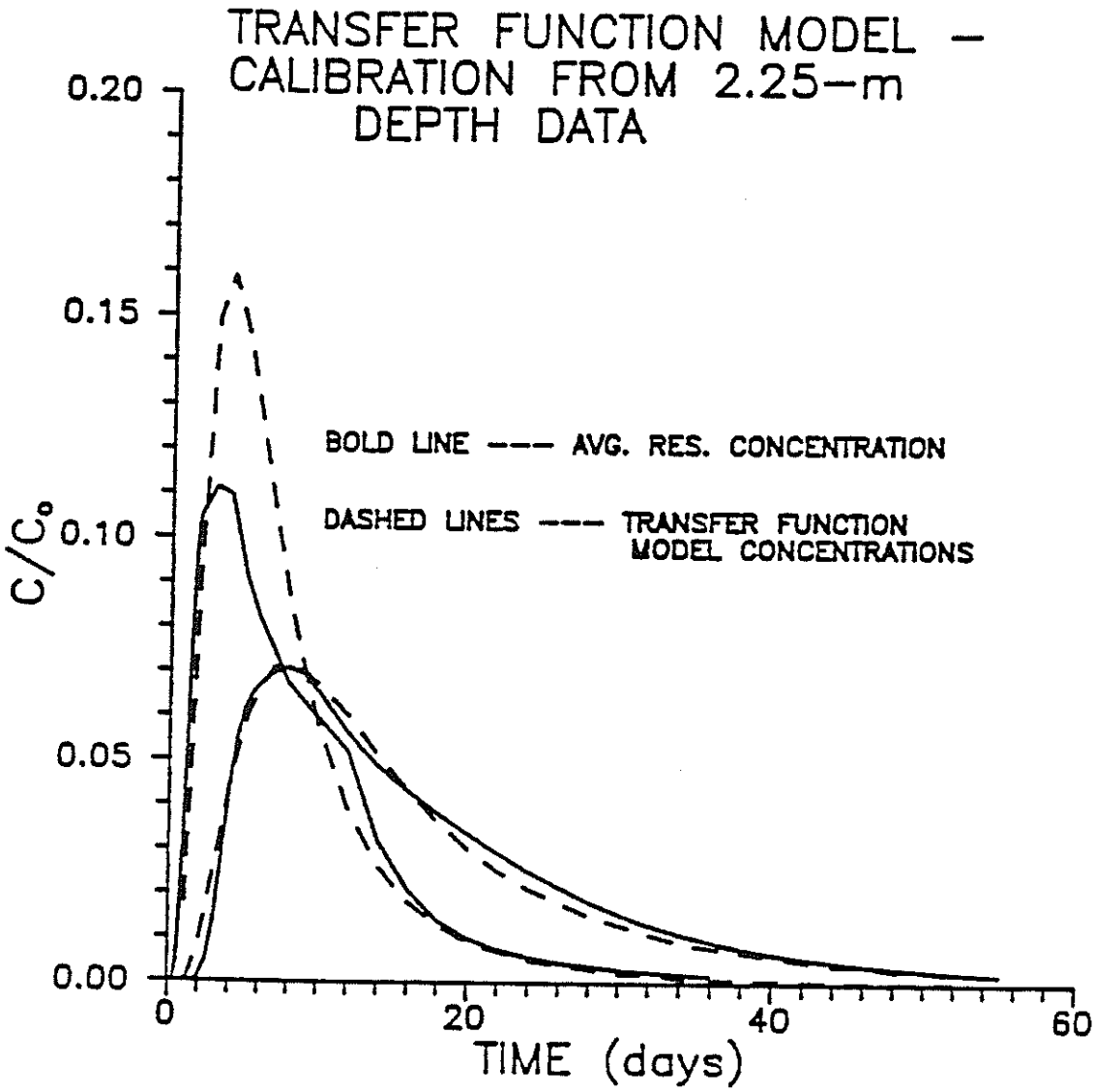

Figure 41. Comparison of ARC curves to curves generated from transfer function calibrated at 2.25 meters.

parameter values from the ARC curve at 2.25 meters. Compared to the 1-D ADE curve generated from CXTFIT, the transfer function model predicts much faster arrival of contaminants at the water table and a longer period of loading on the aquifer, but not as high a peak concentration (fig. 42).

There are several problems inherent in applying the transfer function model to the actual data. The model does not allow for increasing or decreasing heterogeneity with depth. It also does not allow for tracer breakthrough at a particular depth until the tracer application at the surface is complete. This model is best therefore when looking at relatively homogeneous soil systems where the amount of time during which the tracer is added at the surface is very short compared to the tracer's travel time to the depth of interest. **General Discussion of Fitting Breakthrough Curves**

There are problems fitting tracer breakthrough curves, where flow is three dimensional, with one-dimensional models. The parameters that the one-dimensional ADE generates do well in creating good-fitting curves to the data, but what actual significance do the parameters really have? The 1-D ADE gives the vertical velocity, neglecting any lateral components, gives the vertical spreading of the tracer pulse as the dispersion coefficient, and the mass under the curve as the pulse length. The time over which the pulse was applied is known to be one day, so that where the fitted pulse length is greater or less than one day, it implies convergent or divergent tracer flow respectively (figures 43 and 44).

Several BTCs show what are apparently double peaks. This occurs because tracer flowing to a particular porous cup sampler can originate from several drip emitters, some tracer flowing to the cup via one flow path, other tracer flowing to the same cup from other routes. Some of these paths will be longer than others, some shorter. The BTC's showing two fluoro-organic tracers illustrate this phenomenon.

A method was developed to look at these double peaks. The concentration data from early tracer breakthrough up to data belonging to the second peak (determined visually) was plugged into the CXTFIT program and parameters determined. These parameters were then used to determine what the concentrations should be for the various sampling times of the second peak if the second peak were nonexistent. These concentrations were subtracted from

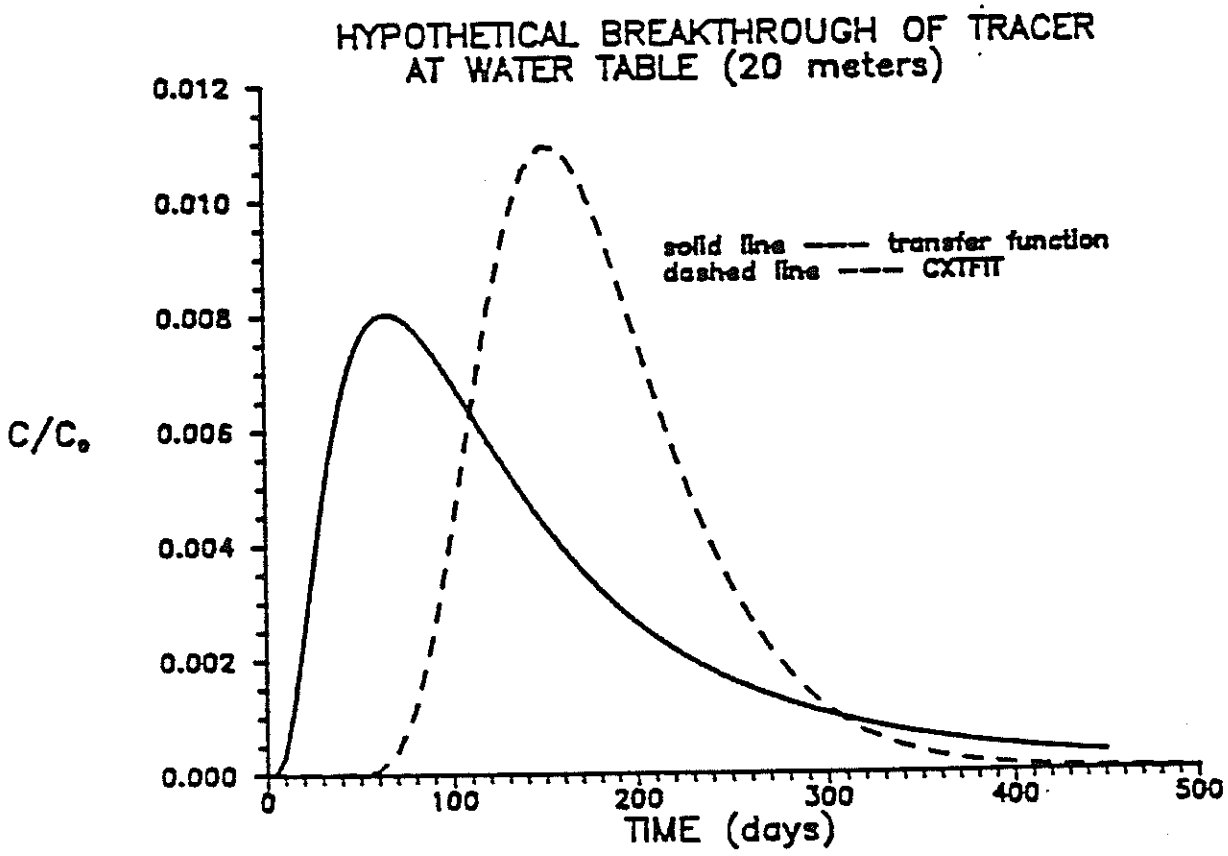

Figure 42. Comparison of predicted loading on water table of tracer by 1-D ADE and from transfer function (both calibrated to 2.25 meter depth).

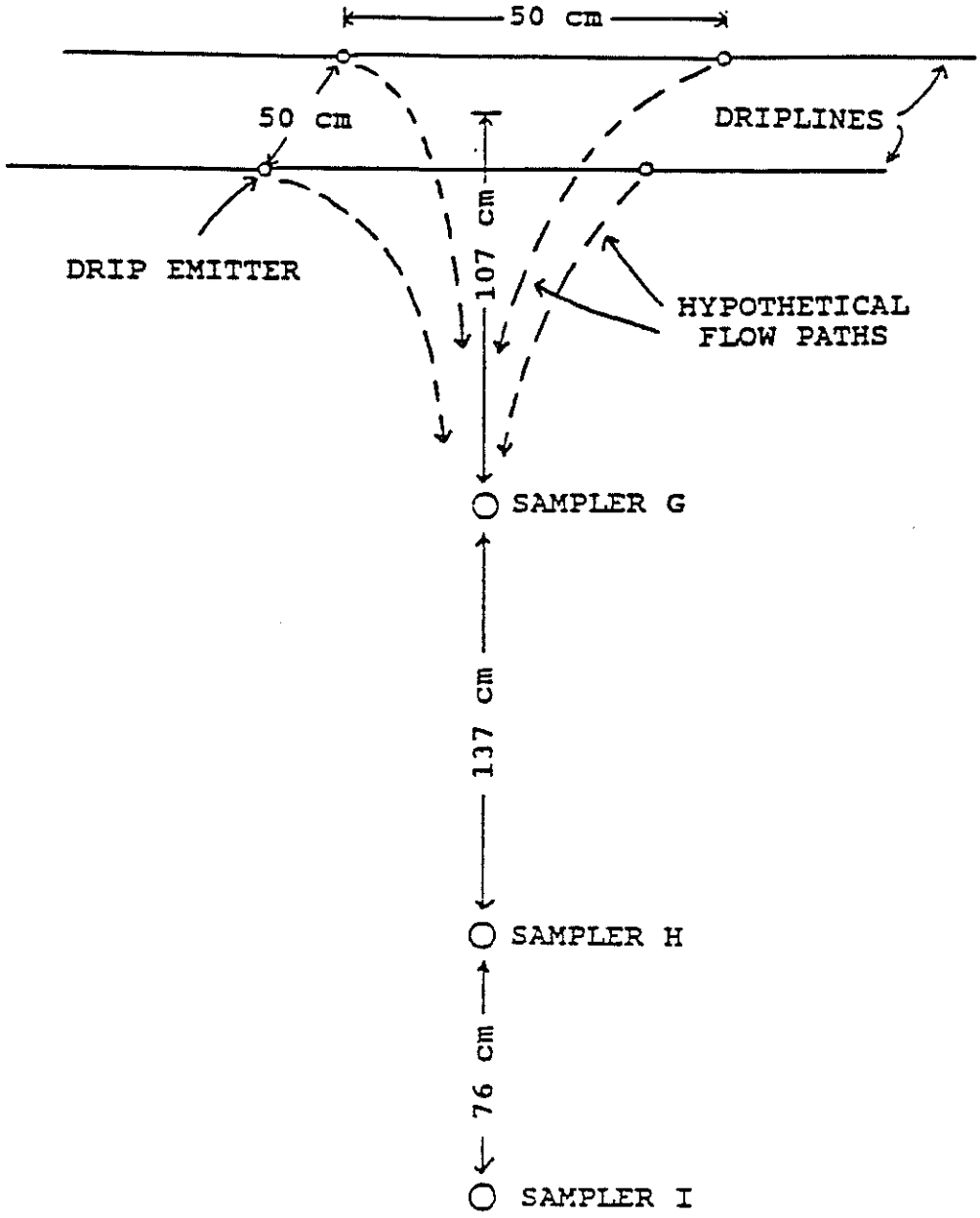

Figure 43. Illustration of convergent flow from multiple sources (from Flanigan 1989).

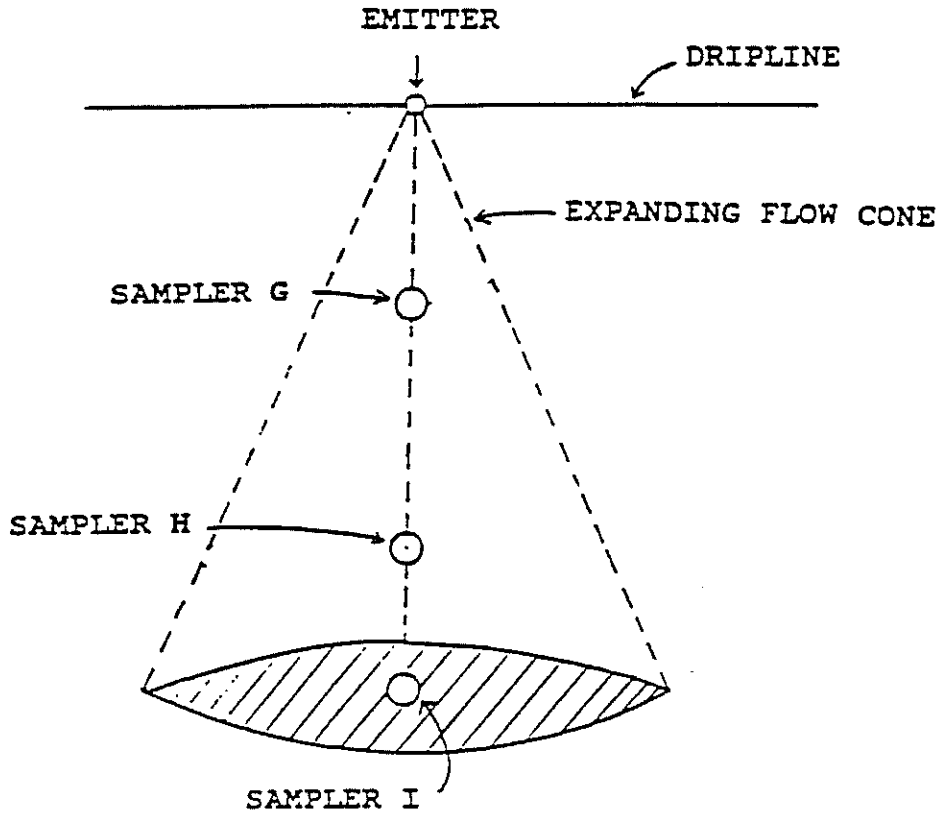

Figure 44. Illustration of divergent flow from a single source (from Flanigan 1989).

the concentrations of the second peak leaving a breakthrough curve of tracer moving through a different flow path minus the effects of the first breakthrough of tracer. The residual concentrations were then input into the CXTFIT program and parameters for the second flow path calculated. In actuality, there were probably many different separate flow paths to a particular sampler, but it seemed impossible to truly determine their number. Only the better fitting of BTCs with double peaks or pronounced tailing was accomplished by this method (figures 45 through 47).

Possible Design Problems

There are some factors that were built into the experiment's design that could possibly taint the data or invalidate some of the assumptions made about flow through this system. One problem was that flow through the emitters was uniform across the site. It is possible that some were clogged, inhibiting flow out the emitter and creating more flow in other emitters in the same section. Also, it is assumed that the flow through the soil is steady state. This is not completely correct. The water is applied to the soil in pulses, four every hour. The moisture content was not seen to noticably change between water applications, so the system was considered steady state. The slight transient nature of the water application might have little effect on moisture contents and suction values, but its effect on actual solute movement might be more noticable (i.e., possibly creating tailing).

Another possible design problem concerns the soil water sampler installation. Ideally, the samplers could have been installed in holes approximately the same diameter as the sampler PVC tube, but this was not possible due to the soils found beneath the surface. Some of the backfill used to fill in the holes does not represent native material, so its hydraulic properties could be greatly different. Also, the silica flour and the bentonite seals could perturb flow paths to the porous cups, thus giving BTCs related more to sampler installation than to flow through the actual native material.

A comparison of fitted v, D, and t of the samplers installed previous to the first tracer test of Flanigan (1989) to the samplers installed later show that suction lysimeters installed earlier have much larger velocities on average than samplers installed later. It is hypothesized that the installation of the earlier samplers was poor, or that the samplers had

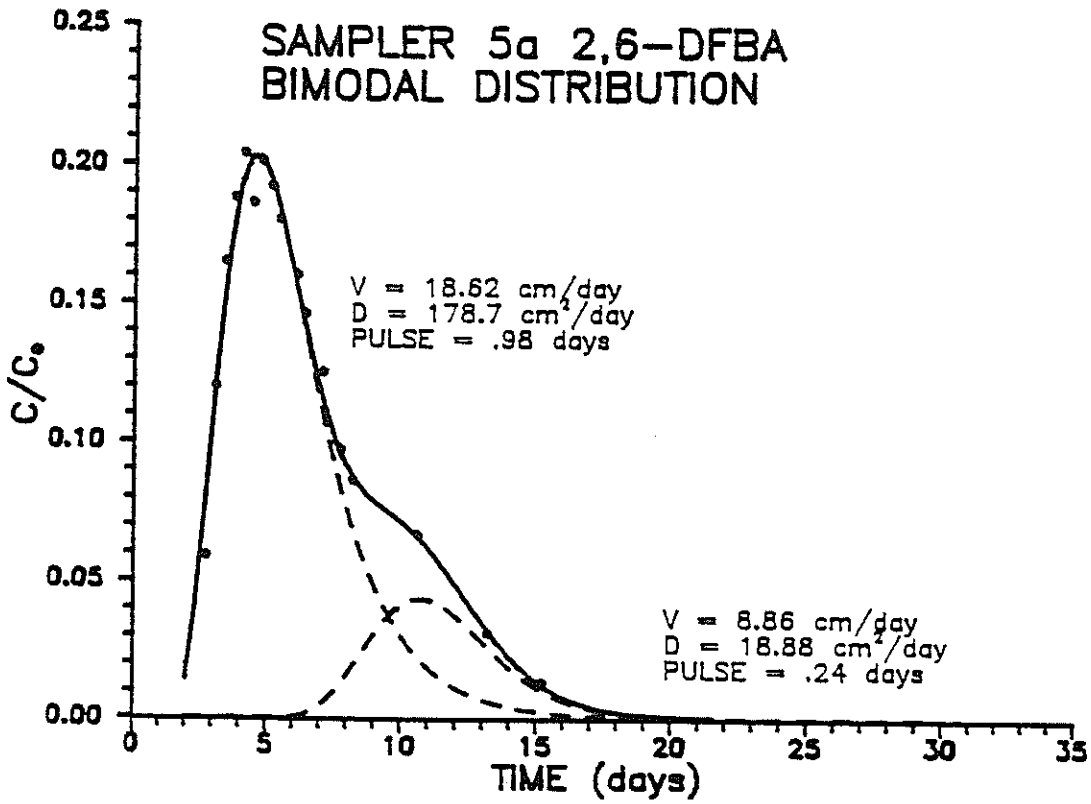

Figure 45. Sampler 5a breakthrough curve using peak addition. V, D and PULSE are parameters used to generate the dashed curves. Solid line is addition of dashed curves.

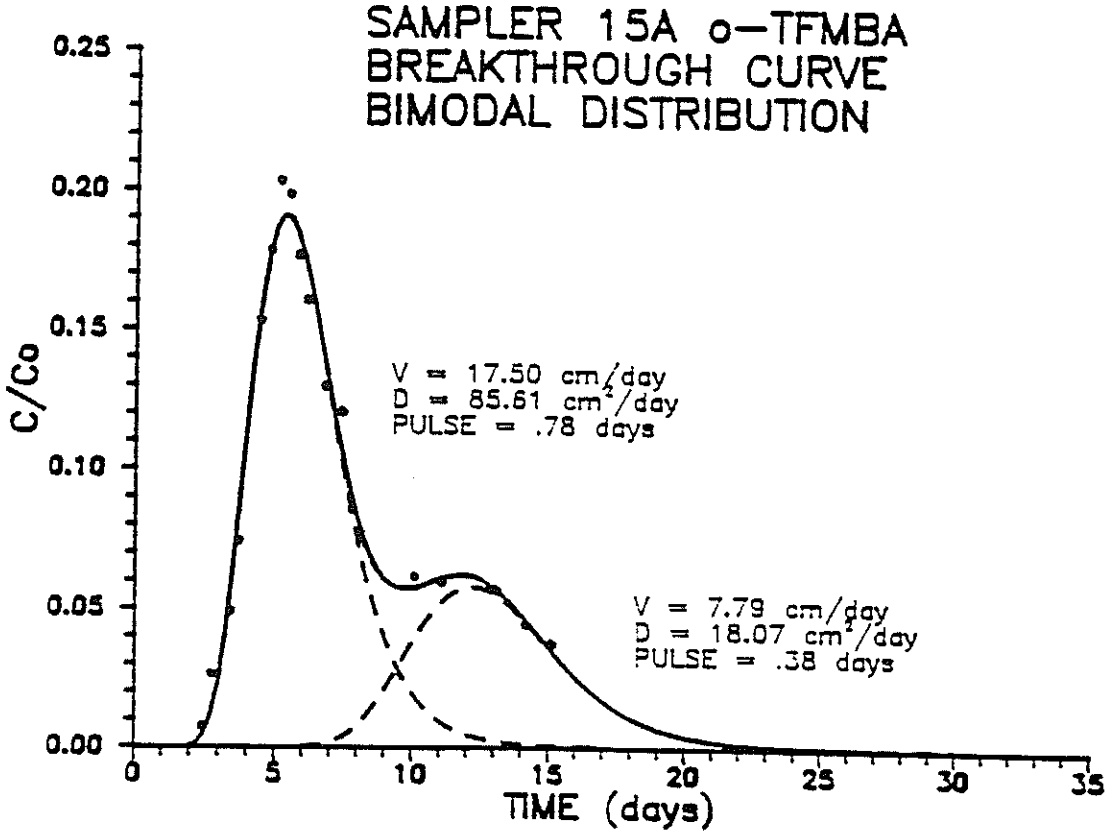

Figure 46. Sampler 15a breakthrough curve using peak addition. V, D and PULSE are parameters used to generate the dashed curves. Solid line is addition of dashed curves.

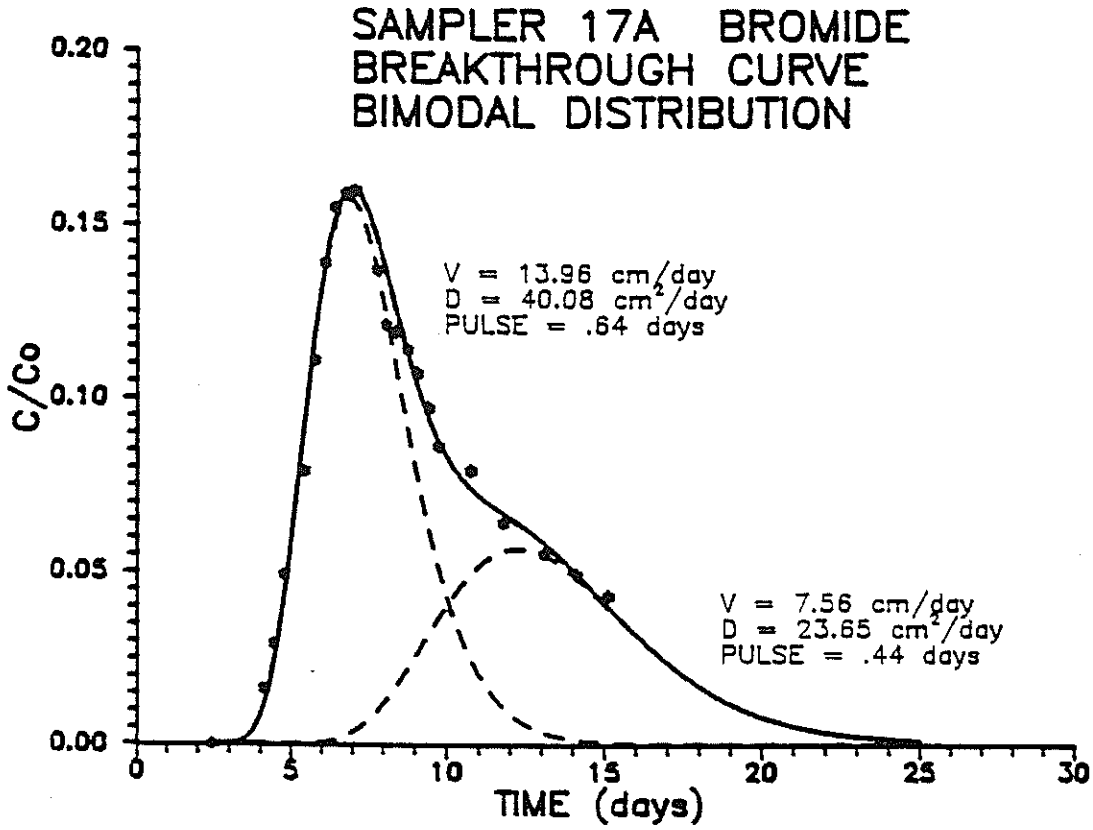

Figure 47. Sampler 17a breakthrough curve using peak addition. V, D and PULSE are parameters used to generate the dashed curves. Solid line is addition of dashed curves.

more established flow paths to them because of prior usage. The suction of soil water through the porous cup may have itself perturged the flow field beneath the site. The different amounts of water pulled infers that some samplers were sampling a greater volume of soil around them than were others. The fact that samples were not taken continuously adds another transient to the system. Finally, stopping the sampling of some of the samplers before the breakthrough of tracer was complete leaves questions as to whether some late time phenomena was missed.

CHARACTERIZATION OF SITE GEOLOGY

Piedmont Slope Facies

Figure 48 shows a map of the western wall of the deep SE-NW trending trench. The western wall was cleaned using shovels, pics, brooms and brushes to take off the slough from the trench digging and to accentuate the structural features and contacts between the units. Approximately 2.5 meters of arroyo facies was exposed (or the entire arroyo section in this spot) and approximately 1 meter of Rio Grande facies was exposed. An additional meter of Rio Grande facies was seen via hand auger samples through the bottom of the trench.

The deep trench exposed a perpendicular or head on view of an arroyo section that contained source material from the Socorro Peak area. The section exposed at the site is approximately 13-feet deep. At 13 feet there is a very undulating contact between the arroyo and the Rio Grande sand that the arroyo deposits moved over.

The following is a geologic description of the arroyo facies and the nature of its contact with the undulating Rio Grande sands. The arroyo facies has been divided into 7 separate stratigraphic beds, based on source differences, grain size distributions, and structural differences. The 7 beds are described from the surface downward.

The first bed, continuous across the face and less than 2-inches thick consists of very recent silty sand with either bedded or suspended sands and gravels. This bed acts as the root zone at the site and its age is not more than 200 years old as pieces of metal were found in the bedded gravels on the southern end of the face. According to J.Hawley (1990 personal communication), this bed is quite a bit younger than the underlying bed as is seen in the pronounced discontinuity on the southern side. The bedded gravels represent a high energy

flow regime. Some places exhibited evidence of soil development with the characteristic desert climate carbonate layers forming within this layer.

It should be noted at this point that according to the Soil Conservation Service (Johnson 1988), the soils found in the study area are characteristic of the local soils that form on bajadas and fan terraces, in alluvium derived dominantly from rhyolite and river deposits. These soils are to have a light brown gravelly sandy loam surface layer with a 12-inch thick light brown and pink gravelly sandy clay loam subsoil. The substratum usually consists of gravelly loam and gravelly loamy sand.

The second bed is also continuous, but more massive. Bed #2 is 1-to-3 feet thick and consists of a massive silty sand with interbedded sands and gravels in its bottom half. It appears that the higher the silt content in this layer, the more massive it appears. The bedded fine to coarse sands and fine to coarse gravels found in the lower half of this unit are subangular to subrounded. These larger grains are more bedded on the southern end of the trench and they mark a high energy event which left a scoured surface at the base of this bed. In places there are small fining upward bedded channel type deposits.

The third unit consists of a 2 to 3 foot thick, massive silty to sandy clay. This bed has up to 30% clay in it with small amounts of gravel and sand lenses. Other characteristics include charcoal scattered throughout, large amounts of bubbles or entrapped air, and on the whole a bubbly texture.

It should be mentioned that the infiltration experiment performed at the site left a pronounced effect on the area cut by the trench. The moisture that left the irrigation plot in the Northeastern direction was seen in the trench wall. Most of it appears to have travelled deeper than 16 feet below the surface by the time of the trench construction, but a substantial amount of moisture was retained in the mostly clay-rich parts of the trench.

Unit 2 was wet on the southern side of the wall (as shown in fig. 48) and unit 5 was almost all wet. The clays and some of the sand in the top 4 feet of the Rio Grande sand that were investigated in this trench were quite moist.

The fourth unit could be considered a subunit of the third unit as it is quite distinct in structure but does not appear to have any distinct contacts with the units above. It does, however, have a very pronounced scoured surface at the base. This unit is up to 1.5 feet

thick and consists of beautifully bedded sands and gravels that had been deposited in a high energy environment. These interbedded fine sands and medium to coarse sands have created very distinct layers with scoured lenses of gravels. The beds within this structure are horizontal at the top but bend down toward the bottom half of the unit, toward the depositional surface. One is able to see that where these beds meet at the depositional surface, there is a locus of deposition. In addition, there are black hematite and manganese stains within this structure.

The fifth bed is the second most clayey bed after unit 2, and is extensive across the wall except for the southernmost 10 feet of the trench where it was interrupted by the 6th unit. This unit was almost all wet from the irrigation experiment (except for the northern most 10 feet) when the trench was first dug. This bed consists of silty sand, some clay and little lenses of sand and gravel. Due to its relatively high clay content and uniform grain size, the texture of this bed appears blocky and smeared. The bed would have been deposited in a low energy environment. This bed has fairly distinct contacts with the units above and below.

Unit 6, located on the southern end of the trench, was deposited in a very high energy environment. From its contact with units 5 and 3, it appears to have flowed down the mountain side as a debris flow displacing unit 5 in that area. Unit 3 was deposited on top of this debris flow. All contacts with this unit are distinct. The debris flow carried cobbles up to 12 inches in diameter suspended in a fine to coarse viscous sand and gravel matrix. A very interesting feature of this unit is that it was surrounded by units that were wet from the irrigation experiment but the pore pressure of the unit never reached a point where it would take in some of the surrounding moisture.

Unit 7 is the deepest unit in the arroyo facies and lies conformably on top of the Rio Grande unit. According to Hawley (personal communication 1990), this was the last discharge event of the Pleistocene (early Holocene at about 7000 years). This is also the first cobble layer described by Parsons (1988) in previous studies. It consists of bedded sand and gravel layers on top of 8-inch cobbles suspended in a moist sand matrix. In the northern section this unit dips upward and consists of bedded sands and gravels below a thick cobble layer. This cobble layer is also suspended in a sand matrix. This unit is approximately 3-feet

thick in the trench but it has the most inconsistent thickness of all the units. Its bottom surface has quite an undulating shape where it meets the Rio Grande sand.

The trench wall was mapped as shown in fig. 48, according to textural and therefore previous energy flow regime conditions. After characterizing the units it was easy to see that they fit into Bull's three product categories very well. There were 7 discernable beds above the axial Rio Grande sands (which are found below unit 7). Below the alluvium at the top (or unit 1) are two mudflow units (units 2 and 3) separated by a discontinuity. Samples from these units had 28% and 33% clay (as found by grain size analyses). Below unit 3 is the only water laid deposit (unit 4) exposed in the trench. Unit 4 is about 1 1/2 feet thick and consists of distinctly bedded sands and gravels that exhibit fining upward and fining downward sequences. Samples taken from unit 4 exhibit 8% and 4% clay. Beneath unit 4 is an intermediate deposit. Samples from this unit contained 20% and 23% clay fractions. Units 6 and 7 are debris flows with gravel to cobble-sized clasts held in suspension within a silt to gravel matrix. Darker colored units were wet from a previous infiltration experiment. Unit 7 exhibits some bedding. Samples of the matrix in unit 6 have a clay content of 4% and 8%. The clay content of the mudflows, water-laid and intermediate deposits agreed very well with Bull's clay content of Fresno County fan deposits.

In addition to studying the alluvial fan units through the deep trench, the shallow trench dug perpendicular to the interpreted lateral water flow direction was mapped. This trench was about one-meter deep, about one-meter wide, and about 40-meters long. The western wall of the shallow trench was mapped using the Unified Soil Classification System (USCS). In addition to noting textural variations and changes, structures such as blocky structure in the clayey units, laminations, fining upward and downward, and crossbedding were noted. Finally, the contact beneath disturbed and undisturbed material, and the areas that were stained with blue dye, were noted. Figure 49 shows a map of the western wall of the shallow trench. In areas where the drip emitter irrigation system had been installed, the top 1/2 meter of section consisted of disturbed material. In other parts of the trench, there was up to 1/10 meter of disturbed material at the surface. The 1-meter deep section contained varying combinations of clay, silt, sand, and gravel with occasional cobbles. The various textural combinations are described on fig. 49.

Arroyo Sequence as Exposed
in SE-NW Trending Trench

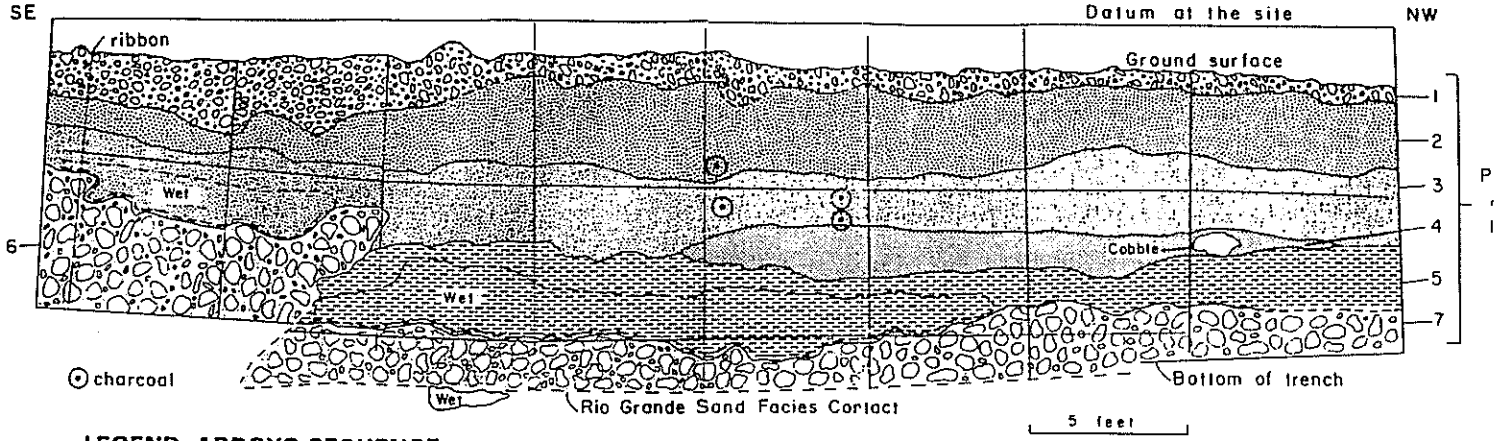

LEGEND: ARROYO SEQUENCE

UNIT 1: A 1 to 2 foot thick continuous silty sand bed with either bedded or suspended sands and gravels. The bedded gravels represent high energy flow. This unit was deposited in the last 200 years.

UNIT 2: A massive and continuous 1 to 3 foot thick silty sand with interbedded subrounded to subangular sands and gravels in bottom half. Bounded by a discontinuity on the top and a scoured surface at the base. This unit contains small fining upward bedded channel deposits.

UNIT 3: A 2 to 3 foot thick silty to sandy clay with little sand and gravel lenses. This unit is characterized by up to 30% clay, scattered pieces of charcoal, entrapped air and a blocky texture. The southern end of this unit became wet due to irrigation experiment.

UNIT 4: A 1½ foot thick distinctly bedded sand and gravel subunit of Unit 3 found on northern side of well. Deposited with substantial amounts of water in a high energy environment. The beds in the lower half of the unit bend down toward the depositional surface. Black hematite and manganese stains are found within this unit.

UNIT 6: A 2 foot thick silty sand with some clay and little lenses of sand and gravel that was interrupted in the southern end of the trench by Unit 6. This unit is characterized by a blocky texture due to its high clay content and low energy depositional environment. Parts of this unit became wet due to the irrigation experiment.

UNIT 6: A high energy debris flow that is seen in southern end of the trench. The debris flow carried cobbles up to 1 foot in diameter suspended in a viscous, fine to coarse sand and gravel matrix.

UNIT 7: An extensive 1 to 3 foot thick high energy debris flow that lies conformably on top of the Rio Grande sands. This unit may represent the last discharge event of the Pleistocene. The unit consists of bedded sand and gravel layers on top of a layer of cobbles suspended in a sand matrix.

Figure 48. Map of NW - SE Trending Trench Face.

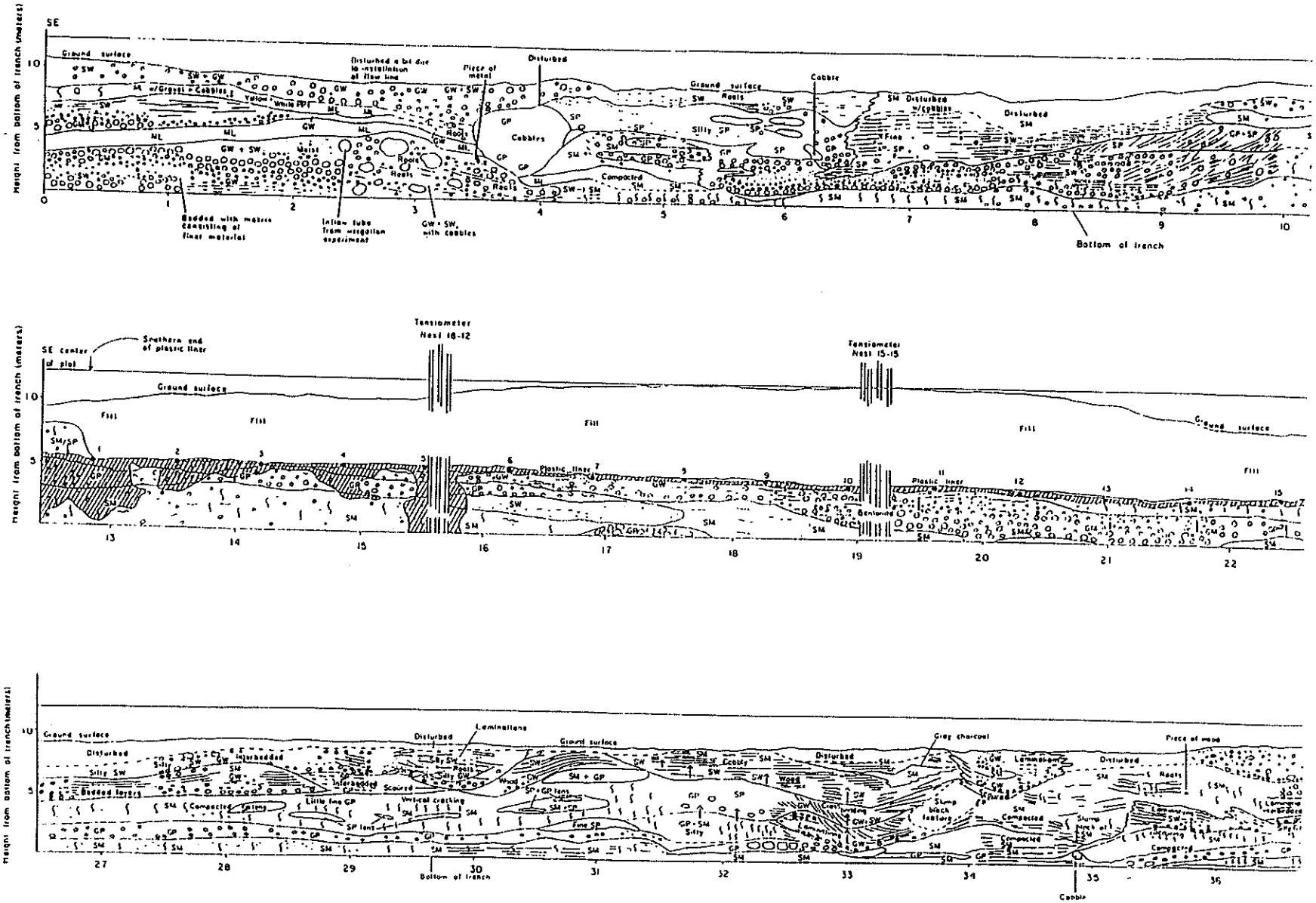

Figure 49. Map of shallow trench face.

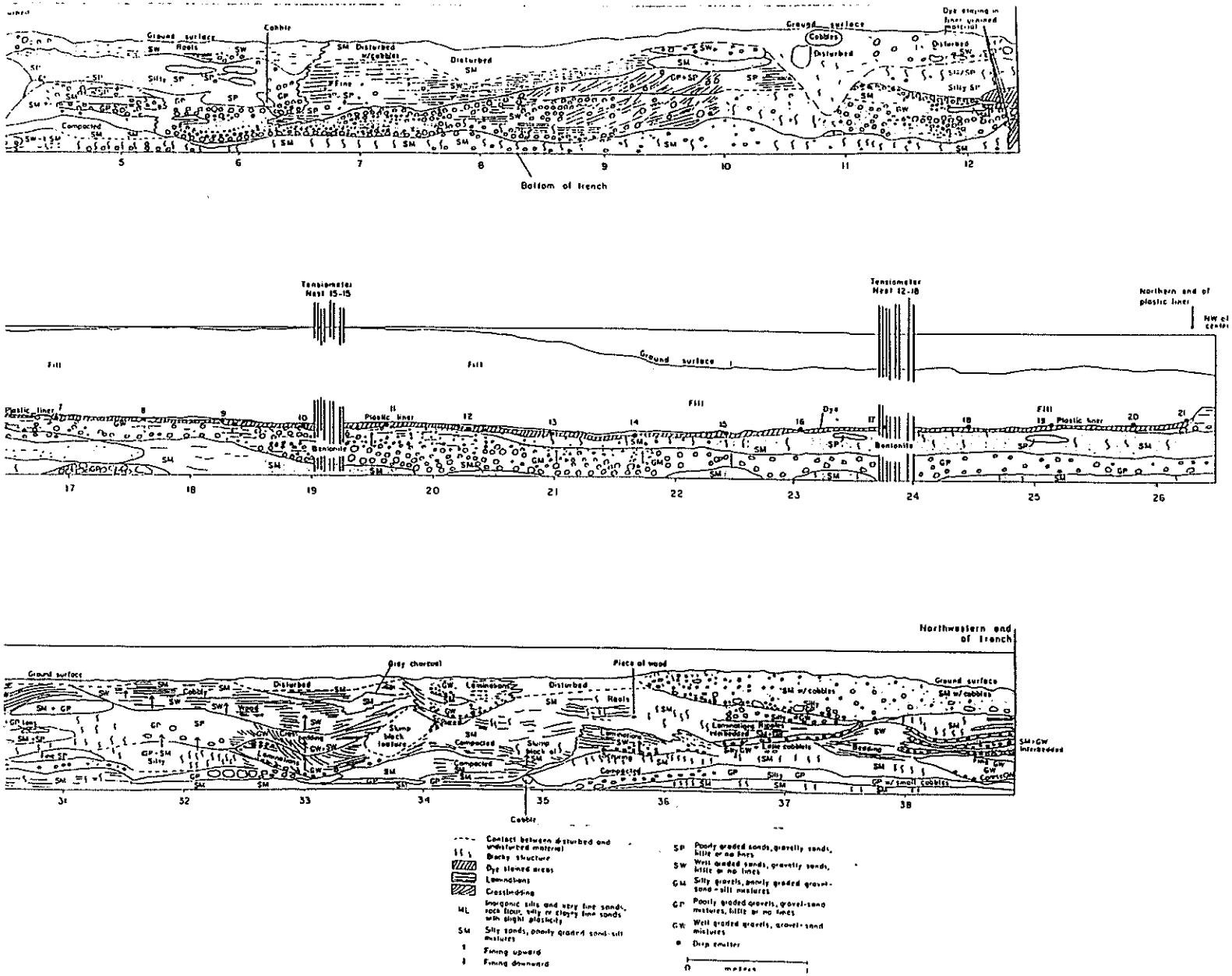

Figure 49 (cont'd)

In terms of the larger scale arroyo unit descriptions used to describe the deep trench facies, we see units 1, 2, and the top of unit 3 (from the surface downward). In the shallow trench, unit 1 is between 1/3 and 2/3 meter thick and consists of horizontally laminated, water-laid, sands and gravels or cobbles entrained in a silty sand matrix. Parts of this unit had been interrupted during the installation of the irrigation system. In addition, the unit contains pieces of metal and wood contributing to the young age of this unit as described earlier. Its lower surface is quite undulating. In this trench, as in the deep trench, unit 1 is found at the surface, underlain by unit 2, which is underlain by unit 3. The floor of the trench was the location of the detailed disc permeameter study. As a result it was prudent to identify the units that intersect the floor of the trench. Starting from the SE and moving toward NW along the floor of trench, unit 1 is seen from 0 to 3.5 meters, unit 2 seen from 3.5 to 19 meters, unit 3 is seen from 19 to 27 meters and unit 2 extends from 27 meters to the NW end of the trench.

As in the deep trench, unit 2 is bounded by a discontinuity on the top and a scoured surface on the bottom. It is approximately 1/3 of a meter thick and consists of a silty sand with interbedded and gravels. There are quite a few structures in this unit with the northern end of the trench containing quite a bit of silt/clay blocky structure and cross-bedding and the southern end of the trench containing a lot of cross bedding and interbedded sands and gravels. Units 2 and 3 show the blue dye stains in the center of the plot (or trench).

Part of unit 3, identified as SM with the USCS, is the lowermost unit seen in the shallow trench. This unit consists of a blocky silty sand with gravel imbedded in it. Unit 3 is not seen in the southern end of the trench. In the center of the plot, this unit is up to 1/3 of a meter thick.

Piedmont slope/fluvial sand facies contact

At the deep trench location, the contact between the Rio Grande sands and the arroyo facies is about 12 ft. and 7.5 inches below the surface or approximately 4.5 meters below datum. Hawley (1990 personal communication) says that the gradient of the arroyo (longitudinally) is about 100 feet/mile. Parsons (1988) estimated the average elevation of the piedmont slope and fluvial sand contact to be about 1412 MASL (5.4 meters below datum). The slope of the surface between the two facies can be determined from 3 different contact

locations and elevation The average attitude of the contact between the piedmont slope facies and fluvial sand facies in the area near the field site is strike N32E, dip 4.5 SE>. The bottom of the arroyo sequence is characterized by a high energy cobble suspended in sand and gravel sequence.

The sand and arroyo contact is highly irregular due to the high energy environment in which the arroyo was deposited. Hawley (personal communication 1991) calls the arroyo an alluvial deposit not under sustained flow. The gradient vs discharge equation would be exponential for such a flow. Locally the contact between the piedmont slope facies and fluvial sands is irregular (Parsons 1988). Prior to the piedmont slope facies deposition, arroyos were created in the ancestral fluvial sands during epirogenic uplift (Chamberlain 1980). Within the site the contact appears to dip slightly to the NE. A direct correlation of the piedmont slope facies and fluvial sand facies from one location to another is not easy because the two facies are known to interfinger.

As pointed out by Chamberlain (1980), the alluvial fan piedmont slope gravels in the Socorro Basin are thought to have graded eastward as Socorro Peak grew, thus burying the ancestral Rio Grande sands and forcing the channel eastward. Accordingly, there may be a transition zone between the two facies site, between two cobble horizons (Parsons 1988). This explanation is supported by the poorly sorted, red brown sand, silt and pebbles which interfinger with well sorted, tan fine sands and silty clays to the east. This depositional sequence suggests that cobbles were washed from western highlands. Subsequently the ancestral Rio Grande encroached onto the field site one last time, leaving fine sand and silty clay deposits before the piedmont slope deposits forced the river to the east. Several outcrops to the west and to the south of the field site exhibit similar characteristics, reinforcing such a hypothesis (Parsons 1988).

Fluvial Sand Facies

Approximately 3 feet of the Rio Grande fan were exposed within the trench (by digging deeper within the center of the trench). The formation consists of very uniform fine to medium sand.

Within the deeper pit (in the middle of the trench) a huge boulder that marks the arroyo sequence. The boulder appears to have descended off the mountain in a very high energy

regime (flow) and plopped into the underlying arroyo sand, producing a scoured gravel from water that was turbulent on the downside of the rock (boulder) and a flame structure within the sand as the sand was being pushed outward from the boulder's impact. The Rio Grande sand is rounded, fine and uniform. Within the sand are wet and dry layers and layers of "Hershey" type clays. The sand contains yellow limonite staining and some black charcoal streaking. There are also ripples within the sand.

Approximately 3 feet below the top of the sand is a very impressive layer of clay 0.5 meter thick. Below that are 0.5 meter of clean sand underlain by 0.3 meter of interbedded sand and clay. These interbedded sands and clays contain orange, brown, and iron-stained sand with flat pebbles in it. At this point there is a cobble layer that was not penetrated by hand auger.

DETERMINATION OF HYDRAULIC PROPERTIES

Field and Laboratory Hydraulic Conductivity Comparisons

Eighty-one of the disc permeameter measurements of hydraulic conductivity conducted at 1.3 cm of tension are regressed against comparable laboratory saturated hydraulic conductivity (fig. 50). A line fit by eye is regressed through the data. This line is more appropriate than a computer generated linear regression because the fit-by-eye gives relatively more weight to outlying data than the mass of measurements in a block near the center of the plot. The mass of log K data pairs ranges from -4.0 to -3.0 on the tension axis and -2.5 to -4.5 on the saturation axis. In general, tension measurements of hydraulic conductivity are slightly higher than saturated values (soil cores) from the disc permeameter test zone. The saturated hydraulic conductivity values throughout the plot are more variable than the tension values. A number of data pairs lie outside the center block and may represent large populations. They can be related to the averaging effects of the disc permeameter as discussed in the laboratory Ks section. For example, in areas of high hydraulic conductivity, the disc permeameter, which averages over a larger surface area to thickness ratio than the soil cores, results in a lower hydraulic conductivity. It is essentially an effective horizontal hydraulic conductivity. Also, the soil cores may contain macropores and disturbances such as sidewall channeling which leads to a higher hydraulic conductivity. In low hydraulic conductivity materials the inverse appears to occur. The disc permeameter

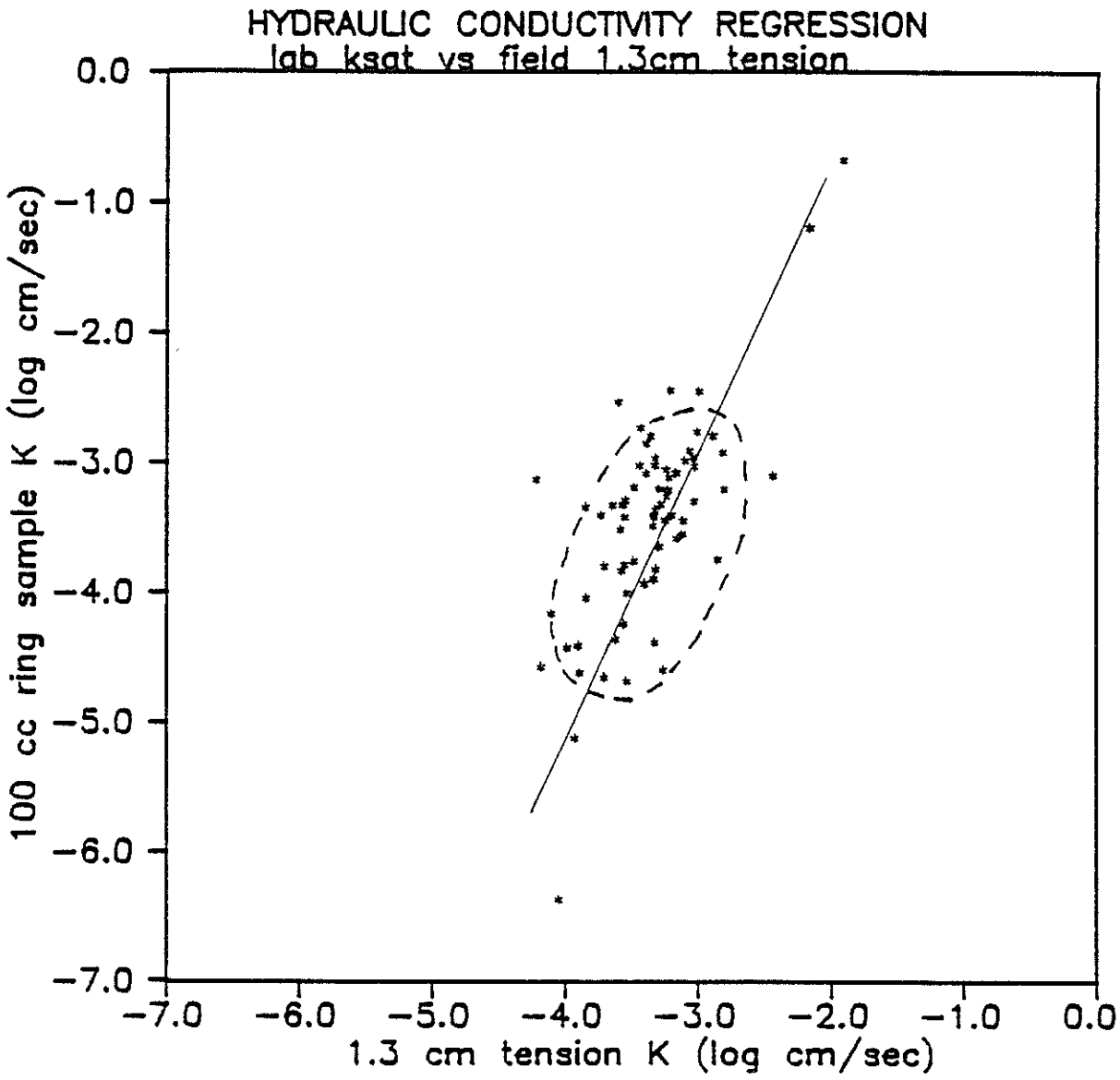

Figure 50. Scatter diagram (regression) of the log laboratory saturated hydraulic conductivity data with the 1.3 cm tension hydraulic conductivity data.

may average over several soils of varying hydraulic conductivity, resulting in a larger effective K than the soil cores. Evaluation of the plot of both lab and field hydraulic conductivity determinations with distance along the transect suggests that the disc permeameter at 1.3 cm tension (Kl.3) produces results which are valid for estimating hydrologic properties at the experimental site (fig. 51). The means of the disc permeameter at 1.3 cm tension and soil core (Ks) data sets differ by approximately 10%, with the Kl.3 mean slightly larger than the lab Ks mean. Due to the different volumes measured by the two methods, the soil cores are about twice as variable as the tension values. In addition, the two distributions show similar trends along the transect, with hydraulic conductivity decreasing toward the center and, then, slowly increasing toward the northwest. The K-S test at the 0.05 level of significance suggests that both the Kl.3 and lab Ks distributions stem from similar log normal distributions (fig. 52). The F-test at the 0.05 level of significance concludes the variances are not equal for the Kl.3 and Ks data sets. Therefore, the T-test cannot be used, and the less powerful largescale test of the hypothesis for the difference of two means (LSTHDTM) is employed for analysis. The LSTHDTM suggests there is insufficient evidence at the 0.05 level of significance to indicate a difference between the Kl.3 and lab Ks means.

Disc Permeameter Discussion

Laboratory values of saturated hydraulic conductivity are plotted along with field hydraulic conductivities measured at the same locations along the transect in fig. 45. The laboratory data are more variable than the field data. A comparison of the laboratory values of saturated hydraulic conductivity and field hydraulic conductivity measured at 1.3 cm tension (fig. 44) showed a majority of the data pairs concentrated in an ellipsoid bounded by an order of magnitude on the tension hydraulic conductivity axis and two orders of magnitude on the saturated hydraulic conductivity axis. Outside the ellipsoid, field hydraulic conductivities are larger than the comparable laboratory saturated hydraulic conductivities for fine textured soils. In coarse textured soils, the opposite behavior is observed. Averaging caused by the disc permeameter's large surface area is a likely explanation for the differences at both ends of the scale. For example, in fine textured soils, a soil core samples a smaller horizontal area and greater soil thickness than the disc permeameter, resulting in a low

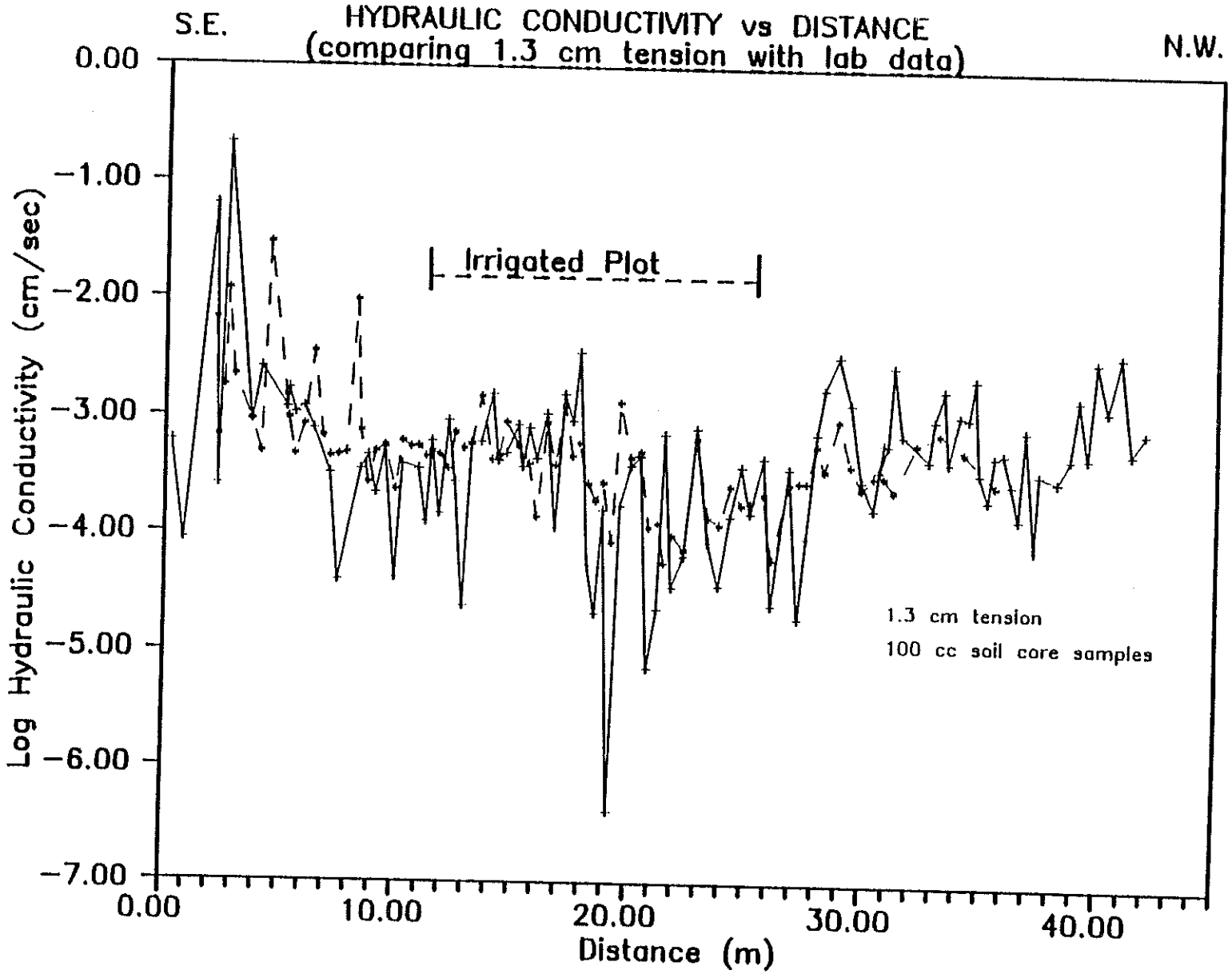

Figure 51. Laboratory saturated hydraulic conductivity and field 1.3cm tension hydraulic conductivity with distance along the transect.

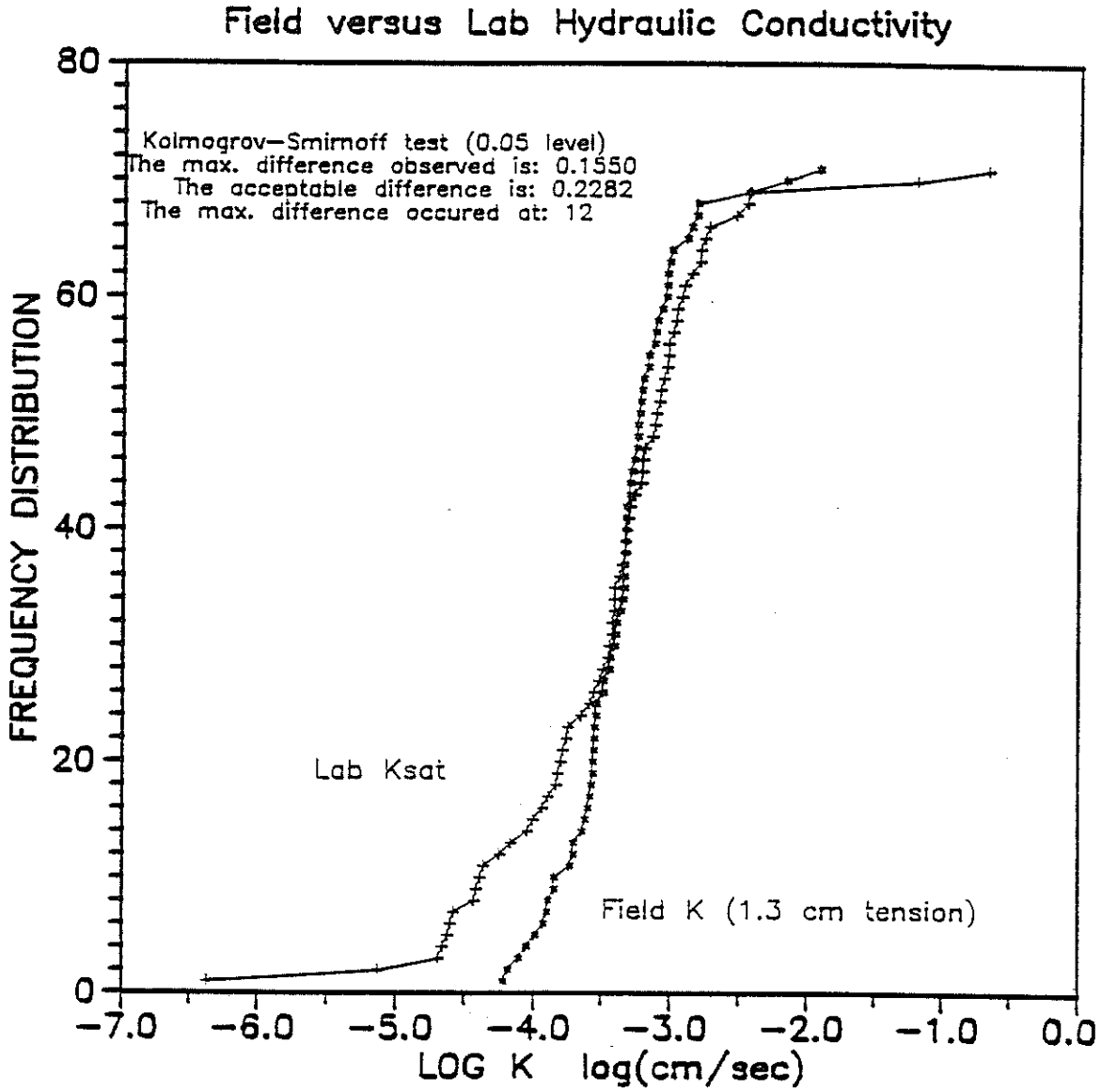

Figure 52. Log laboratory saturated hydraulic conductivity distribution compared with log 1.3 cm tension hydraulic conductivity. They are observed to be similar at the 0.05 level of significance with the Kolmogorov-Smirnoff test.

effective vertical hydraulic conductivity determination. The disc permeameter, on the other hand, may sample the fine textured unit as well as surrounding higher conductivity materials, resulting in a effective horizontal hydraulic conductivity that is larger than the soil core value. Low hydraulic conductivity soils are more likely to contain macropores not sampled by the soil core than higher hydraulic conductivity materials. Also, low hydraulic conductivity soils may swell in the soil core preventing sidewall channeling. This may not occur in sandy soils. Soil cores of coarse soils may have hydraulic conductivities greater than the field values. Therefore, the disc permeameter will yield values of hydraulic conductivity that are smoothed, less varied, as compared to the soil cores.

Measurement Limitations

A number of limitations were encountered during use of the disc permeameter. In its present form it is limited to hydraulic conductivity determinations ranging from approximately 1.0 x 10-2 cm/sec to approximately 1.0 x 10-5 cm/sec. The accuracy of measurements is greatly reduced for coarse textured, high hydraulic conductivity materials. Bubbling, caused by air entry into the reservoir, is so great and the water level drops so quickly that the data contains significant scatter. Determinations of sorptivity are then especially difficult. Although measurements can be conducted with fair results, an automated device (Ankeny et al. 1988) would result in less scatter and, therefore, better results.

In fine textured, low hydraulic conductivity materials, care must be taken to limit outside influences on the disc permeameter. Below 1.0 x 10-4 cm/sec, direct exposure of the disc permeameter reservoir and wetted soil region around the permeameter base to the sun can increase flow from the instrument. Increasing flow rate with time occurred in a number of disc permeameter measurements on fine textured materials. The exposure of the permeameter reservoir to intense sunlight, as is common in the southwestern United States in the spring and summer, caused heating and expansion of air within the reservoir perhaps inducing flow from the disc. Sun exposure to the wetted region about the permeameter base results in evaporation. The effect is very important in this study for measurements of hydraulic conductivity in fine textured soils. Evaporation can induce a gradient from the soil surface toward the disc base, thereby inducing flow from the reservoir. One or both of the effects could have resulted in the increased flow. To limit the problem, the disc

permeameter and measurement areas were shielded from the sun with good result to calculated hydraulic conductivities of 6.0 x 10-5 cm/sec.

In coarse to medium textured soils (gravels to silty-sands), flow from the disc can reach steady state in 1 to 10 minutes. In fine-textured materials (silts and clays), however, the disc permeameter measurement must be conducted for longer time periods to ensure steady state flow. Even after significant time (20 to 30 minutes), the wetted region about the disc may be of larger lateral extent than thickness. Capillary forces may still have considerable effect on the flow rate. Because the measurements would be disrupted, no quantitative data of this phenomena was recorded. Instead, extra measurement time was allotted for the wetted region to expand and for steady state to occur. For hydraulic conductivity determinations below 5.0 x 10-5 cm/sec, 3 to 4 hours should be allowed for reasonable hydraulic conductivity determinations.

CHARACTERIZATION OF SOLUTE FLOW PATHS

The first excavation and drafting performed was along the "lateral" sections. Before the wooden trench was removed, sections A3 and C1 were exposed. Flow through the lateral region A3 was primarily saturated in nature as the "holes" or blank spots were composed of silty clay (fig. 53). Thick layers of clayey sandy silt and thin layers of silty sandy fine gravel were dyed an intense blue from laterally flowing water. Toward the base of the section, the dye broke into large lobes penetrating finer material as the saturated regime became progressively more unsaturated.

For section C1, saturated flow was prevalent in the upper 10 cm of the zone, but became more unsaturated toward the base (fig. 54). The "hole" here was composed of sand and small cobbles. A large cobble (blue tinged on edges only) was found just below the left lobe of dye. Soil in the fight dyed lobe is similar in nature to the dyed pathway near the base of A3.

The third cut was along the northeast face of the trench (fig. 55). The numbers mark the crossing points of the driplines. Note that driplines protrude out of the paper at an angle. Also note that when dripline locations are referenced, the two-dimensional region around the "crossing point" is the subject of the reference. The thick zone of dye in the southeastern part of this cross-section was primarily due to ponding effects in the wooden trench.

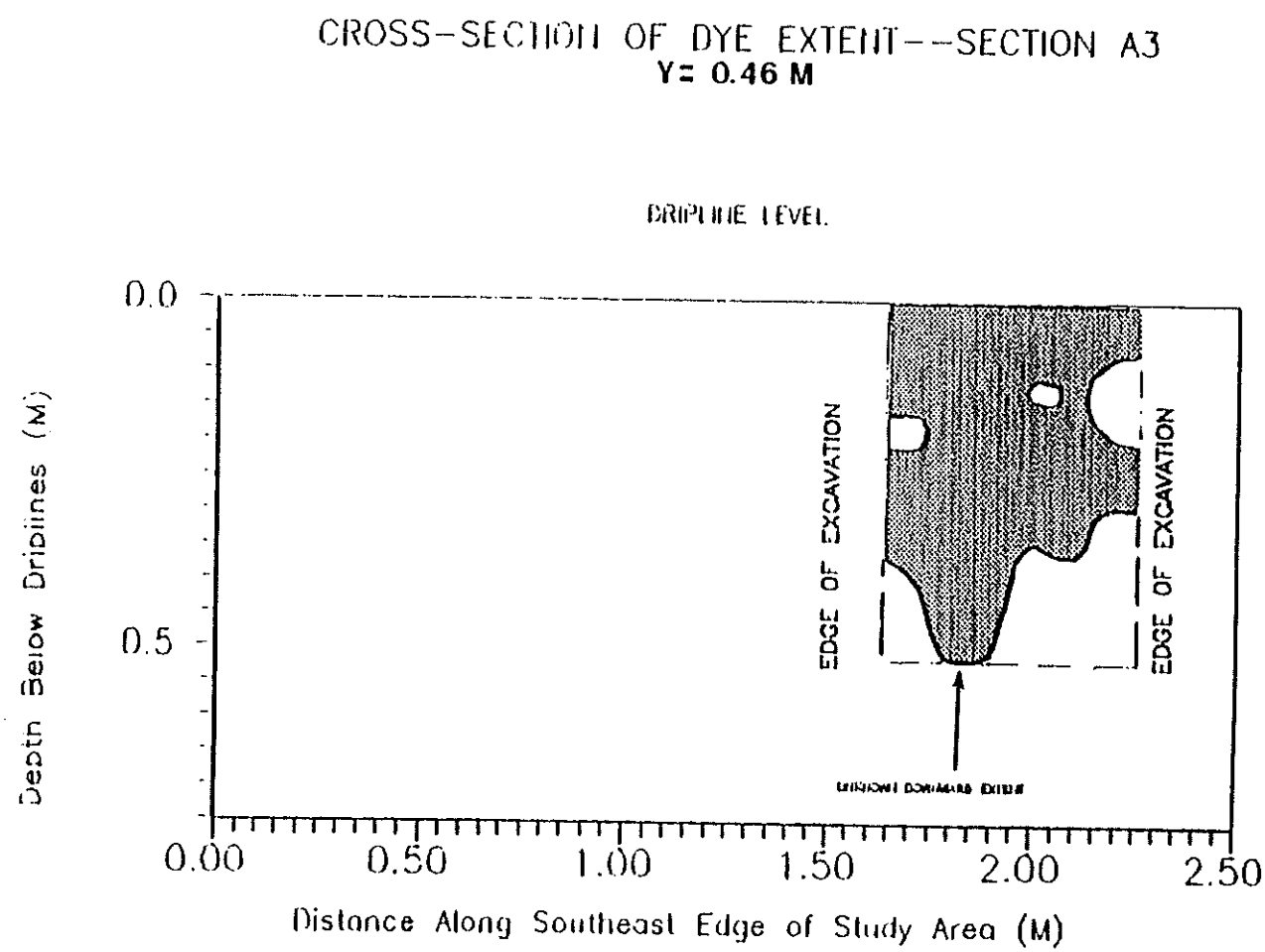

Figure 53. Cross-section of dye extent -- Section A3.

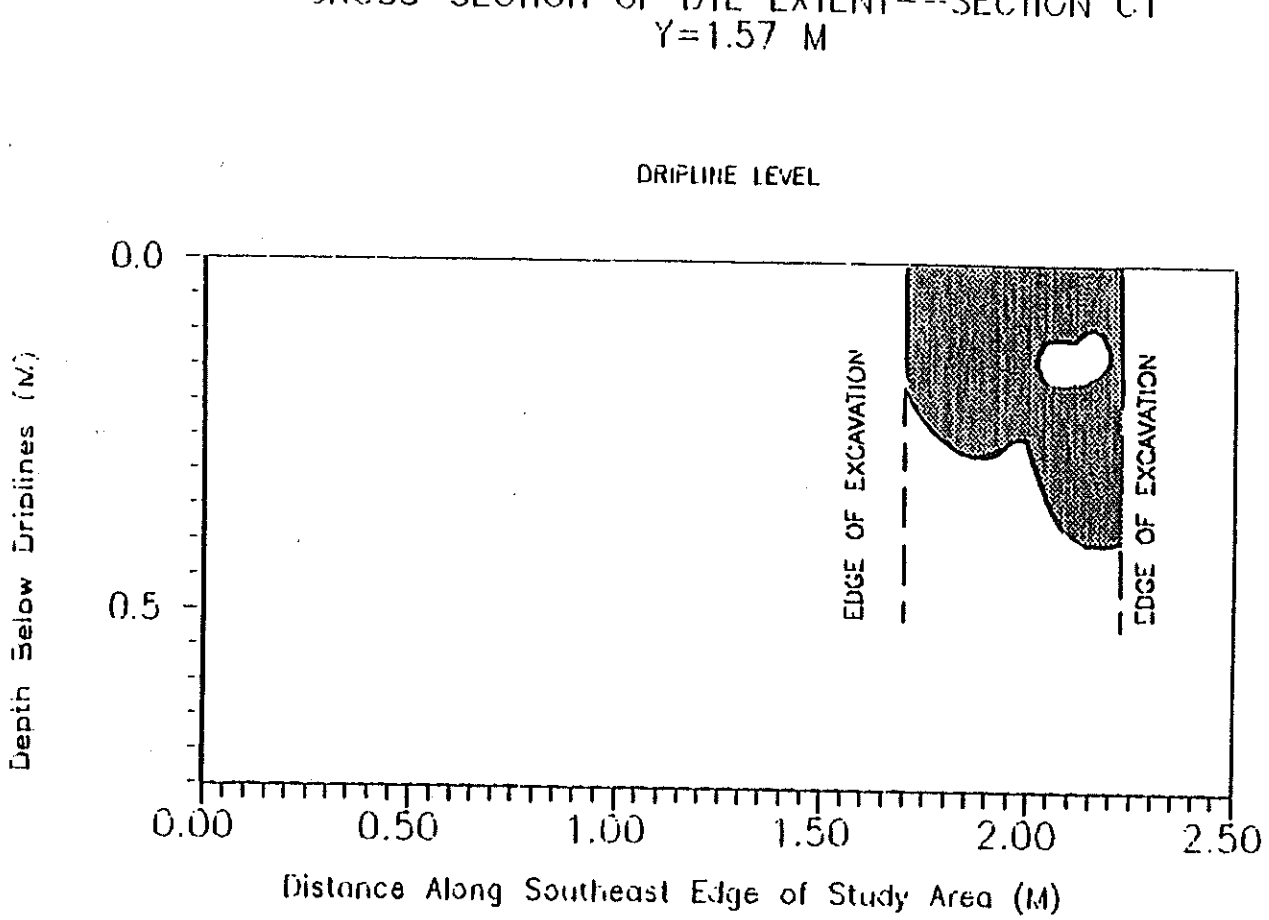

Figure 54. Cross-section of dye extent -- section C1.

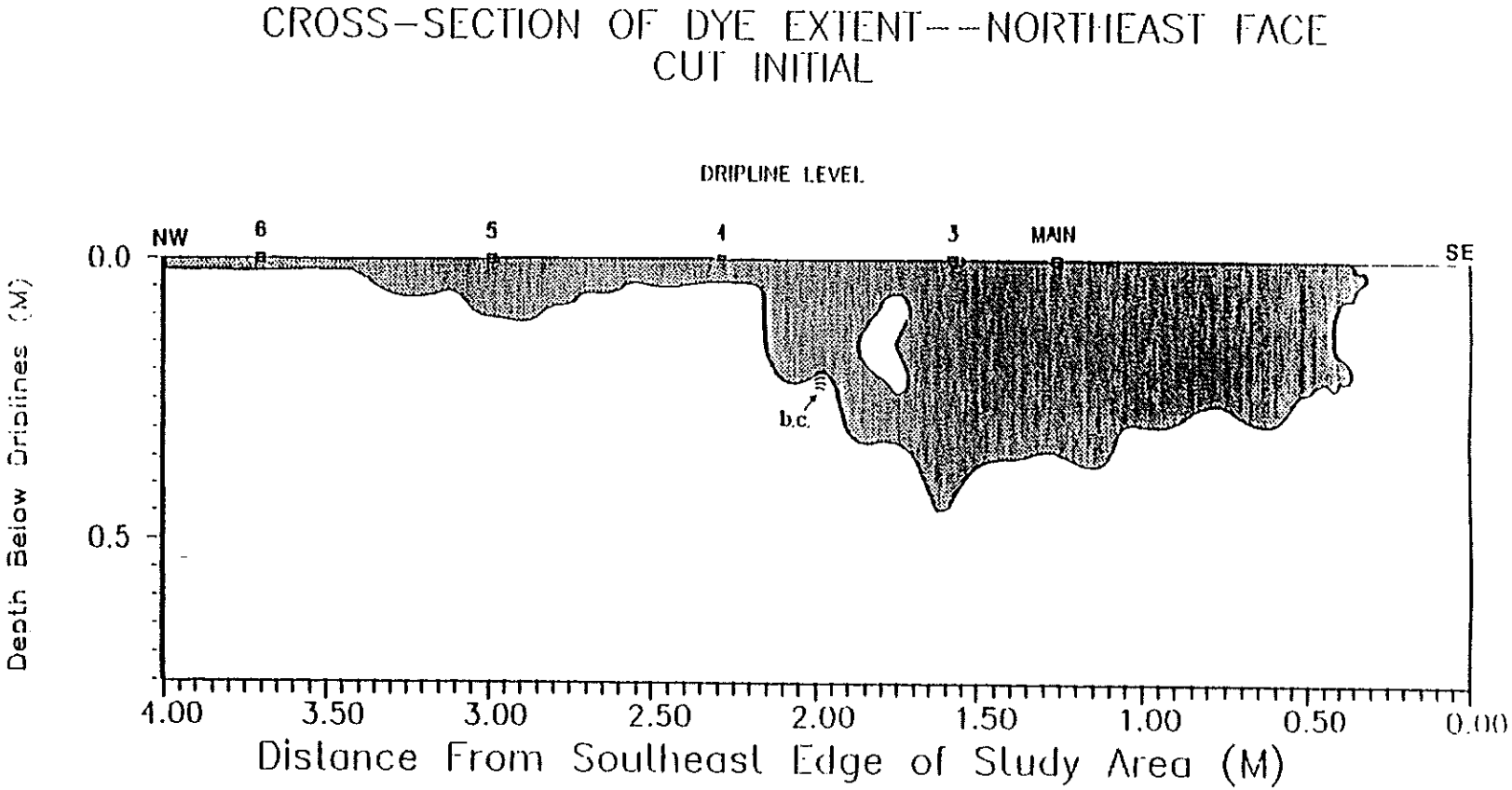

Figure 55. Cross-section of dye extent -- northeast face.

Because so much water was added to the site at once, some of it "backflowed" to the trench and formed a small pond. The water eventually soaked in, but this produced virtually saturated conditions in the vicinity of the main line. This extensive lobe of moisture spread laterally to the southeast along and through coarse layers, while seeping vertically into the underlying clayey silt layer. Small bulges corresponded to movement along coarse layers while undulating, large bulges indicated finer, thicker layers. Beyond the wooden trench some moisture was pulled upward (above dripline level) by capillary forces into finer (clayey silt) layers overlying coarse material.

The deepest penetration of dye along this transect was 45 centimeters below dripline 3. The spreading of the dye appeared to be an almost radial phenomenon in the vicinity of the main line. However, a hole appeared near dripline 3. This hole is composed of fine material overlying coarser (sandy gravelly) soil. The first emitter on dripline 3 is found in the proximity of this hole and may not have produced steady flow due to damage. This region, on the other hand, may have been simply bypassed due to preferential flow through the coarse layers to the left (missing the bedded clay--"b.c.") and from the strong pulse of moisture around the main line. The first emitter on dripline 4 may have contributed significantly to flow producing the lobe just northwest of the bedded clay. Material consisting of coarse sand and medium gravel persisted upward to this dripline's level. Moving northwest, the dyed water preferred the fine cover sand (around the driplines) and the underlying sandy silt. Although participating in the 4-day injection period, this region about dripline 5 showed relatively low amounts of dyed soil. Once again, this could have been due to a clogged emitter and/or prevalent lateral flow. Dyed soil is present only in the sand around dripline 6.

The fourth transect was along the original southwest face of the trench (fig. 56). The expansive region of dyed soil to the southeast was also associated with the slightly ponded conditions around the main line. Dyed water penetrated and evenly stained soils ranging from bedded clay to coarse pebbles and gravel before breaking into lobes having a wavy front. The water traveled vertically 50 cm through clayey silt before becoming impeded by small, thin coarse sand-gravel lenses. The water also avoided a large cobble as it flowed more laterally into layers of sand and fine gravel.

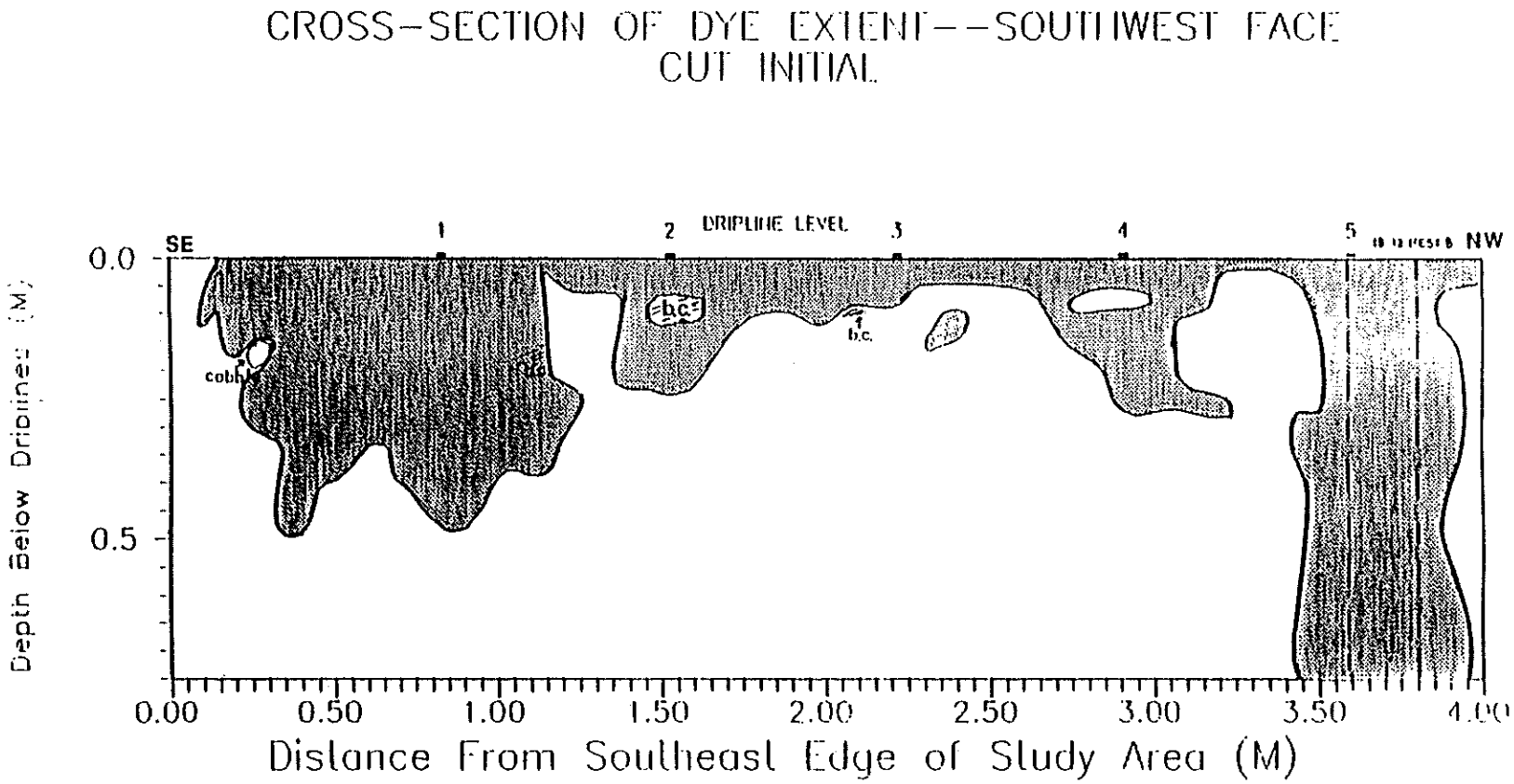

Figure 56. Cross-section of dye extent -- southwest face cut initial.

While water flow in the vicinity of dripline 1 was distributed somewhat radially, flow about dripline 2 was more laterally directed. Saturated flow was prevalent as evidenced by a lens of bedded clay that was bypassed completely. Also, the dyed front terminated at the coarse/fine soil boundary. This silty sand/clayey silt contact was continuous to the northwest and explained the migration of the dyed water below dripline 4. Lateral flow is also suggested by the small isolated patch of dyed soil. The hole just below dripline 4 may have been missed during lateral flow. A thin coarse sand and gravel lens at its lower boundary may have prompted this event. In terms of emitter uniformity, those in the vicinity of driplines 2 and 4 appeared to have contributed somewhat equal amounts of flow.

Water apparently piped along tensiometer nest B at Station 18-12. Bentonite seals and backfill in the shallow portions of the profile were not sufficient to deter water movement along the tubes. The extent of the piping was unclear, but a 5-meter deep tensiometer removed from the nest was stained blue along its length. The strong flow here of dyed water supported the lack of dyed soil between driplines 4 and 5 as well as around dripline 5 in the northeast face of the trench.

Cut A revealed a narrow but deep stretch of dyed soil below dripline 1 (fig. 57). A nearby emitter contributed all or part of flow in this region. The pulse penetrated the cover sand initially, then silty sand, followed by sandy, pebbly gravel and clayey, sandy silt. The smooth dye trace is indicative of flow through the extensive clayey silt. The infiltrating water avoided a circular lens of bedded clay and protruded slightly to the northwest along the coarse sandy gravel.

While the lobes of dyed soil below driplines 1 and 3 are similar in size and extent, the region beneath dripline 2 is only half as extensive. Dyed water may have flowed laterally here as the hole below dripline 2 was composed of the same material which was dyed to either side. However, the lower boundary of the dyed soil does not mark a contact. Rather, it lay below the sandy gravel mentioned above. If lateral flow occurred here during irrigation, then drainage may have caused the water to move vertically from the coarse layer into the underlying fine layer.

Dyed water infiltrated to an unknown depth below dripline 3 and avoided tensiometer nest A. Two layers of bentonite were effective here in keeping moisture away from the

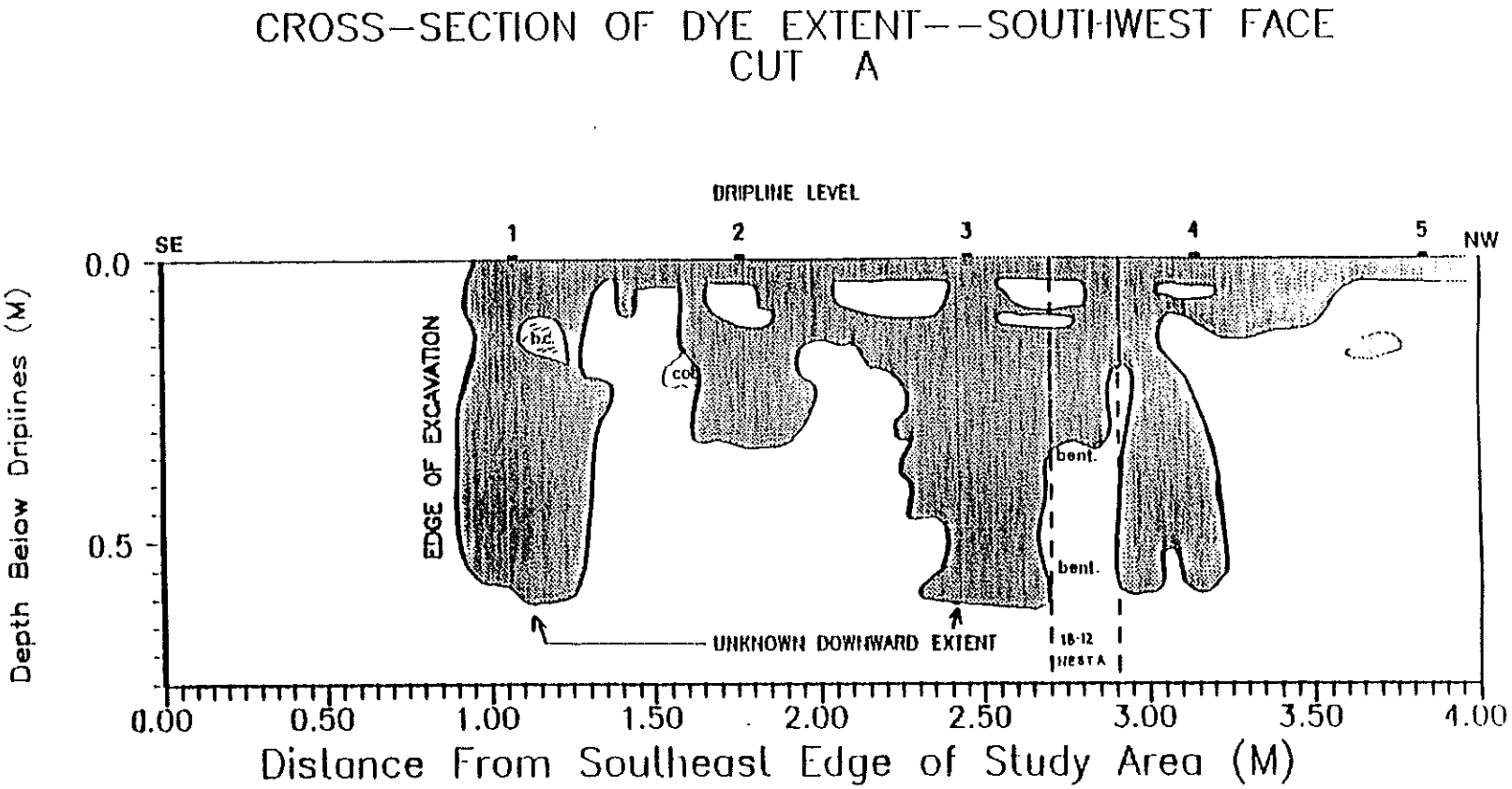

Figure 57. Cross-section of dye extent -- southwest face cut A.

shallow reaches of the instruments. This observation suggested that these tensiometers would not provide biased values of pressure head based on moisture present in the upper layers. The holes found in the near driplines 3 and 4 were bypassed by lateral flow through the cover sand and flow eventually channelled around the tensiometer nest. Finally a small spot of dyed soil near dripline 5 signified some lateral flow in the area, perhaps toward the sink at tensiometer nest B.

The fifth transect, cut B, was oriented at a slight angle north of the SE-NW main trench (fig. 58). The dripline crossover points are therefore closer together. The dye trace extended down to 65 cm and deeper below dripline level. A wavy border marks an expansive zone of dyed soil in the southeastern portion of the cut. Flow through this area may have been primarily vertical as certain holes were missed due to textural variations. Several jagged lenses of silty, sandy gravel persisted in the upper 25 cm of the profile. The dyed water penetrated these lenses and then proceeded into the pervasive clayey silt. The front was not smooth, however, and this may have been due once again to local textural variability producing preferential broad "fingering" of the dye trace. The neutron probe access tube in fig. 58 has also suffered some piping along its outer walls. Clean bentonite was still intact along the tube. However, additional blue-stained bentonite was smeared onto the metal suggesting lateral flow of dyed water around the tube and northwestward into the clayey silt. The erratic pattern of the dyed front also suggested lateral flow "into the paper" owing to close proximity emitters. The dye trace was of unknown downward extent below the trench floor. This signified vertical flow of dyed water through the fill around the access tube. An analysis of moisture content data collected at shallow depths from this access tube is still underway.

The closest emitter to cut B was along dripline 4 (fig. 59). Little dyed soil was found in this area suggesting either the emitter was disabled or that substantial lateral gradients swept the dyed water away.

One cross-section was excavated parallel to dripline 1 (fig. 59). The intersection with cuts A and B are shown. The emitter locations (from dripline 1) are actually 10 cm away (out from the page) from this "side cut." It was unusual that there wasn't dye present in the side cut near emitter 1 when there was extensively dyed soil around dripline 1 in figure 57.

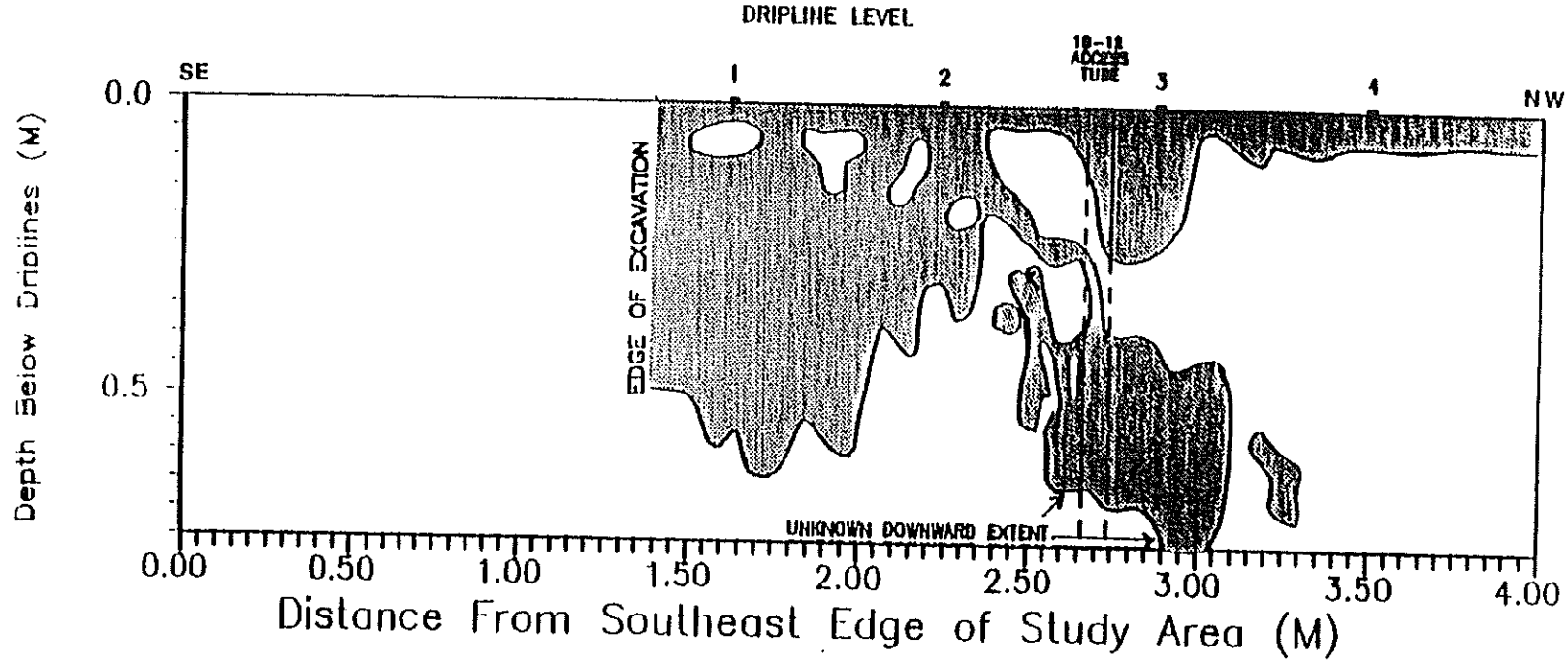

Figure 58. Cross-section of dye extent -- southwest face cut B

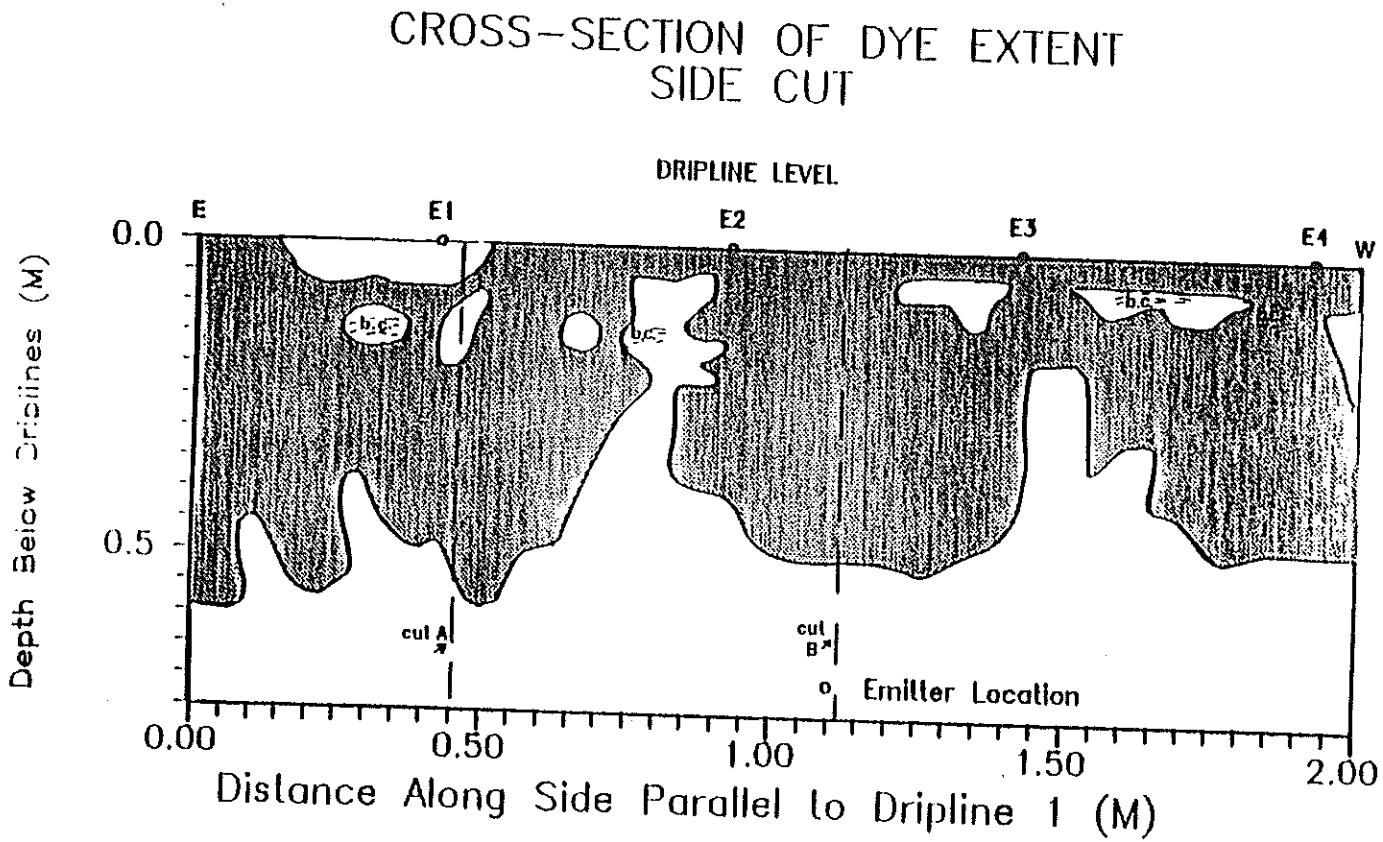

Figure 59. Cross-section of dye extent side cut.

The dyed water may have been initially channeled away from the wall and then back toward the side cut at depths below 10 cm. Lenses of bedded clay were common at the 15 cm depth in figures 58 and 59, in the vicinity of dripline 1. Dyed water avoided these lenses, but strong pulses are found below them. A change in texture from fine clayey silt to coarser gravelly clayey silt may have accounted for the unstable dye trace in the eastern region of the side cut. Flow from fine to coarse layers can promote wetting front instabilities. Also, Parsons (1988) assigned a saturated conductivity value of 2.5 E(-4) cm/s to the region containing the clayey silt. The flux rate was 1.0 E(-4) cm/s. Because the flux rate is less than the Ksat of the clayey silt, instabilities can occur.

Another large lobe of dyed soil was present midway between emitters 2 and 3. The trace was rather smooth indicating a more uniform texture in the clayey silt along the cut. The soil appeared to be dyed by flow from both emitters. The hole in the side cut to the right of the cut B intersection appeared continuous with the hole in cut B just below dripline 1. Dyed water again avoided a section of bedded clay between E3 and E4, but penetrate a smaller lens due west. Flow was channelled through this small lens and into a silty sand. This coarser layer was dry upon excavation while the underlying clayey silt was damp. During drainage the coarser layer may have released some moisture to the fine layer. The sharp point in the dye trace marked part of the contact between the coarse and fine layer.

Figures 60 and 61 are of cut D and section C3C (cut C). An emitter on dripline 5 was located practically on top of cut D. However, only a small amount of dyed soil was present. This emitter either produced little or no water or produced a uniform amount which was immediately piped in part to the sink at tensiometer nest B. Section C3C's dye distribution also emphasized a faulty or biased emitter. Dyed soil was spotty in this section. Lateral flow was indicated by single patches of dyed soil.

The following can be concluded from the dye study: Dyed flow pathways are good qualitative indicators of instrument performance. Supportive data analysis is necessary to allow a sufficient quantitative assessment of performance. Saturated flow was prevalent at very shallow depths and in the southeastern corner of the irrigated plot. Backflow and ponding appear to have promoted pseudoradial growth of the dye trace from the source. Emitters in this region are apparently not entirely uniform in distribution of moisture to the

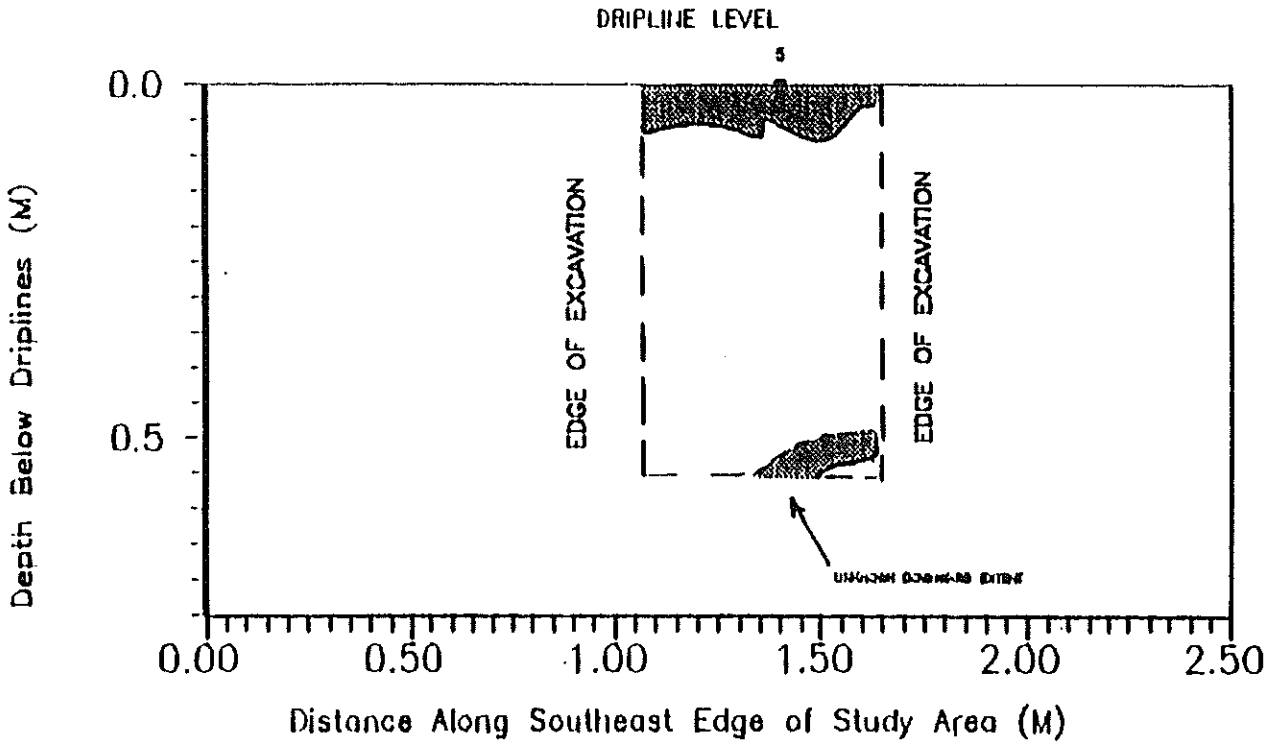

Figure 60. Cross-section of dye extent -- D2BB-D2AA Y=3.80 M.

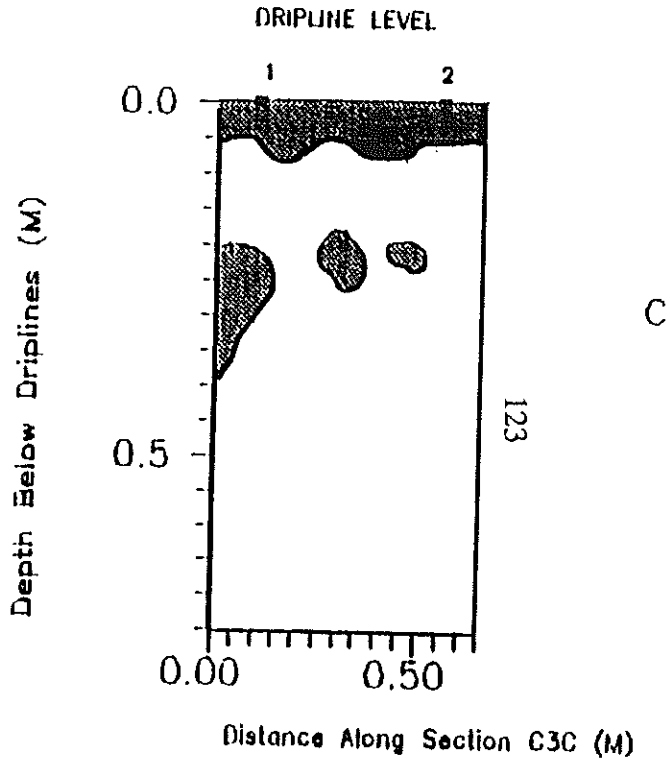

Figure 61. Cross-section of dye extent section C3C.

plot. Emitters could have been clogged or damaged, or the underlying soil could have enticed fluid flow in one direction or another. Heterogeneity and anisotropy in the soil would result in discontinuous pulses of dyed fluid flow (which is what we see). Local conditions determined the dominance of lateral or vertical fluid flow. For instance, loosely packed instruments promoted vertical infiltration. Uneven or jagged dye traces signify textural change in an otherwise uniform media. The trace was wide and smooth from flow through the thick clayey silt units. It became narrow and pointed when the fluid penetrated coarser, horizontally oriented layers. Finally, fluid flow did not have an affinity for a particular soil. Both thinly bedded clay and large cobbles (up to 15 cm in diameter) were stained blue in some areas and untouched in others.

SUMMARY AND CONCLUSIONS

This project provided a comprehensive analysis of the geologic, hydrologic, and solute transport properties of a heterogeneous vadose zone. The field site is representative of stratified alluvial deposits common throughout the western United States.

The results of this study lead to the following specific conclusions:

1. Water and tracer transport at the field site is controlled by anisotropy, heterogeneity, the orientation of the stratified layers, and differences in hydraulic properties between adjacent stratigraphic units. Significant lateral movement of tracer was observed. Beneath the tracer application area, fluoro-benzoate tracer was detected as much as 0.75 meters north of its application area at a depth of 1 meter. Bromide and fluoro-benzoate tracer were observed as much as 6 meters outside the plot at a depth of 5.6 meters after approximately 23 days.

2. A wide distribution of transport parameters was observed. Seepage velocity, dispersion coefficient, and dispersivity were log-normally distributed across the site. The amount of tracer seen and the average volume of soil water sampled were normally distributed.

3. By weighting the concentration seen at a particular point by the assumed water flux passing that point and averaging over a horizontal area, a better representation of the total mass of solute passing through the plane at that depth was obtained. This method predicted much faster movement of tracer than by aerially averaging resident concentrations or by simply averaging the transport parameters.

4. The transfer function model did not adequately describe solute movement in the top 2.5 meters of soil. This was probably due to the large degree of heterogeneity at the site, lateral movement of solute, and the tracer boundary condition to the soil surface. The transfer function predicted much faster tracer loading on the water table than the classical one-dimensional advection dispersion equation.

5. The horizontal spatial variability of hydraulic conductivity can be characterized at a number of scales at the field site, ranging from 1.5 to 2.5 meters to greater than 20 meters.

6. Log reduced sorptivity, 1.3 cm tension hydraulic conductivity ($K_{1.3}$), d_{10}, and van Genuchten's α-values exhibited ranges of correlation (2 m to 3 m) similar to those of the small scale hydrologic analysis.

7. The disc permeameter was a good device for estimating effective horizontal hydraulic conductivity in relatively dry soils over at least 3 orders of magnitude ranging from 1.0×10^{-2} cm/sec to approximately 1.0×10^{-5} cm/sec.

8. The initial moisture content and grain size distribution of the alluvial fan beds were quite a bit more variable than those of the Rio Grande facies. This quantitative analysis agreed with the ponding events and possible lateral flow during drainage through the alluvial fan units.

9. The vertical spatial variability of grain size, and saturated water content within the Rio Grande facies, ranged from about 0.5 to 2.0 meters. Up to 2-meter thick deposits were not unusual for a meandering river such as the Rio Grande to leave behind. The average thickness of beds within the Rio Grande material were about 1-meter. Therefore these correlation lengths may be attributed to the various deposits left by an ancestral meandering river.

10. Hydraulic conductivity within the Rio Grande sands was found to be about 10^{-2} to 10^{-3} cm/sec, confirming previous studies.

11. The disc permeameter study presented hydraulic conductivity values within the individual alluvial fan units that ranged from 1.05×10^{-2} cm/sec to 3.31×10^{-4} cm/sec. The waterlaid and debris flow deposits had unusually low hydraulic conductivities due to their fine matrix.

12. The detailed geologic investigation revealed a very complex set of clayey, sandy, and cobble-filled beds interrelated in such a way as to create conduits and barriers to drainage. All three types of alluvial fan deposits were found within the deep trench; debris flow, intermediate deposits, and waterlaid deposits. These deposits were overlying the finer grained ancestral Rio Grande sands.

The first and third objectives of the proposed research were fully achieved, as was a portion of the second objective. Quantitative information on hydraulic conductivities, infiltration rates, solute transport, and their spatial relationships was obtained for the field

site. The geologic controls on hydrologic flows and transport were determined in a semiquantitative manner. The analysis illustrated how a good understanding of site geology at various scales can lead to estimates of hydrologic characteristics.

The objective of testing the capability of multidimensional flow models to predict flow and transport at the experimental site was not fully achieved. This was partially due to our initial underestimation of the complexity of the site's subsurface geology. The poor correlation among hydrologic properties over short lateral distances was also unexpected.

Despite the lack of a full multi-dimensional analysis, we were able to partially explain patterns of tracer transport in terms of multidimensional flow. The extensive data base resulting from this study, as detailed in Arnet (1991), Grabka (1991), Schmidt-Petersen (1991), and in a forthcoming study by Stark (personal communication 1991) is available for future analysis and modeling work related to the well-characterized field site.

REFERENCES

Albrecht, K.A., B.L. Herzog, L.R. Follmer, I.G. Krapac, R.A. Griffin, and K. Cartwright. 1989. Excavation of an instrumented earthen liner: Inspection of dyed flow paths and morphology. Hazardous Waste and Hazardous Materials. 6:3:269-279.

Allen, J.R. 1970. Physical Processes of Sedimentation, American Elsevier Publishing Company, Inc. New York.

Ankeny, M. D., M. Ahmed, T. C. Kaspar, and R. Horton. 1990a. A simple field method for determining unsaturated hydraulic conductivity. Soil Sci. Soc. Am. J. , in preparation.

Ankeny, M. D., T. C. Kaspar, and R. Horton. 1990b. Characterization of tillage and traffic effects on unconfined infiltration measurements. Soil Sci. Soc. Am. J. 54:837-840

Ankeny, M. D. ,T. C. Kaspar, and R. Horton. 1988. Design for an automated tension infiltrometer. Soil Sci. Soc. Am. J. 52:893-896

Arnet, P. 1991. Field simulation of waste impoundment seepage in the vadose zone: Geologic and hydraulic characterization of a heterogeneous vadose zone with respect to fluid transport. Unpublished Independent Study paper, New Mexico Institute of Mining and Technology, Socorro, NM.

Bachman, G.O., and H.H. Mehnert. 1978. New K-Ar dates and the late pliocene to Holocene geomorphic history of the Central Rio Grande region, New Mexico. Geol. Soc. Am. Bull. 89:283-292.

Baldwin, B. 1963. Geology and water resources of the Santa Fe area, New Mexico. USGS Water Supply Paper, 1528: 21-89.

Biggar, J.W., and D.R. Nielsen, 1976. Spatial variability of the leaching characteristics of a field soil. Water Resour. Res. 12:78-84.

Blissenbach, E. 1954. Geology of alluvial fans in semiarid regions. GSA Bulletin. 65:75-190.

Bowman, R.S., 1984. Analysis of soil extracts for inorganic and organic tracer anions via high performance liquid chromatography. Journal of Chromatography. 285:467-477.

Bull, W.B., 1962. Relation of textural (CM) patterns to depositional environment of alluvial-fan deposits. J. Sed. Petrology, 32:211-216.

_____. 1963. Alluvial-fan deposits in western Fresno County, CA. Jour. Geology. 71:243-251.

_____. 1964. Alluvial fans and near surface subsidence in western Fresno County, CA. USGS Professional Paper. 437-A.

_____. 1972. Recognition of ancient sedimentary environments. Soc. Econ. Paleontologists and Mineralogists, Special Publ. 16:68-83, Tulsa.

_____. 1977. The alluvial fan environment. Progr. Phys. Geogr., 1:222-270.

CSIRO. 1988. Disk permeameter instruction manual. Commonwealth Science, Industry, and Research Organization, Canberroa, Australia.

Chamberlain, R.M. 1980. Cenezoic stratigraphy and structure of the Socorro Peak volcanic center, Central New Mexico. New Mexico Bureau of Mines and Mineral Resources, Open File Report 118:2:495.

Chapin, C.E., R.M. Chamberlain, G.R. Osburn, D.L. White, and A.R. Sanford. 1978. Exploration framework for the Socorro geothermal area, New Mexico. New Mexico Geol. Soc. Spec. Publ. 7:114-129.

Chisholm, R.H., B.J. Bridge, and R.E. Prebble. 1987. A rapid in situ method for measuring soil hydraulic properties and structure with the disc permeameter. Abstr, conference and workshop series-Queensland department of primary industries. In Proceedings National Workshop, Toowoomba, Queensland, 7-10 Seat. 1987. Ed. by K.J. Coughlan and P.N. Truong.

Chong, S.K., and R.E. Green. 1983. Sorptivity measurement and its application. p82-91. In Advances in Infiltration, Proc. Natl. Conf. Advances in Infiltration. Chicago, IL. 12-13 Dec. ASAE, St. Joseph, MI.

Clothier, B.E., and I. White. 1981. Measurement of sorptivity and soil water diffusivity in the field. Soil Sci. Soc. Am. J. 45:241-245

Debrine, B., Z. Speigal, and D. Williams. 1963. Cenozoic sedimentary rocks in Socorro Valley, New Mexico. Guidebook of the Socorro Region, New Mexico 14th Field Conf., New Mexico Geol. Soc., 123-131.

CSIRO Instruction Manual, Disc. Permeameter. 1988. Canberra, Australia.

Denny, C.S. 1940. Tertiary geology of the San Acacia area, New Mexico. J. of Geol. 48:73-106.

Dirksen, C. 1975. Determination of soil water diffusivity by sorptivity measurement. Soil Sci. Soc. Am. Proc. 39:22-273

Dixon, R.M. 1975. Design and use of closed-top infiltrometers. Soil Sci. Soc. Am. Proc. 39:755-763

Flanigan, K.G., 1989. Field simulation of waster impoundment in the vadose zone: Non-reactive solute transport through a stratified, unsaturated field soil. Unpublished M.S. Independent Study Paper, New Mexico Institute of Mining and Technology, Socorro, NM.

Ghodrati, M. and W.A. Jury. 1990. A field study using dyes to characterize preferential flow of water. Soil Sci. Soc. of Amer. J. 54:1558-1563.

Gibbens, J.F. 1989. An evaluation of several fluorinated benzoic acids for use as soil and groundwater tracers. Unpublished M.S. thesis, New Mexico Institute of Mining and Technology, Socorro, New Mexico.

Grabka, D.P. 1991. Field simulation of waste impoundment seepage in the vadose zone: Multiple-tracer transport experiment in a stratified, heterogeneous, unsaturated field soil. Unpublished Independent Study, New Mexico Institute of Mining and Technology, Socorro, NM.

Greene, R.S.B., and D.J. Tongway. 1989. The Significance of (surface) physical and chemical properties in determining soil surface condition of red earths in rangelands. Aust. J. Soil Res. 27:213-225

Hawley, J.W., F.E. Kottlowski, W.S. Strain, W.R. Seager, W.E. King, and D.V. Lemore. 1969. The Santa Fe Group in the south-central New Mexico border region. New Mexico Bureau of Mines and Mineral Resources Circ. 104:52-76.

Hawley, J. 1976. Quaternary stratigraphy in the Basin and Range and Great Plains provinces, New Mexico and Western Texas. In Quaternary Stratigraphy of North America. Dowden, Hutchinson, and Ross, Inc. 235-279.

Jarvis, N.J., P.B. Leeds-Harrison, and J.M. Dosser. 1987. The use of tension infiltrometers to assess routes and rates of infiltration in a clay soil. Jour. Soil Sci. 38:633-640

Johnson, W.R. 1988. Soil Survey of Socorro County Area, New Mexico. Soil Conservation Service, USDA.

Kottlowski, F.E. 1958. Geologic history of the Rio Grande near El Paso, West Texas Geological Society, Guidebook 1958 field trip. 46-54.

Machette, M.N. 1978. Geologic map of the San Acacia quadrangel, Socorro County, New Mexico, USGS Map GQ-1415 1:24,000.

Mack, G.H. and K.A. Rasmussen. 1984. Alluvial-fan sedimentation of the Cutler Formation near Gateway, Colorado. Geological Society of America Bulletin. 95:109-116.

Mattson, E.D., 1989, Field simulation of waste impoundment in the vadose zone: Experimental design and two-dimensional modeling. Unpublished M.S. Independent Study Paper, New Mexico Institute of Mining and Technology, Socorro, NM.

McLemore, V.T. and M.R. Bowie. 1987. Guidebook to the Socorro area, New Mexico, 24th Annual Meeting of the Clay Minerals Society and 36th Annual Clay Minerals Conference, New Mexico Bureau of Mines and Mineral Research.

McPherson 1987. Fan-deltas and braid deltas: Varieties of coarse-grained deltas. Geol. Soc. of America Bulletin, 99:331-340.

Nielsen, D.R., J.W. Biggar, and K.T. Erh. 1973. Spatial variability of field measured soil-water properties, Hilgardia. 42:215-259.

Omoti, U. and A. Wild. 1979. Use of fluorescent dyes to mark the pathways of solute movement through soils under leaching conditions: 2. Field experiments. Soil Science. 128(2):
98-102.

Parker, J.C., and M. Th. van Genuchten. 1984. Determining transport parameters from laboratory and field tracer experiments. Bulletin. 84-3, Va. Agric. Exp. Sta., Blacksburg.

Parsons, A.M. 1988. Field simulation of waste impoundment seepage in the vadose zone: Site charaterization and one-dimensional analytical modeling. Unpublished Independent Study Paper, New Mexico Institute of Mining and Technology, Socorro, New Mexico.

Perroux, K.M., and I. White. 1988. Designs for disc Permeameters. Soil Sci. Soc. Am. J. 52:5

Schmidt-Petersen, R.I. 1991. Field simulation of waste impoundment seepage in the vadose zone: Horizontal spatial variability of the geologic and hydraulic properties of an alluvial fan facies. Unpublished Independent Study Paper, Mexico Institute of Mining and Technology, Socorro, NM.

Smettem, K.R.J., B.E. Clothier. 1989. Measuring unsaturated sorptivity and hydraulic conductivity using multiple disc permeameters. Jour. Soil Sci. 40:3:563-568

Smiles, D.E., and A.G. Harvey. 1973. Measurement of moisture diffusivity in wet swelling systems. Soil Sci. 116:391-399

Sully, M.J., and I. White. 1987. A rapid in situ method for measuring soil hydraulic properties and structure with the disc permeameter. In Proc. National. Workshop., Toowoomba, Queensland. 7-10 Sept. 1987. Ed. by K.J. Coughlan and P.N. Truong. (abstr.)

Talsma, T. 1969. In situ measurements of sorptivity. Aust. J. Soil Res. 7:269-276.

Watson, K.M. and R.J. Luxmoore. 1986. Estimating macroporosity in a forest watershed by use of a tension infiltrometer. Soil Sci. Soc. Am. J. 50:578-582

White, I., and K.M. Perroux. 1989. Estimation of unsaturated hydraulic conductivity from field sorptivity measurements. Soil Sci. Soc. Am. J. 53:324-329.

White, I., and M.J. Sully. 1989. Use and hydrological robustness of time-to-incipient-ponding. Soil Sci. Soc. Am. J. 53:5:1343-1346.

Wilson, G.V. and R.J. Luxmoore. 1988. Infiltration, macroporosity, and mesoporosity distributions on two forest watersheds. Soil Sci, Soc. Am. J. 52:329-335

Wooding, R.A. 1968. Steady infitration from a shallow circular pond. Water Resources Research. 4:1259-1273